Electronic Supplementary Information (ESI)

A new set of metal-organic frameworks synthesised from diisophthalate-based, 2'-phosphorus-substituted *m*-terphenyl linker molecules

Timo Stein, Frank Hoffmann, and Michael Fröba*

Institut für Anorganische und Angewandte Chemie, Universität Hamburg, Martin-Luther-King-Platz 6, 20146 Hamburg, Germany.

TABLE OF CONTENTS

GENERAL DETAILS

Synthetical Details

3,5-(Dimethoxycarbonyl)phenylboronic acid[1] and *trans*-chloro(1-naphthyl)bis(triphenylphosphine)nickel(II)[2] have been prepared according to literature-reported syntheses. As-received anhydrous K_3PO_4 was dried in an oven at 140 °C for three days and stored in a desiccator cabinet over activated 10X molecular sieves. Even though the exact degree of hydration of K_3PO_4 is not known, the presence of water was not observed to have detrimental effect on the outcome of the Suzuki-Miyaura cross-coupling reactions conducted herein.

Unless otherwise stated, all reactions were performed in dry and degassed solvents under an inert atmosphere of argon gas using standard Schlenk technique. All chemical reagents were obtained from common commercial suppliers. Solvents and 1,3-Dichlorobenzene were degassed in an ultrasonic bath under a slow stream of argon gas and subsequently statically dried over activated molecular sieves 3 Å. Molecular sieves 3 Å were activated in dynamic vacuum (10^{-3} mbar) at 300 °C for 8 h and then allowed to cool down to room temperature under an argon atmosphere. 10X molecular sieves were activated in an oven at 140 °C for a minimum of three days until reuse.

TLC was conducted using standard silica layers on aluminium (ALUGRAM® Xtra SIL G/UV254; MACHEREY-NAGEL GmbH & Co. KG). Liquid chromatography was performed using silica gel 60 (0.063 mm – 0.200 mm; MACHEREY-NAGEL GmbH & Co. KG) as a stationary phase under ambient pressure. Alternatively, silica gel 60 (0.04 mm – 0.063 mm; MACHEREY-NAGEL GmbH & Co. KG) was used to perform flash chromatography.

Microwave reactions were done in a CEM Discover SP microwave.

Analytical Methods

Scanning electron microscopy (SEM) was done using a Hitachi TM-1000 Tabletop with an acceleration voltage of 15 kV.

High performance liquid chromatography (HPLC) was performed using a Dionex Ultimate 3000 HPLC with an SRD-3400 solvent rack, an LPG-3400 pump, a VWD-3400 variable wavelength detector, and a Rheodyne manual injection valve equipped with a 10 µL sample loop. The device is equipped with PEEK tubing. Data was collected using Chromeleon 6.80 SR15. A wavelength of 230 nm was detected. The chromatography was done at room temperature using a MACHEREY-NAGEL NUCLEODUR C18 HTec (3 µm, 3.0 mm × 150 mm) column (program 1, program 2) or a MACHEREY-NAGEL NUCLEODUR HILIC (3 µm, 3.0 mm × 150 mm) column (program 3).

- program 1: 0.300 mL/min; 3 min. MeCN/H_2O 70/30, linear ramp to MeCN/H_2O 30/70 over 17 min, 25 min. MeCN/H_2O 30/70, linear ramp to MeCN/H_2O 100/0 over 3 min.
- program 2: 0.350 mL/min, linear ramp from MeOH (0.1 % HCOOH)/H_2O 50/50 to MeOH (0.1 % HCOOH)/H_2O 100/0 over 40 min.
- program 3: 0.350 mL/min, linear ramp from H_2O (50 mmol/L NH_4OAc)/MeCN 30/70 to H_2O (50 mmol/L NH_4OAc)/MeCN 100/0 over 15 min.

Mass spectrometry (MS) was done by the mass spectrometry facility of the Department of Chemistry at the University of Hamburg. ESI-HRMS spectra were obtained at an Agilent Technologies 6224 Accurate-Mass TOF-MS.

Nuclear magnetic resonance (NMR) spectra from solution were obtained by the NMR facility of the Department of Chemistry at the University of Hamburg at room temperature using one of the following spectrometers: Fourier 300, AVANCE 400, AVANCE II 400, AVANCE III HD 400, DRX 500, AVANCE 500, AVANCE III 600, AVANCE 700 (all Bruker BioSpin GmbH), or Gemini 2000 (Varian, Inc.). Chemical shifts are referenced to (a) TMS (^{1}H NMR), (b) chemical shifts of literature-known (residual) resonance(s)[3] of the deuterated solvent used (^{1}H and ^{13}C NMR), or (iii) according to the IUPAC recommended Unified Scale[4,5] (all nuclei but ^{1}H). Phase-sensitive ^{13}C{^{1}H} spectra were recorded as APT (Attached Proton test) or DEPTQ (Distortionless Enhancement by Polarisation Transfer with retention of Quaternaries) experiments. Where required, COSY (Correlation Spectroscopy), HSQC (Heteronuclear Single Quantum Coherence) or HMQC (Heteronuclear Multiple-Quantum Correlation), and HMBC (Heteronuclear Multiple Bond Correlation) spectra were acquired. Where appropriate, higher spin systems were treated like the spin system of first order. Where this approximation did not seem adequate, coupling constants and chemical shifts were obtained by iterative spin simulation using the NUMMRIT routine implemented in SpinWorks 4 (Kirk Marat, University of Manitoba).

IR spectra (4000 cm^{-1}–450 cm^{-1}) were done on KBr pellets on a Bruker VERTEX 70.

X-ray powder diffraction experiments were performed using Cu radiation on (a) a STOE Stadi P (STOE & Cie GmbH) in transmission geometry according to Debye-Scherrer or (b) a Panalytical MPD X'Pert Pro in reflection geometry (Bragg-Brentano).

Single crystal X-ray experiments were performed using a SuperNova four-circle diffractometer in Kappa geometry with 50 W Cu and Mo microfocus tubes, an Atlas CCD detector (Rigaku Oxford Diffraction), and a Cryostream 700 Plus cooler (100 K–300 K, Oxford Cryosystems Ltd). Data collection, cell refinement, data reduction, and absorption correction were done using CrysAlis^{Pro}.[6] Alternatively, a Bruker AXS SMART APEX three-circle diffractometer with an APEX I CCD detector and a 30 W Mo source (Microfocus Source IμS, incoatec GmbH) and an Oxford Cryosystems Ltd cryosystem (100 K–300 K) was used. In this case, data collection was done using SMART, cell refinement and data reduction was done by SAINT. A numerical absorption correction using SADABS was done.[7] In both cases, intensities were measured using omega scans.

Single crystal X-ray data was solved and refined as follows. The space group was determined using XPREP (Bruker AXS Inc.) and the phase problem was solved either (a) using the iterative charge flipping routine provided with SUPERFLIP[8] where primary atom sites are assigned using EDMA,[9] (b) structure-invariant direct methods by SHELXS,[10] or (c) using the dual-space algorithm implemented with SHELXT.[11] In every case, full-matrix least-squares refinement was done on F^2 using SHELXL.[12] WinGX[13] and OLEX2[14] were used for visualization purposes during the refinement process. Missing secondary atom sites were located from the difference Fourier map. If possible, non-hydrogen atoms were refined using individual, anisotropic displacement parameters. The fully refined data was reviewed using PLATON.[15] Carbon atom-bound hydrogen atoms were positioned geometrically and refined riding on their respective parent atoms. U_{iso}(H) was fixed at 1.5 (OH, CH_3) or 1.2 (all other H atoms) of

the parent atom's isotropic displacement parameter. The coordinates of heteroatom-bound hydrogen atoms were assigned using the CALC-OH routine in WinGX, which is an implementation of Nardelli's HYDROGEN method.[16] Bond lengths were set to 0.95 Å ($C_{aromatic}$–H), 0.98 Å (C_{methyl}–H), and 0.99 Å ($C_{methylene}$–H). Hydrogen atoms of methyl groups were fitted to the experimentally observed electron density by allowing free rotation along the C—C bond (HFIX 137). Dihedral angles between planes apply to the corresponding least-squares planes. Estimated standard deviations (e.s.d.'s) concerning those as well as all other parameters of geometry were obtained considering the full matrix. Whenever necessary, site occupancy factors (s.o.f.'s) were obtained *via* occupancy refinement. PLATON/SQUEEZE was used to account for electron density contributions that could not modelled by chemically sensible units.[17]

Elemental analyses were done by the elemental analysis facility of the Department of Chemistry at the University of Hamburg by combustion. Analysers vario EL III (Elementar Analysensysteme GmbH) and EuroEA Elemental Analyzer with a high temperature pyrolysis system (HEKAtech GmbH) were used. It was not possible to assay the oxygen content in the presence of phosphorus.

Physisorption measurements were performed using a QUADRASORB SI-MP or Autosorb iQ instrument (Quantachrome Instruments). Data was evaluated using Quantachrome QuadraWin. The Micropore BET Assistant was used to assure that a meaningful BET range was chosen.[18]

Uptakes in quantities of specific volumes STP adsorbed V_{ads} [cm^3 (STP) g^{-1}] were converted to units of specific amounts of substance n_{ads} [mmol g^{-1}], specific masses m_{ads} [mg g^{-1}], and wt.-% using the following equations:

$$n_{ads} = \frac{V_{ads,\,STP} \cdot \rho_{adsorptive,\,STP} \cdot 1000}{M_{adsorptive}}$$

$$m_{ads} = V_{ads,\,STP} \cdot \rho_{adsorptive,\,STP} \cdot 1000$$

$$\text{wt.-\%} = \frac{m_{ads} \cdot 100}{(m_{ads} + 1000)}$$

Herein, $\rho_{adsorptive,\,STP}$ [g cm^{-3}] is the fluid density for the respective adsorptive at STP conditions (p = 1 bar, T = 273.15 K) as retrieved from NIST Chemistry WebBook ($\rho_{adsorptive,\,STP}(CO_2)$ = 0.0019508 g cm^{-3}, $\rho_{adsorptive,\,STP}(CH_4)$ = 0.00070805 g cm^{-3}).[19] Molar masses of $M(CO_2)$ = 44.009 g mol^{-1} and $M(CH_4)$ = 16.043 g mol^{-1} were used.

Isosteric heat of adsorption calculations were done using the Quantachrome QuadraWin software. Two adsorption isotherms for the gas in question at temperatures T_1 = 273 K and T_2 = 298 K were acquired. Plots of surface coverage θ as a function of pressure reveal pressures corresponding to equal coverages at the different temperatures studied. An Arrhenius plot of the identified pressures and temperatures ln$P$ versus 1/T is then constructed and the heat of adsorption Q_{st} at a given coverage θ can be calculated from the slope, as can be seen from the equation

$$Q_{st} = -R\left(\frac{\partial \ln P}{\partial 1/T}\right)_{\theta}.$$

This approach assumes (a) the heat of adsorption being constant within the temperature range under study, (b) ideal behaviour of the bulk gas phase, and (c) a negligible molar volume of the adsorbate.[20]

Simultaneous thermal analysis (STA) combined with MS techniques (TG-DTA/MS) was done using a TG 449 F3 Jupiter® coupled to a QMS 403 C Aëolos® (NETZSCH-Gerätebau GmbH) in the temperature interval of 20 °C–900 °C using a constant heating rate of 5 °C/min in an Ar/O_2 atmosphere (80/20) at a gas flow of 20 mL min^{-1}. Data evaluation was done using NETZSCH Proteus® Thermal Analysis.

In Silico Methods

Indexing of reflections was done using the X-Cell routine[21] implemented in Materials Studio 5.5 (Accelrys, Inc.).

Homology modelling was done to prove or falsify the isostructural relationship of a compound to be tested with a powder X-ray diffractogram available towards a compound that has been structurally elucidated, e.g. by single crystal X-ray diffraction. It was performed *in silico* using Materials Studio 5.5 (Accelrys, Inc.) according to a procedure described by Loiseau et al.[22] The linker molecule(s) of a MOF to be tested was (were) removed and the new linker molecule(s) inserted instead. Symmetry restrictions were removed by choosing the space group *P*1. Open metal sites were coordinated with oxygen atoms. The structure including the cell were minimised in energy by the Universal Force Field method[23] provided by the Forcite module using the following force field atom types: Cu3+1, O_R (carboxylate oxygen atoms), O_2 (phosphane oxide oxygen atoms and oxygen atoms used to saturate open metal sites), C_R (all carbon atoms except for alkyl chain carbon atom atoms), C_3 (alkyl chain carbon atoms), P_3+5 (phosphane oxide or sulfide phosphorus atoms), and H_ (all hydrogen atoms). Convergence criteria of 10^{-4} kcal/mol (energies), 0.005 kcal/mol/Å (forces), and $5 \cdot 10^{-5}$ Å (displacement) were chosen. Van der Waals interactions were treated in terms of a classical 12-6 Lennard-Jones potential up to a cutoff distance of 15.5 Å. After that, cell parameters were manually set to those acquired from X-Cell indexing and a powder X-ray diffractogram was calculated from the generated structure. The comparison with the experimentally obtained powder X-ray diffractogram validates or falsifies the initial assumption.

Poreblazer 3.0.2[24] was used for ***in silico* calculations of void volumes, He volumes, and accessible specific surface areas**. These parameters were obtained using structural data derived from homology modelling or single crystal structure analyses. The structures were carefully freed from disorder as well as free and metal-coordinated solvent molecules or fragments thereof to give an idealised structure. The default calculation parameters of Poreblazer were used, except for the void volume determinations were the He atom sigma was set to σ = 0 Å. The default UFF parameters for the framework atoms included with Poreblazer were used. Table S1 summarises the values obtained.

Table S1: Comparison of calculated void volumes, He volumes, densities, and specific surface areas for the MOFs presented herein. All data obtained and derived with help of Poreblazer. The values were obtained using structural models of activated materials, therefore free of guest molecules or additional ligands coordinated to the metal ion apart from carboxylate functional groups.

MOF	void volume / %	He volume / $cm^3\ g^{-1}$	specific surface area / $m^2\ g^{-1}$
UHM-60	76	0.999	1950
UHM-61	76	0.989	1879
UHM-62	73	0.868	1337
UHM-63	74	0.801	1199

Topological analyses were carried out using ToposPro.[25] Thus-obtained nets were further evaluated using Systre 1.2.0 beta2 and the related tiling representations were visualised using 3dt 0.6.0 beta2. Both Systre and 3dt are part of the Gavrog project.[26] The procedure used herein has been described by Sartor *et al.*;[27] These resources are now available on YouTube.[28] If a deconstruction of a bent diisophthalate linker to a 4-c node is conducted, thus-derived nets are denoted as *basic* nets. However, we prefer a description where the bent diisophthalate is regarded as a set of two interconnected 3-c nodes. Those nets were also designated as nets *derived* from the corresponding basic net. Hereafter, we omit the expression 'derived' and simply express *the underlying net* of a MOF, unless we explicitly mean to refer to the basic net.[29]

Twist angles and fold angles.

Figure S1 illustrates the construction of twist (Fig. S1b) and fold angles (Fig. S1c) based on a *m*-terphenyl linker molecule shown in Fig. S1a.

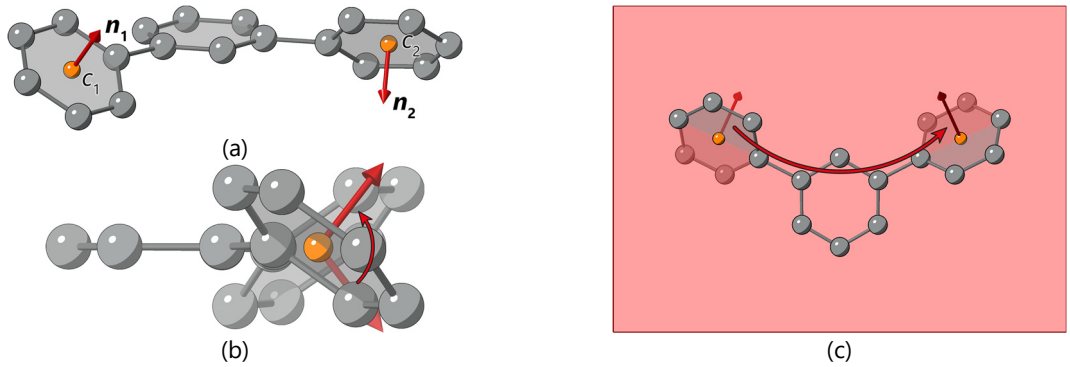

Figure S1: (a) A *m*-terphenyl molecule without H atoms. Least-squares mean planes (LSMPs) for the three aryls are shown in grey colour. Centroids c_1 and c_2 of the peripheral aryls are depicted in orange colour, plane normals $\boldsymbol{n_1}$ and $\boldsymbol{n_2}$ as red vectors. (b) The twist angle is included by the plane normals projected onto a plane orthogonal to the centroid-centroid connecting line c_2-c_1. (c) For the fold angle, the definition of a fold plane depicted in red colour is useful. The fold plane is constructed from two vectors: (i) The centroid-centroid connecting vector c_2-c_1 and (ii) the sum of plane normals $\boldsymbol{n_1} + \boldsymbol{n_2}$. The angle included by the projection of the plane normals onto the fold plane is the fold angle.

Please note that the latest stable version of OLEX2 at the time of preparation of this manuscript (1.2.10, Compilation Info: 2018.05.29 svn.r3508) created fold angles of 0° in cases where the vector $\boldsymbol{n_1} + \boldsymbol{n_2}$ became nearly parallel to the vector c_2-c_1. The values were obtained with an alpha version of OLEX2 (1.3.0, Compilation Info: 2019.04.02 svn.r3582) giving meaningful values in these cases.

IAST selectivities were calculated using the pyIAST package by Simon *et al.*[30] The single-component CO_2 and CH_4 adsorption branches at 273 K and 298 K, respectively, were converted to .csv files containing respective pressures [bar] and uptakes [mmol g^{-1}]. The isotherms were then fitted to the Langmuir model (equation 1) for CH_4 or the dual-site Langmuir (DSLangmuir) model (equation 2) for CO_2. L represents gas uptake, P pressure, M_n the saturation loading, and K_n the Langmuir constant.

$$L(P) = M_1 \frac{K_1 \cdot P}{1 + K_1 \cdot P} \tag{1}$$

$$L(P) = M_1 \frac{K_1 \cdot P}{1 + K_1 \cdot P} + M_2 \frac{K_2 \cdot P}{1 + K_2 \cdot P} \tag{2}$$

In the case of DSLangmuir fitting, the parameter guess for the pyIAST fitting routine was obtained by a fitting procedure with help of OriginPro 2019. In the following example, single-component CO_2 and CH_4 adsorption branches at 273 K were fitted to the DSLangmuir (note that in this example, the parameter guesses were all set to '1') and Langmuir models, respectively, the isotherms are plotted, and the model parameters are printed. Afterwards, the mole fraction of the feed gas of interest as well as the feed gas pressure points required are set, and the IAST calculation of CO_2 and CH_4 loadings q_1 and q_2 is run.

```
import pyiast
import pandas as pd
import numpy as np
df_co2_273 = pd.read_csv("/home/timostein/pyiast/uhm62co2273.csv")
df_ch4_273 = pd.read_csv("/home/timostein/pyiast/uhm62ch4273.csv")
co2_273_isotherm = pyiast.ModelIsotherm(df_co2_273,
                                        loading_key="Loading(mmol/g)",
                                        pressure_key="Pressure(bar)",
                                        model="DSLangmuir",
                                        param_guess={"M1": 1,"M2": 1,"K1": 1,"K2": 1})
ch4_273_isotherm = pyiast.ModelIsotherm(df_ch4_273,
                                        loading_key="Loading(mmol/g)",
                                        pressure_key="Pressure(bar)",
                                        model="Langmuir")
pyiast.plot_isotherm(co2_273_isotherm)
pyiast.plot_isotherm(ch4_273_isotherm)
co2_273_isotherm.print_params()
ch4_273_isotherm.print_params()
feedcomp = np.array([0.50, 0.50])
pressures = [0.01, 0.10, 0.20, 0.30, 0.40, 0.50, 0.60, 0.70, 0.80, 0.90, 1.00]
for val in pressures:
                                        print(pyiast.iast(val * feedcomp, [ch4_273_isotherm, co2_273_isotherm]))
```

The selectivity at a given pressure was then calculated by

$$S = \frac{q_1 \cdot p_2}{q_2 \cdot p_1} \tag{3}$$

With p_n being the partial pressure of the respective component at the respective feed gas pressure. The model parameters and root-mean-square errors (RMSE) for the relevant fits of **UHM-62** adsorptions are given in Table S2.

Table S2: Model parameters and RMSE values for Langmuir (CH_4) and dual-site Langmuir (CO_2) fits of the adsorption branches of CO_2 and CH_4 at temperatures of 298 K and 273 K, respectively.

	CO_2		CH_4	
	298 K	273 K	298 K	273 K
M_1	0.285775	1.126053	9.188564	4.705413
K_1	3.547043	7.798482	0.086590	0.293866
M_2	59.340195	23.277479		
K_2	0.063100	0.212041		
RMSE	0.004484	0.006937	0.002211	0.002035

SYNTHESIS OF ORGANIC COMPOUNDS

The synthetical concepts for the preparation of organic compounds used in this work are shown in Figures S2—S5.

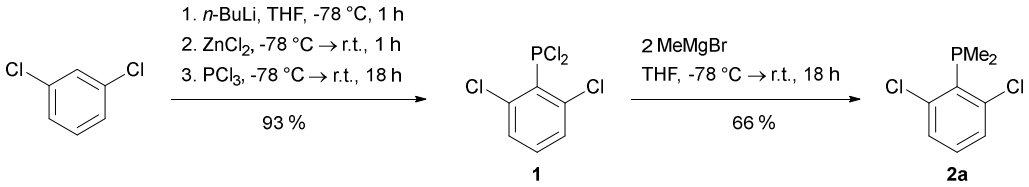

Figure S2: The cross-coupling nucleophile **2a** has been synthesised as follows. 1,3-Dichlorobenzene was subjected to directed ortho lithiation and subsequent metathesis with $ZnCl_2$ to give the arylzinc compound. Selective monosubstitution at PCl_3 gave the aryldichlorophosphane **1**. Substitution of **1** with MeMgBr at the phosphorus atom gave the aryldimethylphosphane **2a**.

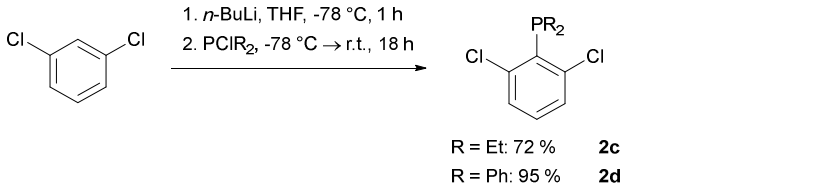

Figure S3: By reacting 2,6-dichlorolithiobenzene with phosphorus electrophiles chlorodiethylphosphane or chlorodiphenylphosphane, the cross-coupling building blocks **2c** and **2d**, respectively, have been obtained.[1]

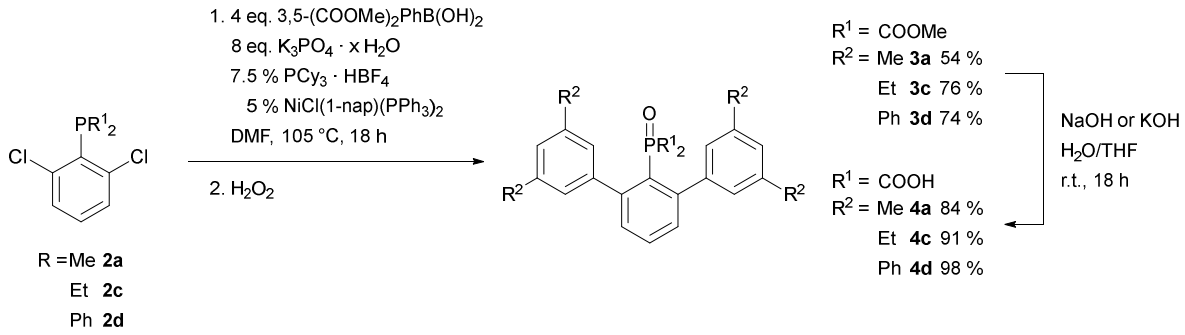

Figure S4: Ni(0)-catalysed cross-coupling reaction of the (2,6-dichlorophenyl)phosphanes **2** with 3,5-(dimethoxycarbonyl)phenylboronic acid[2] und subsequent oxidation with H_2O_2 yielded the *m*-terphenyl-based phosphane oxides **3**. Saponification of the ester functional groups yielded the linker molecules **4**.

[1] **2c** was also prepared by substitution of **1** by two equivalents of ethylmagnesium bromide in 65 % yield similar to the prodecure for the preparation of **2a**. Due to the affordability of $PClEt_2$ and $PClPh_2$ in contrast to $PClMe_2$, we decided to use the Grignard substitution route only for the preparation of **2a**.

[2] For the sterically less demanding aryldimethylphosphane **2a**, [$NiCl_2$(dppp)] (dppp: 1,3-bis(diphenylphosphino)-propane) was also found to be an efficient (pre-)catalyst for Suzuki-Miyaura coupling with 3,5-$(COOMe)_2PhB(OH)_2$ using Han and co-workers procedure.[88]

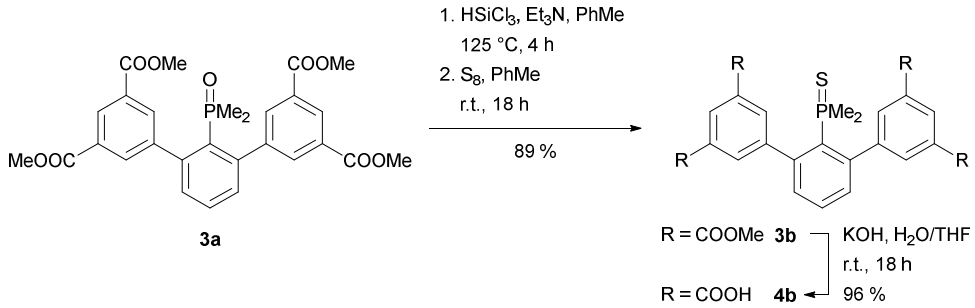

Figure S5: The aryldimethylphosphane sulfide-based linker molecule was prepared by a P(V) → P(III) reduction of **3a** by trichlorosilane[31] and subsequent reaction with elemental sulfur to give the tetramethyl ester of the phosphane sulfide **3b**. Saponification gave the linker molecule **4b**.[3]

(2,6-Dichlorophenyl)dichlorophosphane (1)

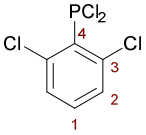

A magnetically stirred solution of 1,3-dichlorobenzene (1.15 mL, 1.48 g, 10.0 mmol) in THF (30 mL) was cooled to −78 °C using an acetone/dry ice bath. A solution of *n*-butyllithium (1.6 mol/L in hexanes, 6.25 mL, 10.0 mmol, 1 eq.) was added slowly over the course of ten minutes *via* syringe. The temperature was maintained at −78 °C for 90 minutes during which colourless precipitate formed. $ZnCl_2$ solution[4] (1.0 mol/L, 12.0 mL, 12 mmol, 1.2 eq.) was added dropwise over five minutes *via* syringe, whereby a colourless solution is formed. The cooling bath is removed, and the reaction mixture allowed to reach room temperature.

In a second flask, phosphorus trichloride (4.4 mL, 50 mmol, 5 eq.) was dissolved in THF (20 mL) and the colourless solution cooled to −78 °C using an acetone/dry ice bath. The organozinc reagent solution is added to the phosphorus trichloride solution *via* syringe transfer over five minutes. The cooling bath was removed, and the reaction mixture allowed to reach room temperature over 18 h. Volatiles were removed in vacuum and the resulting colourless viscous oil was magnetically stirred with *n*-hexane (20 mL) for five minutes. Stirring was stopped and the top layer of *n*-hexane was removed *via* cannula transfer. Using this procedure, the crude oil was extracted two more times and the combined *n*-hexane phases were freed from volatiles *in vacuo* to yield 2.31 g (9.32 mmol, 93 % based on 1,3-dichlorobenzene) of a colourless liquid.

^{1}H NMR (400 MHz, C_6D_6): δ [ppm] = 6.62 (dd, 2 H; ^3J(H,H) = 8.1 Hz, ^4J(H,P) = 2.5 Hz, H_2), 6.24 (t, 1 H; ^3J(H,H) = 8.1 Hz, H_1).

^{1}H NMR (400 MHz, $CDCl_3$): δ [ppm] = 7.30 (**A_2**BX, 2H; ^3J(H,H) = 8.1 Hz, ^4J(H,P) = 2.5 Hz, H_2), 7.27 (A_2**B**X, 1H; ^3J(H,H) = 8.1 Hz, ^5J(H,P) = 0.1 Hz, H_1).

^{13}C{^{1}H} NMR (75 MHz, C_6D_6): δ [ppm] = 133.5 (C_4), 129.5 (C_3).[5]

^{31}P{^{1}H} NMR (162 MHz, C_6D_6): δ = 153.0 ppm.

---

[3] In principle, the phosphane sulfide **3b** can also be obtained by direct conversion of **3a** using 2,4-bis(4-methoxyphenyl)-1,3,2,4-dithiadiphosphetane-2,4-dithione (Lawesson's reagent). However, this method gave relatively low yields around 25 %.

[4] A solution of $ZnCl_2$ in THF can be prepared by melting commercially available anhydrous $ZnCl_2$ three times in dynamic vacuum (10^{-3} mbar) using a heat gun. After cooling to room temperature, the mass of $ZnCl_2$ is redetermined and the material dissolved in an appropriate volume of dry THF. More conveniently, solutions of $ZnCl_2$ in diethyl ether are also commercially available.

[5] The quaternary carbon resonances could not be detected due to a low concentration of analyte.

(2,6-Dichlorophenyl)diorganophosphanes (2)

(2,6-Dichlorophenyl)dimethylphosphane (**2a**)

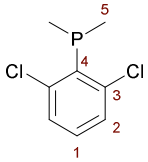

The dichlorophosphane **1** (2.31 g, 9.32 mmol) was dissolved in THF (15 mL) and the magnetically stirred colourless solution cooled to −78 °C with help of an acetone/dry ice bath. A solution of methylmagnesium bromide (3.0 mol/L in diethyl ether, 6.5 mL, 19.5 mmol, 2.1 eq.) was added dropwise over the course of ten minutes. The cooling bath was removed, and the reaction mixture was allowed to reach room temperature over 18 h. First, methanol (5 mL) was added in order to quench any unreacted Grignard reagent, then, volatiles were removed in vacuum. The residue was extracted three times with *n*-hexane (three times with 20 mL each) *via* cannula filtration. The combined organic phases were concentrated in vacuum and transferred to a Kugelrohr distillation apparatus. Distillation was conducted at 10^{-3} mbar up to 120 °C to yield 1.27 g (6.13 mmol, 66 % based on **1**) of a colourless liquid with an unpleasant odour.

ESI-HRMS: *m/z* = calc. for $[C_8H_9Cl_2P + H]^+$: 206.9892; found: 206.9896.

HPLC (230 nm, program 1): retention time = 16.91 min *for the oxide (2,6-Cl_2Ph)POMe_2*.

^{1}H NMR (400 MHz, C_6D_6): δ [ppm] = 6.91 (dd, 2 H; ^3J(H,H) = 8.0 Hz, ^4J(H,P) = 1.5 Hz, H_2), 6.44 (t, 1 H; ^3J(H,H) = 8.0 Hz, H_1), 1.38 (d, 6 H; ^2J(H,P) = 6.6 Hz, H_5)

^{13}C{^{1}H} NMR (75 MHz, C_6D_6): δ [ppm] = 142.2 (d; ^2J(C,P) = 16.0 Hz, C_3), 136.5 (d; ^1J(C,P) = 35.6 Hz, C_4), 130.4 (s; C_2).

^{31}P{^{1}H} NMR (162 MHz, C_6D_6): δ = −31.9 ppm.

(2,6-Dichlorophenyl)diethylphosphane (**2c**)

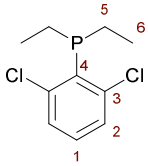

1,3-Dichlorobenzene (2.00 mL, 2.58 g, 17.6 mmol, 1.0 eq.) was dissolved in THF (50 mL) under magnetic stirring. The colourless solution was cooled to −78 °C using an acetone/dry ice bath. *n*-Butyllithium solution (1.6 mol/L in hexanes, 50 mL) was added over ten minutes *via* syringe. The mixture was stirred at −78 °C for 90 minutes, forming colourless precipitate. In a second flask, chlorodiethylphosphane (2.15 mL, 2.20 g, 17.7 mmol, 1.0 eq.) was dissolved in THF (15 mL). The chlorophosphane solution was added dropwise *via* syringe to the aryllithium suspension over ten minutes. Care has to be taken to contain the strongly exothermic reaction and prevent thermal decomposition of 2,6-dichlorolithiobenzene.[32] After the addition had been completed, the cooling bath was removed and the yellow coloured solution warmed to room temperature while stirring over the course of 18 h. The volatiles were removed *in vacuo* and the residual red oil was extracted with *n*-hexane (three times with 15 mL each) using cannula filtration. A small amount of solid might precipitate from the combined *n*-hexane phases that are concentrated *in vacuo* and transferred to a Kugelrohr distillation apparatus. Distillation was carried out from 100 °C—140 °C at 10^{-3} mbar. A colourless to slightly yellow liquid **2c** (2.96 g, 12.6 mmol, 72 %) was obtained.

ESI-HRMS: *m/z* = calc. for $[C_{10}H_{13}Cl_2P + H]^+$: 235.0210; found: 235.0208.

^{1}H NMR (400 MHz, $CDCl_3$): δ [ppm] = 7.22 (**A_2**BX, 2 H; $^3J(H_A,H_B)$ = 8.0 Hz, $^4J(H_A,P_X)$ = 1.5 Hz, H_2), 7.09 (A_2**B**X, 1 H; ^3J(H,H) = 8.0 Hz, $^5J(H_B,P_X)$ = 0.4 Hz, H_1), 2.23 (**A**BM_3X, 2 H; $^2J(H_A,H_B)$ = 13.6 Hz, $^3J(H_A,H_M)$ = 7.7 Hz, $^2J(H_A,P_X)$ = 2.4 Hz, H_5), 1.94 (A**B**M_3X, 2 H; $^2J(H_B,H_A)$ = 13.6 Hz,

$^{3}J(H_B,H_M)$ = 7.7 Hz, $^{2}J(H_B,P_X)$ = 6.5 Hz, H_5), 1.06 (AB**M$_3$**X, 6 H; $^{3}J(H_M,H_A)$ = 2.4 Hz, $^{3}J(H_M,H_B)$ = 7.7 Hz, $^{3}J(H_M,P_X)$ = 17.5 Hz, H_6).

^{13}C{^{1}H} NMR (100 MHz, CDCl$_3$): δ [ppm] = 142.9 (s; C_4), 133.9 (s; C_3), 130.7 (s; C_1), 129.1 (s; C_2), 18.3 (d; ^{1}J(C,P) = 12.2 Hz, C_5), 10.8 (d; ^{2}J(C,P) = 18.6 Hz, C_6).

^{31}P{^{1}H} NMR (162 MHz, CDCl$_3$): δ = −2.3 ppm.

(2,6-Dichlorophenyl)diphenylphosphane (**2d**)

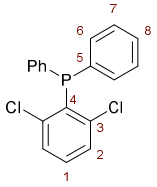

A solution of 1,3-dichlorobenzene (2.58 mL, 3.32 g, 17.6 mmol) in THF (25 mL) was cooled to −78 °C under magnetic stirring. *n*-Butyllithium solution (1.6 mol/L in hexanes, 11.0 mL, 17.6 mmol, 1.0 eq.) was added dropwise over the course of 10 min. The reaction mixture was stirred for 90 minutes while colourless precipitate formed. Chlorodiphenylphosphane (3.15 mL, 3.76 g, 17.5 mmol, 1.0 eq.) was added dropwise over 10 min. The cooling bath was removed, and the red solution further stirred for 18 h, during which it reached room temperature. Demineralised water (0.5 mL) was added and volatiles were removed *in vacuo* to give a deep red oil. The following steps were conducted at ambient conditions. The residue was taken up in EE (150 mL) and the organic phase washed with demineralised water (two times with 50 mL each). The organic phase was stirred over sodium sulfate, subjected to filtration over cotton wool and the organic solvent was removed from the filtrate by rotary evaporation. The crude was purified by column chromatography (SiO_2; PE/THF = 95/5) to yield a colourless oil which soon crystallised. During the chromatographic workup, crystallisation of the compound on the column and within the test tubes was observed. On the one hand, this made elution more time-consuming, on the other hand, single crystals suitable for X-ray structural analysis of **2d** were obtained. When **2d** was crystallised from an ethanol solution at −20 °C for several days, single crystals of (2,6-dichlorophenyl)diphenylphosphane oxide formed as proven by single crystal X-ray diffraction.

R$_f$ = 0.65 (PE/THF = 95/5; detection *via* UV activity).

ESI-HRMS: *m/z* = calc. for $[C_{18}H_{13}Cl_2P + H]^+$: 331.0210; found: 331.0230.

HPLC (230 nm, program 1): retention time = 45.81 min.

^{1}H NMR (300 MHz, CDCl$_3$): δ [ppm] = 7.46—7.20 ppm (m; H_1, H_2, H_6, H_7, H_8).

^{13}C{^{1}H} NMR (75 MHz, CDCl$_3$): δ [ppm] = 143.0 (d; ^{1}J(C,P) = 16.7 Hz, C_4), 134.7 (d; ^{1}J(C,P) = 13.2 Hz, C_5), 133.5 (d; ^{2}J(C,P) = 26.4 Hz, C_3), 132.6 (d; ^{2}J(C,P) = 20.1 Hz, C_6), 131.6 (s; C_1), 129.7 (d; ^{3}J(C,P) = 1.0 Hz, C_2), 128.5 (d; ^{3}J(C,P) = 6.3 Hz, C_7), 128.5 (s; C_8).

^{31}P{^{1}H} NMR (162 MHz, CDCl$_3$): δ = −2.0 ppm.

IR (KBr): $\tilde{\nu}$ [cm^{-1}] = 3435 (br m), 3134 (w), 3080 (w), 3065 (m), 3046 (w), 2998 (w), 2363 (w), 2342 (w), 1941 (w), 1892 (w), 1822 (w), 1794 (w), 1583 (w), 1567 (m), 1548 (m), 1478 (m), 1434 (s), 1415 (s), 1395 (m), 1328 (w), 1307 (w), 1272 (w), 1246 (w), 1186 (s), 1145 (w), 1122 (w), 1093 (w), 1069 (w), 1039 (w), 1069 (w), 1039 (w), 1024 (w), 998 (w), 972 (w), 781 (s), 771 (s), 754 (s), 740 (s), 710 (m), 694 (s), 518 (s), 499 (m), 457 (w), 429 (m).

(3,3‘‘,5,5‘‘-Tetramethoxycarbonyl-1,1‘:3‘,1‘‘-terphen-2‘-yl)diorganophosphane (chalcogenides) (3)

The linker phosphane oxides **3a**, **3c**, and **3d** can be readily purified by column chromatography (SiO_2, DCM/MeOH = 9/1) and/or recrystallisation from ethanol, methanol, acetonitrile, or mixtures of the solvents mentioned. If present, the homocoupling product of the boronic acid, 3,3',5,5'-tetra(methoxycarbonyl)biphenyl, will tend to crystallise at 0 °C. However, the biphenylic by-product was mostly obtained only after extended periods of crystallisation exceeding two days or from follow-up crops, when the mother liquor was concentrated under reduced pressure and left to crystallise at low temperature again. Therefore, fractional crystallisation is relatively easy to achieve. In one case, partial transesterification was observed when ethanol was used during recrystallisation.

For the cross-coupling reactions involving the liquid dichloroaryls **2a** and **2c**, the following procedure proved to be useful: A volume of approximately 0.2 mL of the cross-coupling nucleophile is drawn into a syringe that is immediately weighed. After injection into a second Schlenk flask, the mass of reactant is determined *via* differential measurement of weight of the syringe. The remaining reaction components are calculated afterwards.

The retention times in HPLC for the homocoupling product (3,3‘,5,5‘-tetramethoxycarbonyl-1,1‘-biphenyl) and the protodeborylation product (1,3-dimethoxycarbonylbenzene) using program 1 are 25.76 min and 17.09 min, respectively.

(3,3‘‘,5,5‘‘-Tetramethoxycarbonyl-1,1‘:3‘,1‘‘-terphen-2‘-yl)dimethylphosphane oxide (**3a**)

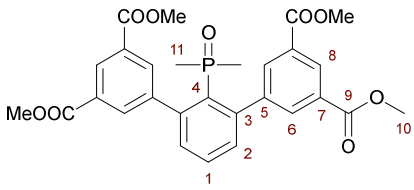

A two-neck Schlenk flask equipped with a reflux condenser, a stopcock and an efficient egg-shaped magnetic stirring bar was charged with a mixture of potassium phosphate (3.30 g, 15.5 mmol, 8 eq.), 3,5-(dimethoxycarbonyl)phenylboronic acid (1.84 g, 7.73 mmol, 4 eq.), *trans*-chloro(1-naphthyl)bis-(triphenylphosphine)nickel(II) (72 mg, 97 µmol, 5 %), and tricyclohexylphosphonium tetra-fluoroborate (53 mg, 0.14 mmol, 7.5 %). The apparatus was carefully evacuated and refilled with argon three times. A solution of (2,6-dichlorophenyl)dimethylphosphane (**2a**, 400 mg, 1.93 mmol) in DMF (20 mL) was added and the resulting orange suspension was heated to 105 °C for 18 h under magnetic stirring. The suspension turned dark-red during the reaction. The temperature was lowered to 80 °C and volatiles were removed *in vacuo*. The following work-up procedure was done at ambient conditions. The solid residue was distributed between chloroform (100 mL) and demineralised water (100 mL) in a separatory funnel. An aqueous solution of hydrogen peroxide (30 %, 2 mL) was added and the mixture was shaken well. After separation of the phases, the organic phase was isolated, and the aqueous phase was further extracted with chloroform (three times with 20 mL each). The combined organic phases were stirred over anhydrous sodium sulfate for five minutes and the resulting mixture subjected to filtration over cotton wool. The filter cake was washed with chloroform (15 mL) and the filtrate was evaporated to dryness using a rotary evaporator. The crude product was intensively dried *in vacuo* (10^{-3} mbar for three hours) to remove traces of DMF. Afterwards, the residue was filtered over a plug of Celite 545 (approximately 5 cm in length and 2 cm in diameter) using chloroform (80 mL). The solvent was reduced under reduced pressure, and the crude product was purified by column chromatography (SiO_2, DCM/MeOH = 9/1) to give an off-white solid

that was further purified by recrystallisation from methanol at 0 °C. 558 mg (1.04 mmol, 54 % based on **2a**) of a colourless crystalline solid were obtained. Single crystals of suitable quality for single crystal X-ray diffraction have been obtained by recrystallisation from ethanol at 0 °C.

R_f = 0.57 (DCM/MeOH = 9:1; detection *via* UV activity).

elemental analysis for $C_{28}H_{27}O_9P$ (percentage): calc. C (62.45), H (5.05), O (26.74), P (5.75); found C [62.74(2)], H [5.15(1)].

ESI-HRMS: *m/z* = calc. for $[C_{28}H_{27}O_9P + H]^+$: 539.1465; found: 539.1458.

HPLC (230 nm, program 1): retention time = 20.00 min.

^{1}H NMR (300 MHz, $CDCl_3$): δ [ppm] = 8.76 (t, 2 H; ^4J(H,H) = 1.6 Hz, H_8), 8.37 (d, 4 H; ^4J(H,H) = 1.6 Hz, H_6), 7.60 (td, 1 H; ^3J(H,H) = 7.7 Hz, ^5J(H,P) = 1.6 Hz, H_1), 7.38 (dd, 2 H; ^3J(H,H) = 7.7 Hz, ^4J(H,P) = 3.3 Hz, H_2), 3.98 (s, 12 H; H_{10}), 1.17 (d, 6 H; ^2J(H,P) = 12.8 Hz, H_{11}).

^{13}C{^{1}H} NMR (75 MHz, $CDCl_3$): δ [ppm] = 166.0 (s; C_9), 145.5 (d; ^3J(C,P) = 8.2 Hz, C_5), 143.4 (d; ^2J(C,P) = 3.9 Hz, C_3), 134.6 (s; C_6), 132.5 (d; ^1J(C,P) = 90.5 Hz, C_4), 131.7 (d; ^3J(C,P) = 9.1 Hz, C_2), 130.7 (s; C_1), 130.7 (s; C_7), 130.3 (s; C_8), 52.7 (s; C_{10}), 22.0 (d; ^1J(C,P) = 71.6 Hz, C_{11}).

^{31}P{^{1}H} NMR (162 MHz, $CDCl_3$): δ = 35.6 ppm.

IR (KBr): $\tilde{\nu}$ [cm^{-1}] = 3426 (br m), 3069 (w), 3008 (w), 2954 (m), 2913 (w), 2849 (w), 2361 (w), 2341 (w), 1845 (w), 1729 (s), 1637 (w), 1600 (w), 1567 (w), 1432 (s), 1335 (s), 1310 (m), 1292 (m), 1251 (br s), 1183 (s), 1137 (m), 1109 (w), 1077 (w), 1055 (w), 999 (m), 981 (m), 938 (m), 917 (m), 859 (m), 813 (w), 788 (w), 755 (s), 721 (w), 689 (w), 639 (w), 517 (w).

(3,3‘‘,5,5‘‘-Tetramethoxycarbonyl-1,1‘:3‘,1‘‘-terphen-2‘-yl)dimethylphosphane sulfide (**3b**)

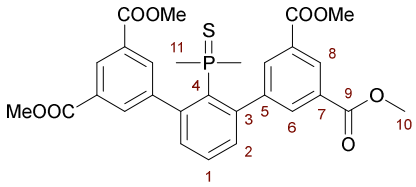

A J. Young ampoule charged with the tetramethyl ester of the phosphane oxide **3a** (363 mg, 674 µmol) was evacuated and flushed with argon three times. The colourless solid was suspended in toluene (20 mL) under magnetic stirring and the suspension added with triethylamine (3.80 mL, 2.77 g, 27.3 mmol, 41 eq.) and trichlorosilane (0.35 mL, 0.47 g, 3.5 mmol, 5.2 eq.). The ampoule was sealed, and the yellow-coloured suspension heated to 125 °C for 4 h. After cooling to room temperature, the reaction mixture was filtered over sintered glass of porosity G3 and the filter cake washed with additional toluene (three times with 20 mL each). Sulfur powder (173 mg, 675 µmol S_8[6]) was added and the mixture stirred at room temperature for 18 h. The following steps were conducted under ambient conditions. The solvent was removed in vacuo and the yellow solid subjected to column chromatography (SiO_2; eluate the excessive sulfur with cyclohexane first and the product afterwards using PE/acetone = 3/2) to yield 334 mg of a colourless solid **3b** (602 µmol, 89 %). Single crystals suitable for single crystal X-ray diffraction were obtained by recrystallisation of the compound from its solution in a solvent mixture of methanol and dichloromethane at 4 °C.

R_f = 0.67 (PE/acetone = 3/2; detection *via* UV activity).

[6] Further experiments showed that a slight excess based on ‘S’ instead of S_8 is sufficient. Heating the toluene solution to 90 °C overnight might be required.

HPLC (230 nm, program 1): retention time = 27.09 min.

ESI-HRMS: *m/z* = calc. for $[C_{28}H_{27}O_8PS + H]^+$: 555.1243; found: 555.1277.

^{1}H NMR (600 MHz, $CDCl_3$): δ [ppm] = 8.78 (t, 2 H; ^4J(H,H) = 1.6 Hz, H_8), 8.70 (d, 4 H; ^4J(H,H) = 1.6 Hz, H_6), 7.58 (td, 1 H; ^3J(H,H) = 7.7 Hz, ^5J(H,P) = 1.7 Hz, H_1), 7.35 (dd, 2 H; ^3J(H,H) = 7.7 Hz, ^4J(H,P) = 3.7 Hz, H_2), 3.99 (s, 12 H; H_{10}), 1.08 (d, 6 H; ^2J(H,P) = 12.3 Hz, H_{11}).

^{13}C{^{1}H} NMR (151 MHz, $CDCl_3$): δ [ppm] = 165.9 (s; C_9), 144.9 (d; ^3J(C,P) = 8.1 Hz, C_5), 142.6 (d; ^2J(C,P) = 4.1 Hz, C_3), 135.5 (s; C_6), 133.0 (d; ^1J(C,P) = 75.2 Hz, C_4), 132.2 (d; ^3J(C,P) = 8.9 Hz, C_2), 130.9 (s; C_7), 130.8 (s; C_8), 130.6 (d; ^5J(C,P) = 2.4 Hz, C_1), 52.7 (s; C_{10}), 26.1 (d; ^1J(C,P) = 58.5 Hz, C_{11}).

^{31}P NMR (243 MHz, $CDCl_3$): δ = 32.3 ppm.

IR (KBr): $\tilde{\nu}$ [cm^{-1}] = 3441 (br m), 3073 (w), 3026 (w), 3002 (w), 2953 (w), 2923 (w), 2850 (w), 2360 (w), 2341 (w), 1725 (s), 1634 (br w), 1602 (w), 1570 (w), 1430 (m), 1333 (m), 1307 (w), 1246 (s), 1194 (w), 1132 (w), 1106 (w), 1078 (w), 1052 (w), 1000 (w), 980 (w), 953 (w), 923 (w), 875 (w), 809 (w), 788 (w), 754 (m), 733 (w), 700 (w), 690 (w), 685 (w), 637 (w), 593 (w).

(3,3‘‘,5,5‘‘-Tetramethoxycarbonyl-1,1‘:3‘,1‘‘-terphen-2‘-yl)diethylphosphane oxide (**3c**)

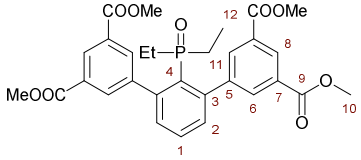

A two-neck Schlenk flask equipped with a reflux condenser, a stopcock and an efficient egg-shaped magnetic stirring bar was charged with a mixture of potassium phosphate (1.37 g, 6.45 mmol, 8 eq.), 3,5-(dimethoxycarbonyl)phenylboronic acid (766 mg, 3.22 mmol, 4 eq.), *trans*-chloro(1-naphthyl)bis(triphenylphosphine)nickel(II) (30 mg, 40 µmol, 5 %), and tricyclohexylphosphonium tetrafluoroborate (22 mg, 60 µmol, 7.5 %). The apparatus was carefully evacuated and refilled with argon three times. A solution of (2,6-dichlorophenyl)diethylphosphane (**2c**, 202 mg, 805 µmol) in DMF (10 mL) was added and the resulting yellow suspension was heated to 105 °C for 18 h under magnetic stirring. The temperature was lowered to 80 °C and volatiles were removed *in vacuo*. The following work-up procedure was done at ambient conditions. The solid residue was distributed between chloroform (50 mL) and demineralised water (50 mL) in a separatory funnel. After separation of the phases, the organic phase was isolated, and the aqueous phase was further extracted with chloroform (three times with 15 mL each). The combined organic phases were stirred over anhydrous sodium sulfate for five minutes and the resulting mixture subjected to filtration over cotton wool. The filter cake was washed with chloroform (15 mL) and the filtrate was evaporated to dryness using a rotary evaporator. Acetonitrile (10 mL) was added and aqueous hydrogen peroxide solution (30 %, 0.50 mL, 4.9 mmol, 6 eq.) was added under magnetic stirring. An exothermic reaction took place and the mixture was stirred for 10 minutes. The solvent was removed by rotary evaporation and the crude product was intensively dried *in vacuo* (10^{-3} mbar for three hours) to remove traces of DMF. Afterwards, the residue was filtered over a plug of Celite 545 (approximately 5 cm in length and 2 cm in diameter) using chloroform (80 mL). The solvent was reduced under reduced pressure and the crude product purified by recrystallisation from a solution of the crude product in an ethanol/acetonitrile mixture (approx. 5 mL, *v/v* = 1/1) at 0 °C to yield 352 mg (621 µmol, 77 %) of a colourless, crystalline solid. Single crystals suitable for X-ray structural analysis where obtained when a solution of **3c** in $CDCl_3$

(10 mg in 0.6 mL of solvent) was layered with cyclohexane (0.5 mL) in a snap-on lid vial. Crystals did not separate at the phase boundary, but by slow evaporation of the solvents after 7 days.

***R*$_f$** = 0.54 (DCM/MeOH = 9:1; detection *via* UV activity).

ESI-HRMS: *m/z* = calc. for $[C_{30}H_{32}O_9P + H]^+$: 567.1784; found: 567.1811.

HPLC (230 nm, program 1): retention time = 22.68 min.

^{1}H NMR (400 MHz, $CDCl_3$): δ [ppm] = 8.73 (t, 2 H; ^4J(H,H) = 1.6 Hz, H_8), 8.27 (d, 4 H; ^4J(H,H) = 1.6 Hz, H_6), 7.56 (td, 1 H; ^3J(H,H) = 7.6 Hz, ^5J(H,P) = 1.6 Hz, H_1), 7.32 (dd, 2 H; ^3J(H,H) = 7.6 Hz, ^4J(H,P) = 3.0 Hz, H_2), 3.97 (s, 12 H; H_{10}), 1.38 (dq, 4 H; ^2J(H,P) = 10.6 Hz, ^3J(H,H) = 7.6 Hz, H_{11}), 0.96 (dt, 6 H; ^3J(H,P) = 17.3 Hz, ^3J(H,H) = 7.6 Hz, H_{12}).

^{13}C{^{1}H} NMR (151 MHz, $CDCl_3$): δ [ppm] = 166.0 (s; C_9), 146.1 (d; ^3J(C,P) = 7.6 Hz, C_5), 143.6 (d; ^2J(C,P) = 3.0 Hz, C_3), 134.3 (s; C_6), 132.1 (d; ^3J(C,P) = 8.8 Hz, C_2), 130.5 (d; ^4J(C,P) = 2.4 Hz, C_1), 130.3 (s; C_7), 130.0 (s; C_8), 129.9 (d; ^1J(C,P) = 80.7 Hz, C_4), 52.5 (s; C_{10}), 25.3 (d; ^1J(C,P) = 68.1 Hz, C_{11}), 6.1 (d; ^2J(C,P) = 5.3 Hz, C_{12}).

^{31}P{^{1}H} NMR (162 MHz, $CDCl_3$): δ = 46.5 ppm.

IR (KBr): $\tilde{\nu}$ [cm^{-1}] = 3425 (br m), 2955 (w), 2362 (w), 1728 (s), 1602 (w), 1562 (w), 1433 (m), 1355 (m), 1249 (s), 1165 (w), 1135 (w), 1109 (w), 999 (w), 918 (w), 876 (w), 810 (w), 756 (m), 720 (w), 638 (w).

(3,3‘‘,5,5‘‘-Tetramethoxycarbonyl-1,1‘:3‘,1‘‘-terphen-2‘-yl)diphenylphosphane oxide (**3d**)

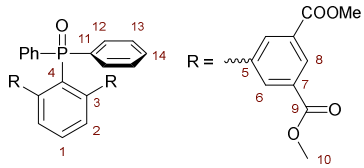

A two-neck Schlenk flask equipped with a reflux condenser, a stopcock and an efficient egg-shaped magnetic stirring bar was charged with a mixture of (2,6-dichlorophenyl)diphenylphosphane (**2d**, 535 mg, 1.62 mmol), potassium phosphate (2.72 g, 12.8 mmol, 8 eq.), 3,5-(dimethoxycarbonyl)phenylboronic acid (1.53 g, 6.43 mmol, 4 eq.), *trans*-chloro(1-naphthyl)bis(triphenylphosphine)nickel(II) (60 mg, 81 µmol, 5 %), and tricyclohexylphosphonium tetrafluoroborate (44 mg, 0.12 mmol, 7.5 %). The apparatus was carefully evacuated and refilled with argon three times. DMF (20 mL) and degassed demineralised water (2 mL) were added and the resulting yellow suspension was heated to 105 °C for 18 h under magnetic stirring. The temperature was lowered to 80 °C and volatiles were removed *in vacuo*. The following work-up procedure was done at ambient conditions. The solid residue was distributed between chloroform (50 mL) and demineralised water (50 mL) in a separatory funnel. After separation of the phases, the organic phase was isolated, and the aqueous phase was further extracted with chloroform (three times with 15 mL each). The combined organic phases were stirred over anhydrous sodium sulfate for five minutes and the resulting mixture subjected to filtration over cotton wool. The filter cake was washed with chloroform (15 mL) and the filtrate was evaporated to dryness using a rotary evaporator. The residue was taken up in acetonitrile (10 mL) and aqueous hydrogen peroxide solution (30 %, 0.50 mL, 4.9 mmol, 9 eq.) was added under magnetic stirring. An exothermic reaction took place and the mixture was stirred for 10 minutes. The solvent was removed by rotary evaporation and the crude product was intensively dried *in vacuo* (10^{-3} mbar for three hours) to remove traces of DMF. Afterwards, the residue was filtered over a plug of Celite 545 (approximately 5 cm in length and 2 cm in diameter) using chloroform

(80 mL). The solvent was reduced under reduced pressure and the crude product purified by column chromatography (SiO_2, DCM/MeOH = 9/1) to yield a yellowish solid.

Further purification was achieved by recrystallisation from ethanol at 0 °C. 795 mg (1.20 mmol, 74 %) of a colourless, crystalline solid was obtained. Single crystals of monoclinic symmetry could be structurally elucidated by single crystal X-ray determination. We prepared and characterised a series of transition metal complexes using the P(III) derivative of **3d** (not reported herein); When we reacted the phosphane with $[Rh(cod)Cl]_2$ (cod: 1,5-cyclooctadiene) in an 1:2 molar ratio in $CDCl_3$, we observed the formation of a Rh(cod)Cl adduct as proven by ^1H and $^{31}P\{^1H\}$ NMR spectroscopy. Gas phase diffusion of *n*-hexane into the $CDCl_3$ solution of the product complex yielded single crystals of the complex as well as single crystals of the oxidized phosphane oxide **3d** in triclinic symmetry, both of which were characterised *via* single crystal X-ray diffraction. Slow evaporation of a solution of **3d** in chloroform gave the solvomorph **3d** · 2 $CHCl_3$ that could also be structurally elucidated by X-ray diffraction.

R_f = 0.61 (DCM/MeOH = 9:1; detection *via* UV activity).

HPLC (230 nm, program 1): retention time = 25.86 min.

ESI-HRMS: *m/z* = calc. for $[C_{38}H_{31}O_9P + H]^+$: 663.1784; found: 663.1781.

^{1}H NMR (400 MHz, $CDCl_3$): δ [ppm] = 8.35 (t, 2 H; ^4J(H,H) = 1.6 Hz, H_8), 8.10 (d, 4 H; ^4J(H,H) = 1.6 Hz, H_6), 7.65 (td, 1 H; ^3J(H,H) = 7.7 Hz, ^5J(H,P) = 1.5 Hz, H_1), 7.37 (dd, 2 H; ^3J(H,H) = 7.7 Hz, ^4J(H,P) = 3.6 Hz, H_2), 7.25—7.17 (m, 2 H; H_{12}), 7.02—6.88 (m, 6 H; H_{13} and H_{14}), 3.94 (s, 12 H; H_{10}).

^{13}C{^{1}H} NMR (100 MHz, $CDCl_3$): δ [ppm] = 165.8 (s; C_9), 147.5 (d; ^3J(C,P) = 9.0 Hz, C_5), 141.8 (d; ^2J(C,P) = 4.8 Hz, C_3), 135.5 (s; C_6), 135.4 (d; ^1J(C,P) = 103.6 Hz, C_{11}), 131.5 (d; ^1J(C,P) = 100.9 Hz, C_4), 131.3 (d; ^2J(C,P) = 9.3 Hz, C_{12}), 131.3 (s; C_{14}), 130.2 (d; ^3J(C,P) = 9.0 Hz, C_2), 130.0 (d; ^4J(C,P) = 2.8 Hz, C_1), 129.9 (s; C_7), 129.6 (s; C_8), 127.9 (d; ^3J(C,P) = 12.0 Hz, C_{13}), 52.4 (s; C_{10}).

^{31}P{^{1}H} NMR (162 MHz, $CDCl_3$): δ = 21.2 ppm.

IR (KBr): $\tilde{\nu}$ [cm^{-1}] = 3441 (br m), 3070 (w), 3051 (w), 3000 (w), 2951 (w), 2846 (w), 2361 (w), 1730 (s), 1602 (w), 1479 (w), 1435 (m), 1348 (w), 1333 (m), 1249 (s), 1194 (w), 1133 (w), 1107 (w), 1079 (w), 1004 (m), 911 (w), 874 (w), 815 (w), 788 (w), 756 (m), 744 (m), 719 (w), 696 (w), 639 (w), 507 (w).

(3,3‘‘,5,5‘‘-Tetracarboxy-1,1‘:3‘,1‘‘-terphen-2‘-yl)diorganophosphane (chalcogenides) (4)

The saponification of ester functional groups was conducted at ambient conditions and was carried out as follows: The tetramethyl ester of the dimethylarylphosphane oxide (**3**) was suspended in a mixture of sodium or potassium hydroxide solution (2.0 mol/L, approximately 10 mL per 200 mg of **3**) and THF (the same volume as for the aqueous alkali hydroxide solutions). The biphasic mixture was emulsified by efficient magnetic stirring and stirred for 18 h at room temperature. Afterwards, THF was removed by rotary evaporation and the clear and colourless aqueous phase was acidified with hydrochloric acid (6.0 mol/L) until pH = 1 was reached. The mixture containing colourless precipitate was cooled to 0 °C for at least three hours to complete precipitation and increase filterability. The solid was isolated by filtration over fritted glass of porosity G4. The filter cake was repeatedly washed with small volumes of

cold demineralised water and dried at 60 °C for 18 h. In some cases of ester saponification reactions, the linker obtained was not entirely soluble in DMSO(-d_6). This is attributed to the presence of residual alkali chloride salt as evidenced from the observation of expectable reflections in powder X-ray diffraction experiments. In this case, the crude was suspended in a small volume of demineralised water and magnetically stirred for 18 h and subsequently subjected to filtration and drying as described above.

(3,3'',5,5''-Tetracarboxy-1,1':3',1''-terphen-2'-yl)dimethylphosphane oxide (**4a**)

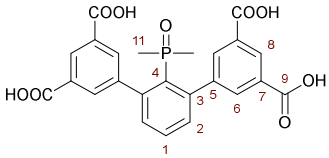

The reaction was done using **3a** (240 mg, 446 µmol) according to the general procedure described above. 180 mg (373 µmol, 84 %) of a colourless solid was obtained.

ESI-HRMS: *m/z* = calc. for $[C_{24}H_{19}O_9P + H]^+$: 483.0839; found: 483.0843.

HPLC (230 nm, program 3): retention time = 7.57 min.

^{1}H NMR (400 MHz, DMSO-d_6): δ [ppm] = 13.40 (s, 4 H; COO**H**), 8.56 (t, 2 H; ^4J(H,H) = 1.6 Hz, H_8), 8.34 (d, 4 H; ^4J(H,H) = 1.6 Hz, H_6), 7.73 (td, 1 H; ^3J(H,H) = 7.7 Hz, ^5J(H,P) = 1.3 Hz, H_1), 7.50 (dd, 2 H; ^3J(H,H) = 7.6 Hz, ^4J(H,P) = 3.2 Hz, H_2), 0.99 (d, 6 H; ^2J(H,P) = 12.8 Hz, H_{11}).

^{13}C{^{1}H} NMR (100 MHz, DMSO-d_6): δ [ppm] = 166.9 (s; C_9), 145.5 (d; ^3J(C,P) = 8.1 Hz, C_5), 143.7 (d; ^2J(C,P) = 3.8 Hz, C_3), 134.8 (s; C_6), 133.2 (d; ^1J(C,P) = 90.3 Hz, C_4), 131.8 (s; C_7), 131.7 (s; C_2), 131.3 (s; C_1), 129.8 (s; C_8), 21.5 (d; ^1J(C,P) = 71.5 Hz, C_{11}).

^{31}P{^{1}H} NMR (162 MHz, DMSO-d_6): δ = 35.6 ppm.

IR (KBr): $\tilde{\nu}$ [cm^{-1}] = 3381 (br m), 3071 (br m), 2918 (br m), 2593 (br m), 1861 (w), 1747 (s), 1601 (m), 1562 (w), 1443 (w), 1419 (w), 1397 (w), 1328 (w), 1276 (s), 1230 (m), 1209 (m), 1184 (m), 1134 (m), 1114 (s), 1051 (w), 936 (m), 926 (m), 898 (w), 865 (w), 817 (w), 758 (s), 731 (m), 691 (m), 680 (w), 632 (w), 517 (br w), 460 (w), 445 (w), 430 (w).

(3,3'',5,5''-Tetracarboxy-1,1':3',1''-terphen-2'-yl)dimethylphosphane sulfide (**4b**)

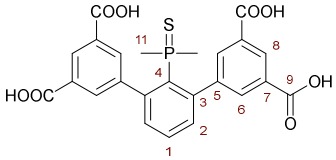

The tetramethyl ester **3b** (221 mg, 399 µmol) was treated according to the general procedure. 192 mg (385 µmol, 96 %) of a colourless solid were obtained. The crude product typically contains ~ 5 % of phosphine oxide **4a**, see also the discussion in the section concerned with the synthesis and characterisation of **UHM-61**.

ESI-HRMS: *m/z* = calc. for $[C_{24}H_{19}O_8PS + H]^+$: 499.0617; found: 499.0621.

HPLC (230 nm, program 3): retention time = 7.89 min.

^{1}H NMR (400 MHz, DMSO-d_6): δ [ppm] = 13.17 (s, 4 H; COO**H**), 8.56 (t, 2 H; ^4J(H,H) = 1.6 Hz, H_8), 8.51 (d, 4 H; ^4J(H,H) = 1.6 Hz, H_6), 7.69 (td, 1 H; ^3J(H,H) = 7.7 Hz, ^5J(H,P) = 1.7 Hz, H_1), 7.43 (dd, 2 H; ^3J(H,H) = 7.7 Hz, ^4J(H,P) = 3.6 Hz, H_2), 1.02 (d, 6 H; ^2J(H,P) = 12.8 Hz, H_{11}).

^{13}C{^{1}H} NMR (100 MHz, DMSO-d_6): δ [ppm] = 166.2 (s; C_9), 144.2 (d; ^3J(C,P) = 8.1 Hz, C_5), 142.2 (d; ^2J(C,P) = 4.0 Hz, C_3), 134.8 (s; C_6), 132.7 (d; ^1J(C,P) = 74.6 Hz, C_4), 131.8 (d; ^3J(C,P) = 8.7 Hz, C_2), 131.2 (s; C_7), 130.6 (s; C_1), 129.7 (s; C_8), 24.8 (d; ^1J(C,P) = 58.1 Hz, C_{11}).

^{31}P{^{1}H} NMR (162 MHz, DMSO-d_6): δ = 33.3 ppm.

IR (KBr): $\tilde{\nu}$ [cm^{-1}] = 3418 (br m), 2362 (w), 1724 (s), 1699 (s), 1601 (m), 1566 (w), 1440 (w), 1399 (w), 1309 (w), 1277 (s), 1247 (s), 1225 (s), 1145 (w), 1109 (w), 1051 (w), 942 (m), 918 (m), 864 (w), 810 (w), 760 (w), 737 (w), 686 (m), 635 (w), 585 (w)

(3,3'',5,5''-Tetracarboxy-1,1':3',1''-terphen-2'-yl)diethylphosphane oxide (**4c**)

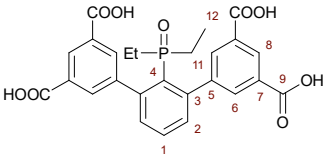

3c (269 mg, 475 µmol) was subjected to saponification correspondent to the procedure described above. 221 mg (433 µmol, 91 %) of a colourless solid was obtained.

HPLC (230 nm, program 3): retention time = 7.33 min.

ESI-HRMS: *m/z* = calc. for $[C_{26}H_{23}O_9P + H]^+$: 511.1158; found: 511.1161.

^{1}H NMR (600 MHz, DMSO-d$_6$): δ [ppm] = 13.33 (s, 4 H; COO**H**), 8.49 (t, 2 H; ^4J(H,H) = 1.6 Hz, H_8), 8.18 (d, 4 H; ^4J(H,H) = 1.6 Hz, H_6), 7.68 (td, 1 H; ^3J(H,H) = 7.6 Hz, ^5J(H,P) = 1.4 Hz, H_1), 7.43 (dd, 2 H; ^3J(H,H) = 7.6 Hz, ^4J(H,P) = 2.9 Hz, H_2), 1.43—1.14 (m, 4 H; H_{11}), 0.74 (dt, 6 H; ^3J(H,P) = 16.9 Hz, ^3J(H,H) = 7.5 Hz, H_{12}).

^{13}C{^{1}H} NMR (151 MHz, DMSO-d$_6$): δ [ppm] = 166.4 (s; C_9), 145.6 (d; ^3J(C,P) = 7.3 Hz, C_5), 143.3 (d; ^2J(C,P) = 3.2 Hz, C_3), 133.6 (s; C_6), 131.5 (d; ^3J(C,P) = 8.6 Hz, C_2), 130.7 (s; C_7), 130.7 (s; C_1), 129.5 (d; ^1J(C,P) = 80.3 Hz, C_4), 129.0 (s; C_8), 24.0 (d; ^1J(C,P) = 68.1 Hz, C_{11}), 5.6 (d; ^2J(C,P) = 5.3 Hz, C_{12}).

^{31}P{^{1}H} NMR (243 MHz, DMSO-d$_6$): δ = 45.7 ppm.

IR (KBr): $\tilde{\nu}$ [cm^{-1}] = 3405 (br s), 2983 (m), 2601 (br m), 1713 (s), 1601 (m), 1561 (w), 1446 (w), 1401 (w), 1326 (w), 1278 (s), 1250 (s), 1218 (s), 1147 (m), 1131 (m), 1109 (s), 1047 (w), 1035 (w), 922 (w), 814 (w), 758 (m), 699 (w), 674 (w), 633 (w), 524 (w), 499 (w), 453 (w).

(3,3'',5,5''-Tetracarboxy-1,1':3',1''-terphen-2'-yl)diphenylphosphane oxide (**4d**)

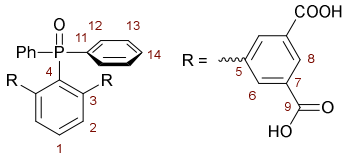

The saponification of **3d** (114 mg, 172 µmol) according to the procedure described above yielded 102 mg (168 µmol, 98 %) of a colourless solid.

ESI-HRMS: *m/z* = calc. for $[C_{34}H_{23}O_9P + H]^+$: 607.1158; found: 607.1155.

HPLC: 230 nm, program 2: retention time = 18.57 min. program 3: retention time = 7.19 min.

^{1}H NMR (400 MHz, DMSO-d$_6$): δ [ppm] = 13.18 (s, 4 H; COO**H**), 8.15 (t, 2 H; ^4J(H,H) = 1.6 Hz, H_8), 8.02 (d, 4 H; ^4J(H,H) = 1.7 Hz, H_6), 7.82 (t, 1 H; ^3J(H,H) = 7.6 Hz, H_1), 7.52 (dd, 2 H; ^3J(H,H) = 7.7 Hz, ^4J(H,P) = 3.6 Hz, H_2), 7.26—7.14 (m, 4 H; H_{12}), 7.06—6.90 (m, 6 H; H_{13} and H_{14}).

^{13}C{^{1}H} NMR (100 MHz, DMSO-d$_6$): δ [ppm] = 166.1 (s; C_9), 147.1 (d; ^3J(C,P) = 8.8 Hz, C_5), 141.5 (d; ^2J(C,P) = 5.0 Hz, C_3), 135.6 (d; ^1J(C,P) = 102.8 Hz, C_{11}), 134.8 (s; C_6), 132.0 (s; C_{14}), 131.2 (d; ^2J(C,P) = 9.0 Hz, C_{12}), 130.5 (s; C_7), 129.7 (d; ^3J(C,P) = 8.5 Hz, C_2), 129.7 (d; ^4J(C,P) = 2.8 Hz, C_1), 128.8 (s; C_8), 127.6 (d; ^3J(C,P) = 11.8 Hz, C_{13}).[7]

[7] C_4 with an expected ^1J(C,P) coupling constant of approximately 100 Hz could not be detected. We assume that the resonance at 130.1 ppm is the lower-ppm part belonging to the expected doublet. In this case, the second part at a 100 Hz higher frequency is overlapped by the anti-phase doublet of C_{12}.

$^{31}P\{^{1}H\}$ NMR (162 MHz, DMSO-d_6): δ = 19.9 ppm.

IR (KBr): $\tilde{\nu}$ [cm^{-1}] = 3449 (br m), 2362 (w), 1704 (s), 1603 (m), 1439 (m), 1414 (m), 1267 (m), 1240 (m), 1176 (m), 1110 (m), 999 (w), 918 (), 814 (w), 759 (w), 719 (w), 700 (w), 686 (w), 674 (w), 635 (w), 543 (m), 527 (w).

SYNTHESIS AND CHARACTERISATION OF METAL-ORGANIC FRAMEWORKS

MOF samples that have been isolated *via* separation from the reaction mixture, washed with a volume of fresh solvent, and dried under mild conditions are denoted as 'as-synthesised'. The individual procedures for removal of guest molecules differ slightly for the materials described herein. In each case, sequential solvent exchange steps gave materials that were pre-dried in a stream of inert gas and treated in vacuum (10^{-3} mbar) at 60 °C for one hour to give materials labelled 'activated'. Before doing physisorption experiments, the samples were finally treated at an elevated temperature for 24 h at 10^{-2} mbar. As-synthesised samples of the Cu(II)-based MOFs were light blue, while those materials solvent-exchanged for methanol, THF, or dichloromethane were dark blue in appearance. During the final thermal activation *in vacuo*, we noticed a colour change to purple.

The linker identity of the MOFs described herein was verified as follows. A sample (typically about 30 mg) of the respective MOF was suspended in a small volume of hydrochloric acid (2 mol L^{-1}) and the mixture treated with ultrasonic irradiation for five minutes. The colourless solid was isolated *via* filtration, washed with demineralised water, and dried at 60 °C for 18 h.

UHM-60

IR (KBr): $\tilde{\nu}$ [cm^{-1}] = 3423 (br m), 2934 (m), 2813 (w), 2490 (br w), 1717 (w), 1629 (s), 1509 (w), 1438 (s), 1398 (s), 1371 (s), 1306 (w), 1257 (w), 1144 (w), 1108 (m), 1084 (m), 1056 (m), 1024 (w), 937 (w), 865 (w), 777 (m), 750 (w), 729 (m), 694 (w), 664 (w), 644 (w), 595 (w), 488 (w).

The material was prepared for physisorption measurements as follows: the solid was suspended in dry methanol (10 mL) and the resulting mixture left standing for 4 d. The supernatant liquor was removed *via* syringe and dry dichloromethane (10 mL) was added and again removed after one day. The dichloromethane exchange was repeated one time. After the final removal of the solvent, the solid was dried at 60 °C *in vacuo* (10^{-3} mbar) for three hours to give samples further denoted as 'activated'. Finally, the solid was treated at 50 °C for 18 h in vacuo. Nitrogen physisorption data is shown in Figure S25. A specific BET surface area of S_{BET} = 1939 m^2 g^{-1} and a total pore volume of 0.89 cm^3 g^{-1} were derived.

Indexing of the reflections obtained from the as-synthesised sample with X-Cell gave possible cubic extinction classes *P*23 (a = 25.93 Å) and $F\bar{4}3c$ (a = 51.86 Å).[8] A comparison of the powder X-ray diffractograms of as-synthesised **UHM-60** and **UHM-25**[33] (space group *P*432, a = 28.943(3) Å, extinction class *P*23) made us hypothesise isostructurality of the two compounds mentioned. *In silico* substitution of the **UHM-25** linker molecule by the linker molecule used in the synthesis of **UHM-60** gave a structural model. Modelling experiments with the 2'-H-substituted *m*-terphenyl diisophthalate linker molecule on **ucp**, **zhc**, and **zmj** topology

[8] The extinction class *P*23 includes space groups *P*23, $Pm\bar{3}$, P432, $P\bar{4}3m$, $Pm\bar{3}m$, the extinction class $F\bar{4}3c$ includes space groups $F\bar{4}3c$ and $Fm\bar{3}c$.[21]

representative materials with optimization of the metric during UFF geometry optimization gave $a = b = c = 25.6$ Å, $\alpha = \beta = \gamma = 90°$ (**ucp**), $a = b = 36.2$ Å, $c = 25.8$ Å, $\alpha = \beta = \gamma = 90°$ (**zhc**), and $a = b = 25.9$ Å, $c = 27.5$ Å, $\alpha = \beta = \gamma = 90°$ (**zmj**). The expected cubic symmetry for a **ucp**-type material was confirmed by powder X-ray diffraction, the expected tetragonal symmetries for a **zhc**- and **zmj**-type materials disproved.

The calculated powder X-ray diffractogram of as-synthesised **UHM-60** and the calculated powder X-ray diffractogram from the homology modelling approach showed good agreement (see Figure S6). Thermal analyses were done on as-synthesised material and activated material (see Figure S8). The residue was characterised *via* powder X-ray diffractometry and identified as $Cu_4O(PO_4)_2$ (see Figure S7). The retention of integrity of the linker molecule was verified by acidic digestion of an **UHM-60** sample and $^{31}P\{^1H\}$ as well as ^1H NMR spectroscopy on the reisolated linker molecule (see Figure S9).

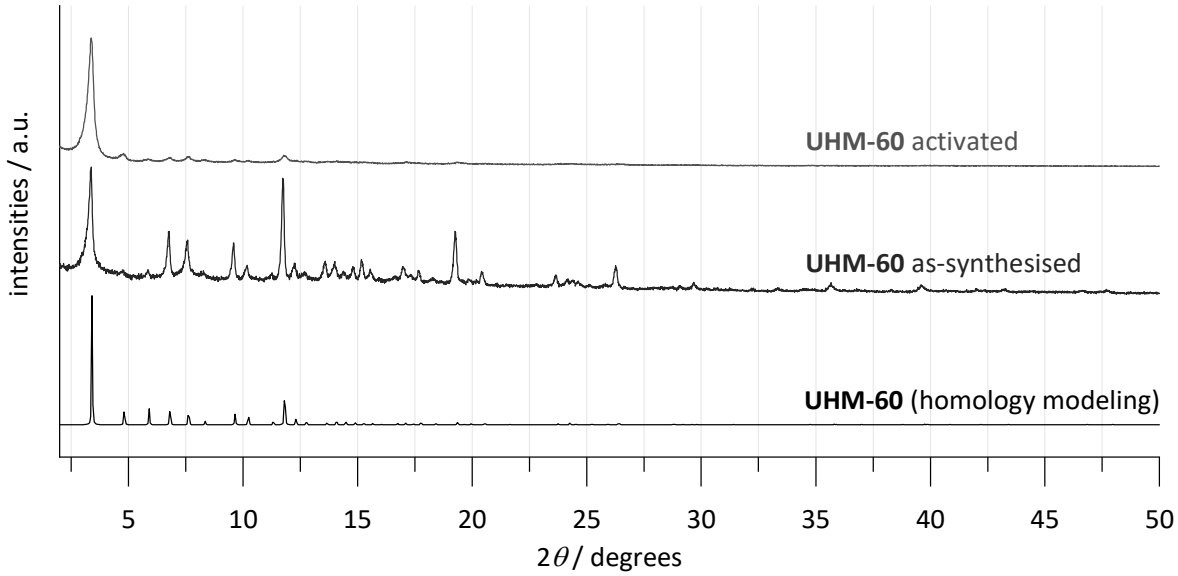

Figure S6: Powder X-ray diffractograms of (from bottom to top) **UHM-60** (calculated from homology modelling), **UHM-60** as-synthesised, and **UHM-60** activated.

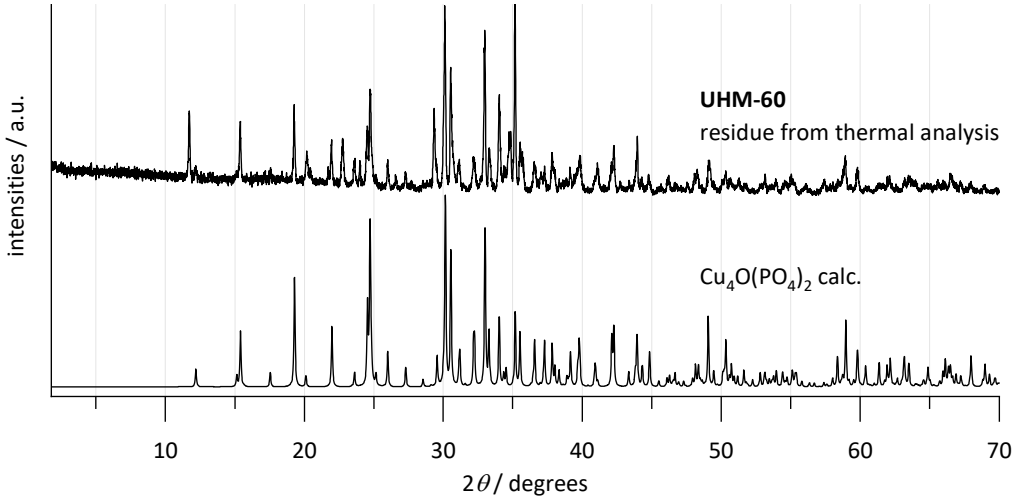

Figure S7: Comparison of the powder X-ray diffractograms of the residue from the thermal analysis of **UHM-60** (upper) and the calculated diffractogram of $Cu_4O(PO_4)_2$[34] (lower).

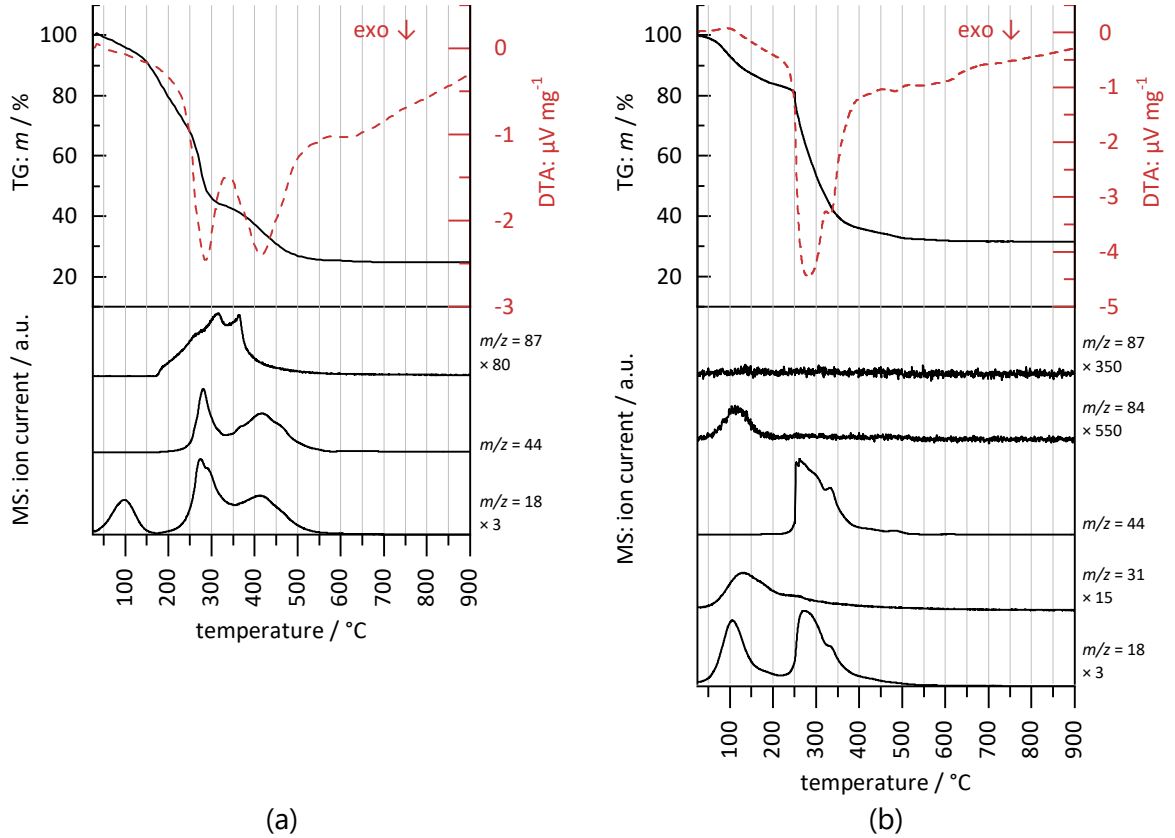

Figure S8: TG-DTA/MS data for (a) **UHM-60** as-synthesised and (b) **UHM-60** activated according to the procedure described. The *m/z* traces possibly correspond to H_2O (18), MeOH (31), CO_2 (44), CH_2Cl_2 (84), and DMA (87).

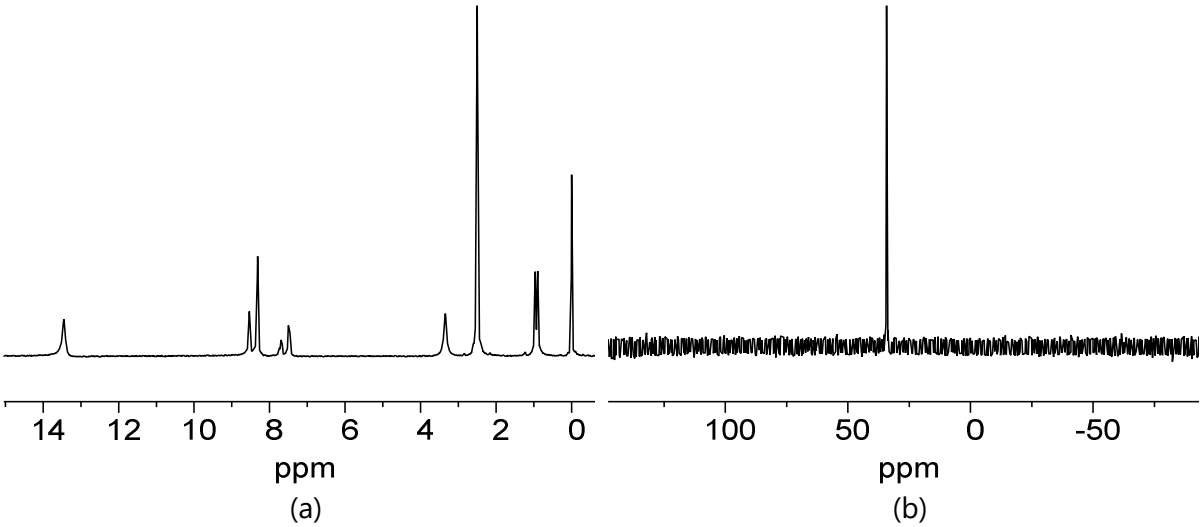

Figure S9: (a) ^{1}H NMR and (b) $^{31}P\{^{1}H\}$ NMR spectra of reisolated linker molecule from **UHM-60** in DMSO-d_6. No decomposition products of the linker molecule were identified.

UHM-61

IR (KBr): $\tilde{\nu}$ [cm^{-1}] = 3433 (br s), 2427 (w), 1703 (w), 1618 (m), 1563 (m), 1435 (m), 1384 (s), 1308 (w), 1139 (w), 1113 (w), 1055 (w), 1021 (w), 937 (w), 864 (w), 840 (w), 777 (w), 749 (w), 725 (w), 694 (w), 694 (w), 663 (w), 642 (w), 482 (w).

For the purpose of checking the linker identity, a **UHM-61** sample was subjected to acidic digestion. The reisolated linker molecule mixture was characterised *via* ^{1}H and $^{31}P\{^{1}H\}$ NMR spectroscopy, see Figure S10. We observed the oxidation of the phosphane sulfide linker

molecule to the corresponding phosphane oxide to an extent of 39 % and 34 % as estimated from deconvolution of ^{1}H and $^{31}P\{^{1}H\}$ NMR spectra, respectively. One of the referees recommended to re-evaluate the IR spectra of the P=O and P=S-based linker molecules **4a** and **4b**, respectively, as well as those of **UHM-60** and **UHM-61** in order to clarify whether oxidation might take place during the acidic digestion of **UHM-61** rather than during the solvothermal synthesis. Figure S11 shows the relevant IR spectra as well as the wavenumber regions where P=O and P=S valence vibrations are expected according to Chittenden and Thomas.[35,36] We were not able to unambiguously assign vibrational bands that are both present within the IR spectrum of the linker and the corresponding MOF. Thus, we were not able to verify the presence (or absence) of the P=O functional group within as-synthesised **UHM-61** by IR spectroscopy.

However, we would like to point out that both the conditions during solvothermal synthesis of **UHM-61** as well those employed in the digestion of the MOF possibly involve oxidation of the thiophosphoryl functional group, while we consider the former to be decisive for the noteworthy degree of oxidation. A typical saponification of the tetramethyl ester **3b** yielded the tetracarboxylate of the phosphine sulfide **4b** with a small contamination by the phosphine oxide **4a**, typically ~ 5 %. The saponification is conducted in a rapidly stirred biphasic mixture of aqueous sodium (potassium) hydroxide solution (2 M) and THF at room temperature for 18 h. After removal of THF, the tetracarboxylic acids are precipitated *via* addition of hydrochloric acid (6 M) over circa one minute until pH = 1 is reached, isolated *via* filtration, washed with water, and dried at 60 °C for 18 h. Possible reasons for oxidation can be the prolonged exposure to aqueous alkali base, the brief exposure to hydrochloric acid, the drying period at 60 °C – or a combination of the aforementioned. The digestion of **UHM-61** is achieved in hydrochloric acid (2 M) over circa one minute. The precipitated tetracarboxylic acids are then further treated as described before. The linker molecule composition of digested **UHM-61** was shown to be approximately 2:1 between **4b** and **4a**. Given that the conditions of MOF digestion are less forcing than those employed in the saponification of **3b**, we conclude that the conditions including prolonged heating in non-degassed DMF in the presence of possibly catalytically active Cu(II) during the synthesis of the MOF are more likely to involve oxidation of the thiophosphoryl functional group.

Indexation using the X-Cell routine gave a cubic extinction class *P*23 with a = 25.96. **UHM-61** was found to be isostructural to **UHM-60** as can be seen from comparison of the powder X-ray diffractograms shown in Figure S12. **UHM-61** was shown to exhibit permanent porosity. Characteristic reflections are preserved in the activated state. The nitrogen physisorption isotherm is shown in Figure S25, argon physisorption data is shown in Figure S26. Specific BET surface areas of $S_{BET}(N_2)$ = 1930 $m^2\ g^{-1}$ and $S_{BET}(Ar)$ = 1772 $m^2\ g^{-1}$, respectively, were derived. Figure S13 shows the TG-DTA/MS data for both as-synthesised **UHM-61** as well as activated material. Figure S14 shows SEM images of **UHM-61**. The cubic symmetry of the material is reflected by the observed morphology of cubes with an edge length of approximately 25 µm.

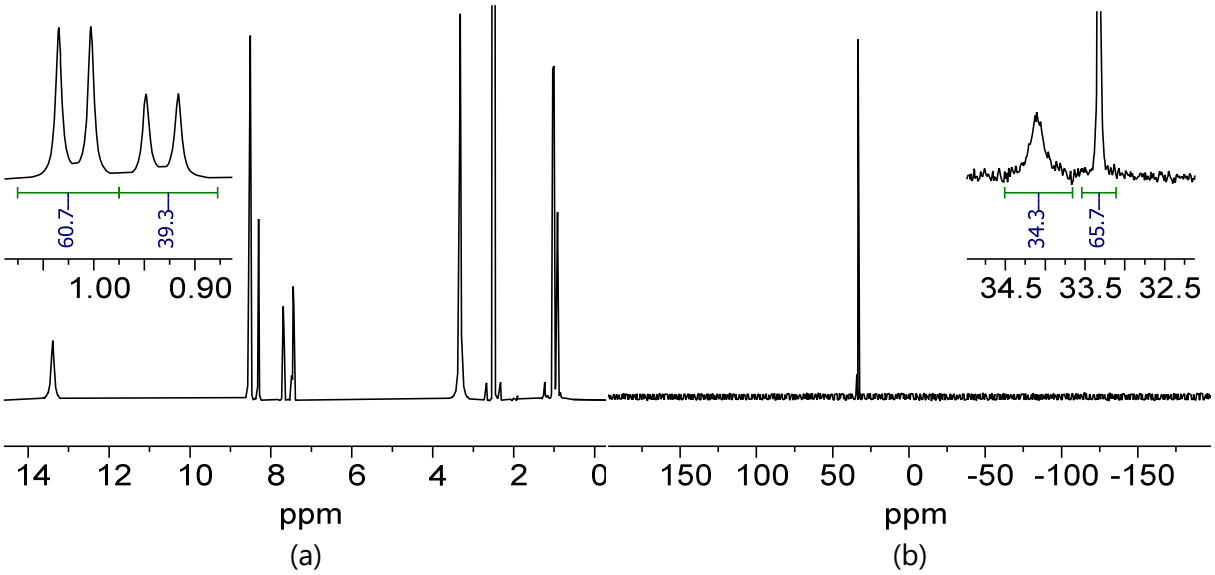

Figure S10: (a) ^{1}H and (b) $^{31}P\{^{1}H\}$ NMR spectra of reisolated linker molecule from **UHM-61** in DMSO-d_6. Deconvolution of the P(=E)$\underline{Me}_2$ (E = O, S) ^{1}H resonances as well of the ^{31}P resonances gave a portion of 61 % and 66 % remaining phosphane sulfide from ^{1}H and $^{31}P\{^{1}H\}$ NMR data, respectively.

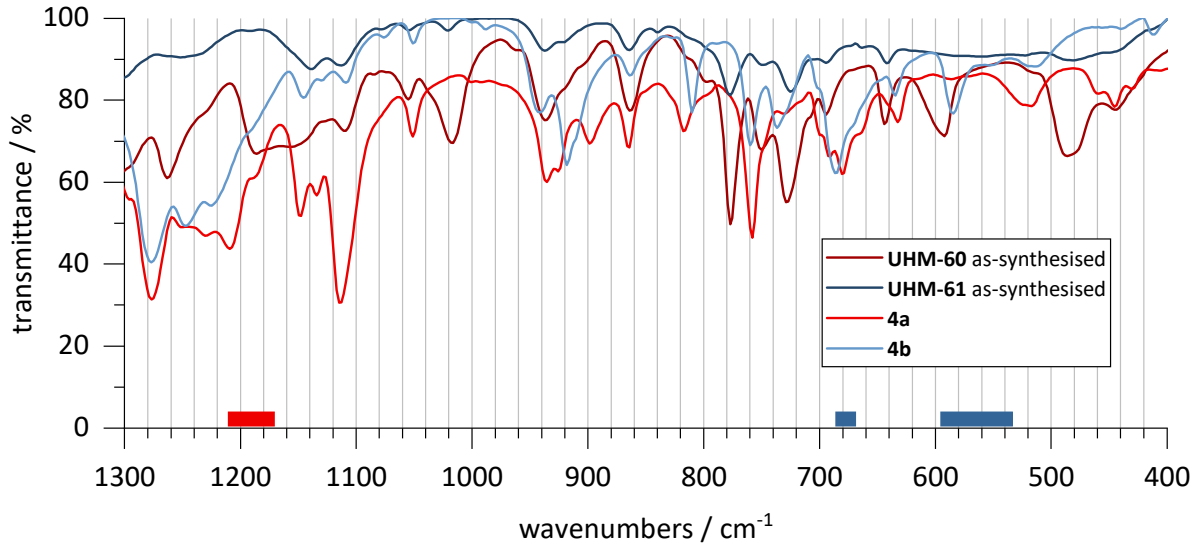

Figure S11: IR spectra (KBr) of **UHM-60** as-synthesised (dark red) and **UHM-61** as-synthesised (dark blue) as well as the linker molecules **4a** (red) and **4b** (blue) the respective MOFs were constructed from between 400 cm^{-1} and 1300 cm^{-1}. Coloured bars indicate the wavenumber ranges P=O (red) or P=S (blue) valence vibrations are expected.[35,36] There is no clear indication for phosphoryl or thiophosphoryl bands that can be assigned beyond doubt for both the linker molecule and the derived MOF.

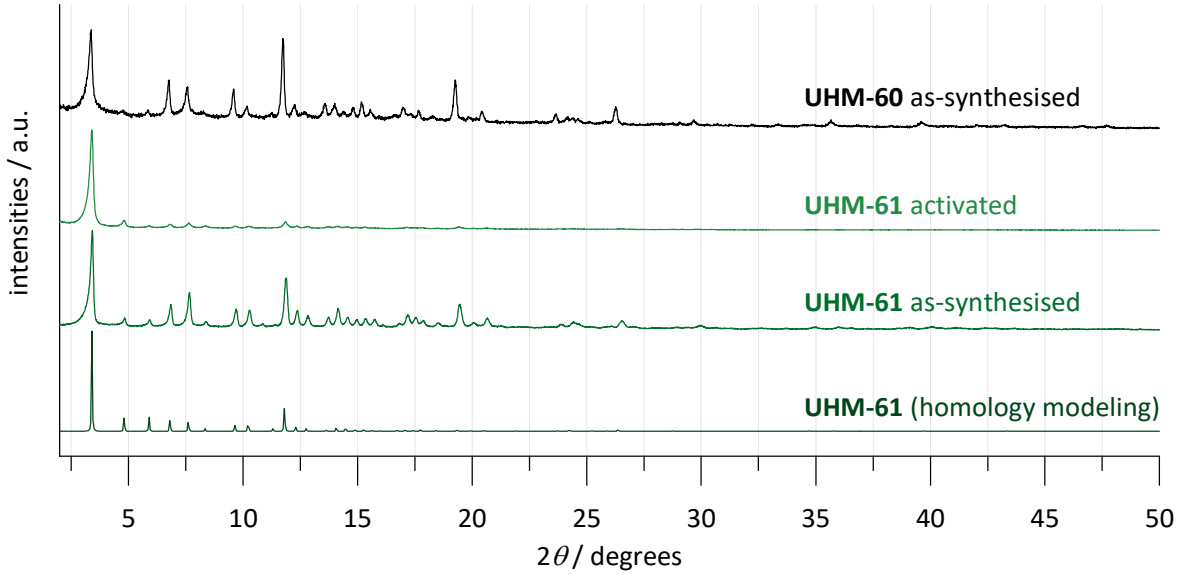

Figure S12: Powder X-ray diffractograms of (from bottom to top) **UHM-61** (calculated from homology modelling), **UHM-61** as-synthesised, **UHM-61** activated, and **UHM-60** as-synthesised for comparison.

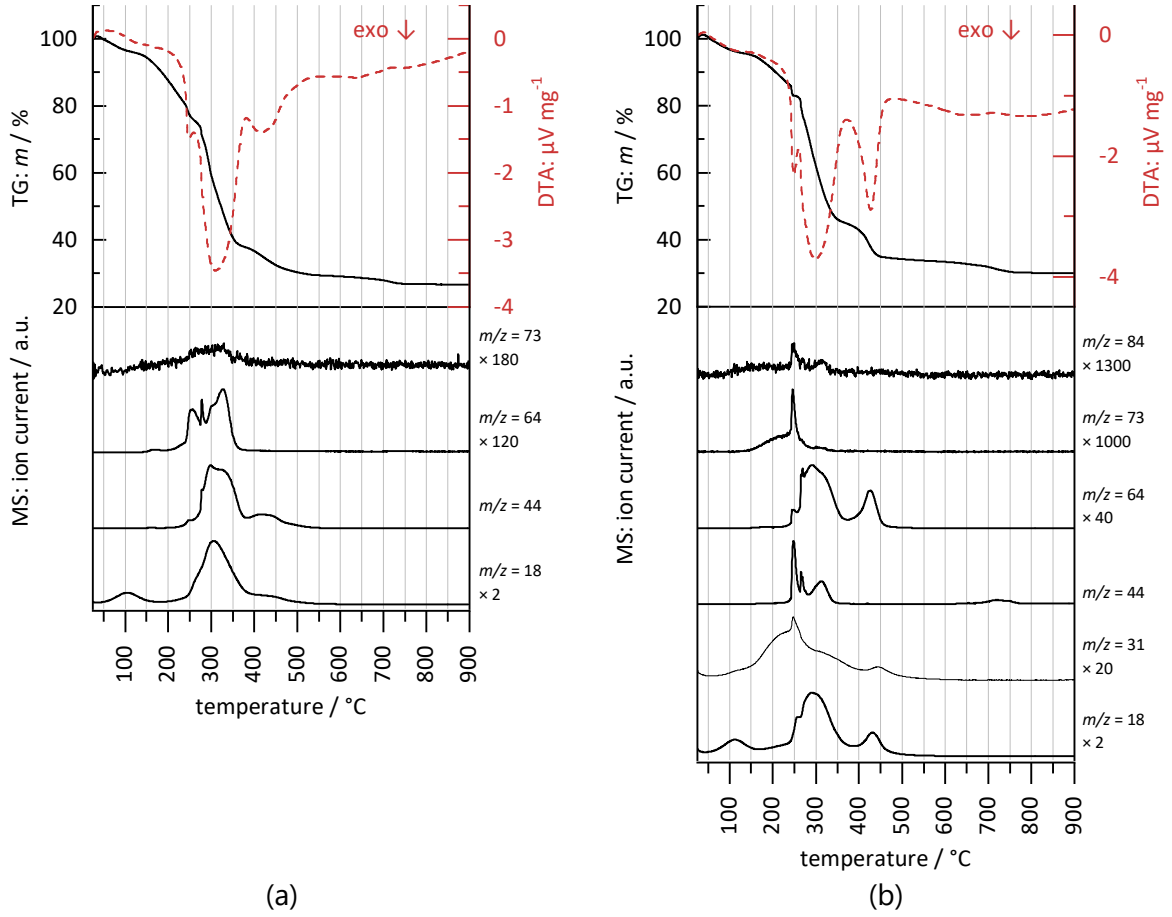

Figure S13: TG-DTA/MS data for (a) **UHM-61** as-synthesised and (b) **UHM-61** activated according to the procedure described. The *m/z* traces possibly correspond to H_2O (18), MeOH (31), CO_2 (44), SO_2 (64), DMF (73), and CH_2Cl_2 (84).

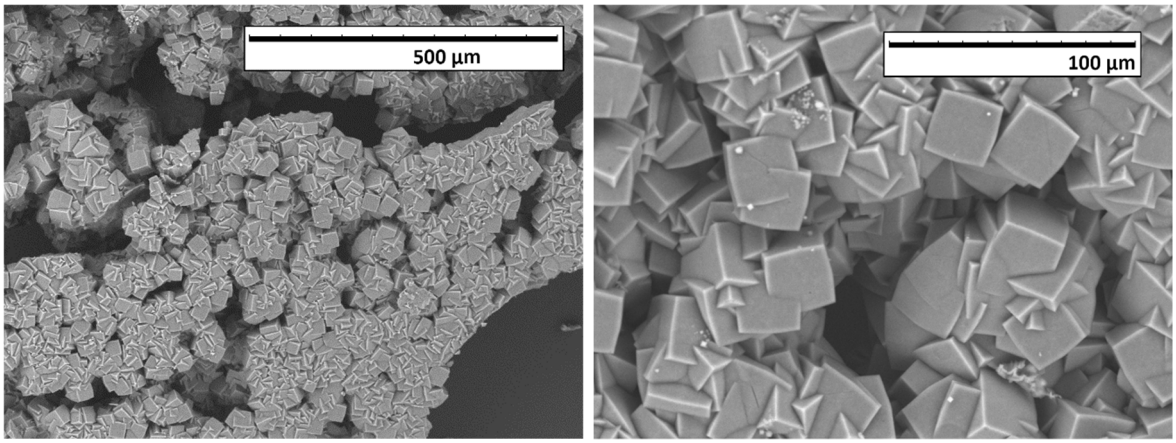

Figure S14: SEM images of as-synthesised **UHM-61.**

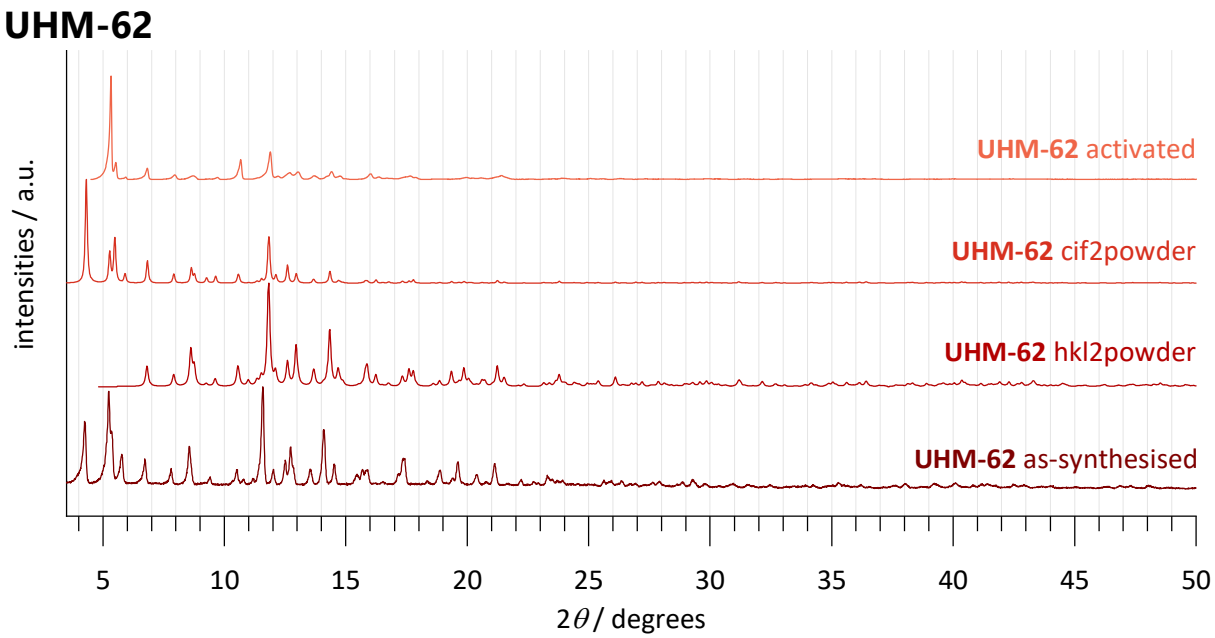

Figure S15: Powder X-ray diffractograms of (from bottom to top) **UHM-62** as-synthesised, **UHM-62** hkl2powder, **UHM-62** cif2powder, and **UHM-62** activated. Please note that hkl2powder and cif2powder data is obtained from a single crystal diffraction experiment at 100 K, while as-synthesised and activated samples were measured at room temperature. The hkl2powder and cif2powder diffractograms are thus shifted to higher 2θ values.

Powder X-ray diffractograms of **UHM-62** as-synthesised as well as the diffractograms calculated from the single crystal data (hkl2powder) and from the structural model established after refinement (cif2powder) are shown in Figure S15. The X-ray diffractogram of activated **UHM-62** is also shown. An expansion of the diffractograms between 2θ = 3°–15° is shown in Figure S16. Even though intensities are modulated considerably upon activation, the reflection pattern consistent with the approximate dimensions of the orthorhombic cell determined *via* scXRD and the expected integral extinctions due to the *I* centering within the *Immm* space group are maintained satisfactorily through this procedure. An anisotropic shift towards higher 2θ angles demonstrating a contraction of the unit cell dimensions is observed. This underlines the structural integrity in the absence of guest molecules. The linker integrity was verified by an acidic digestion of the MOF and NMR spectroscopy of the reisolated linker molecule (see Figure S17). TG-DTA/MS data of as-synthesised as well as activated material is shown in Figure S18, SEM images of as-synthesised material in Figure S19.

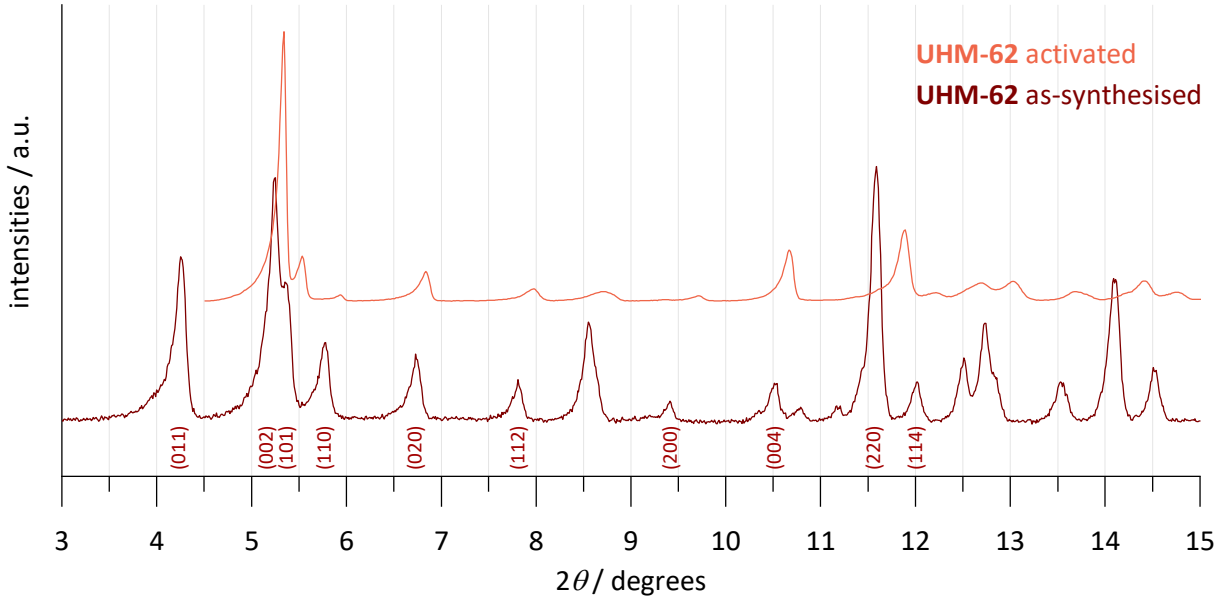

Figure S16: Powder X-ray diffractograms of **UHM-62** activated and **UHM-62** as-synthesised between 2θ angles of 3° and 15°. Reflections for **UHM-62** as-synthesised that can be assigned without doubt are labelled. Please note that the (011) reflection could not be observed with the method used for the measurement of **UHM-62** activated.

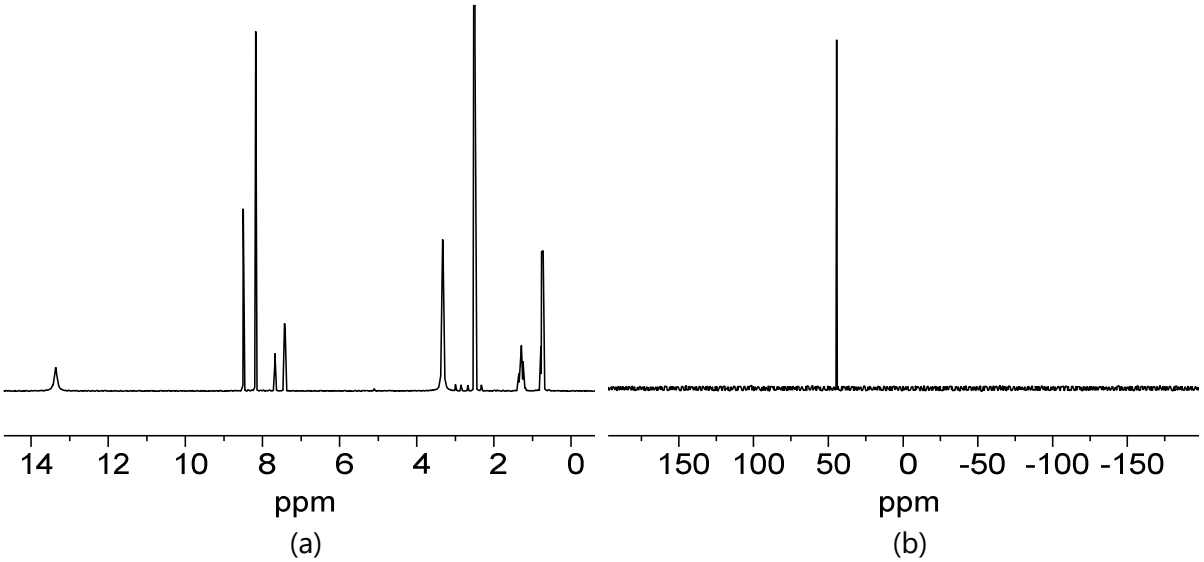

Figure S17: (a) ^{1}H NMR and (b) ^{31}P{^{1}H} NMR spectra of reisolated linker molecule from **UHM-62** in DMSO-d_6. No decomposition products of the linker molecule were identified.

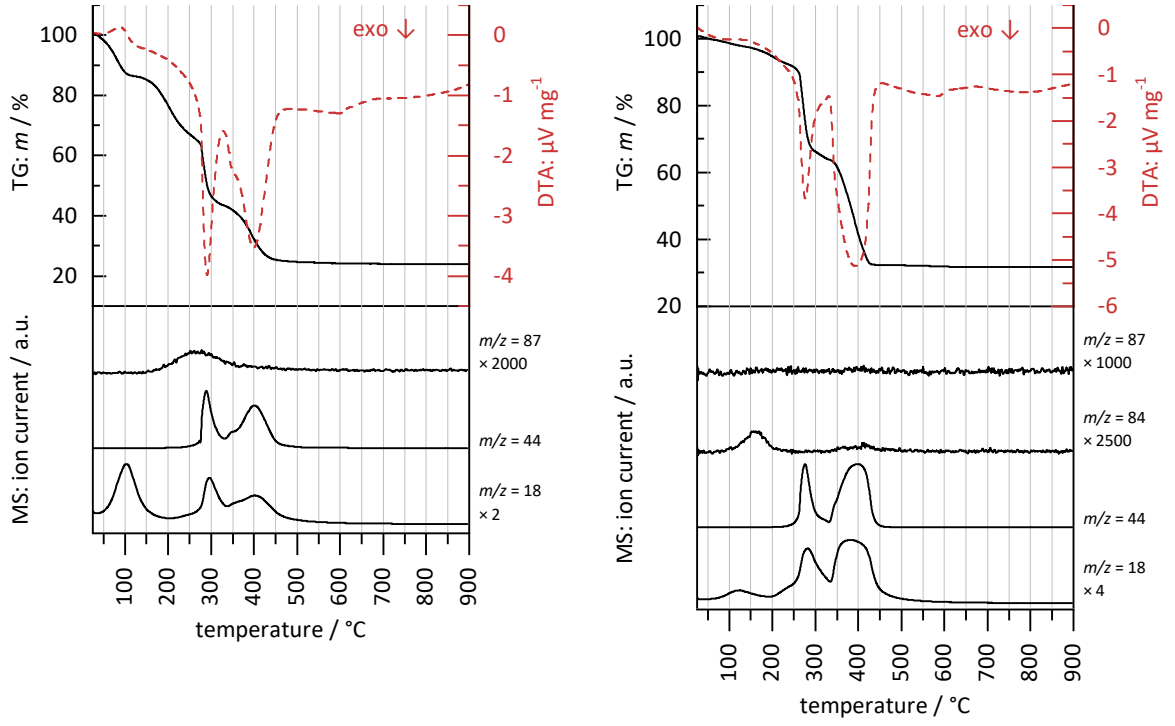

Figure S18: TG-DTA/MS data for (a) **UHM-62** as-synthesised and (b) **UHM-62** activated according to the procedure described. The *m/z* traces possibly correspond to H_2O (18), CO_2 (44), CH_2Cl_2 (84), and DMA (87).

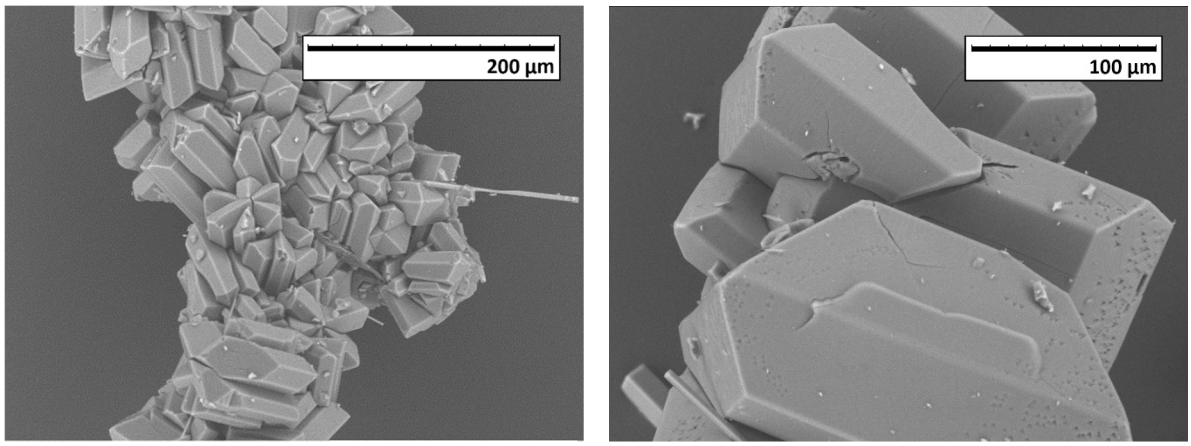

Figure S19: SEM images of as-synthesised **UHM-62**. Crystals belong to the crystallographic point group *mmm* that belongs to the orthorhombic crystal class. A high degree of aggregation is observed. Distinct faces are (001), (101), and (01$\bar{1}$).

UHM-63

Powder X-ray diffractograms for **UHM-63** as-synthesised, diffractograms calculated from single-crystal X-ray data (hkl2powder) as well as the .cif obtained after refinement of the single crystal data (cif2powder), an experimental diffractogram of **UHM-62** at the activated state, as well as a comparison with the powder diffractogram of **UHM-62** as-synthesised are shown in Figure S20. It becomes evident that **UHM-63** is isostructural to **UHM-62**. Figure S21 compares the powder diffractograms of as-synthesised and activated **UHM-63** between 3°–15°. The reflection intensities are remarkably modulated and shift anisotropically to higher 2θ angles during the activation procedure (see discussion for **UHM-62** above). Again, the linker integrity was verified by NMR methods (see Figure S22). TG-DTA/MS data of as-synthesised and activated **UHM-63** is given in Figure S23, and SEM images of the material are shown in Figure S24.

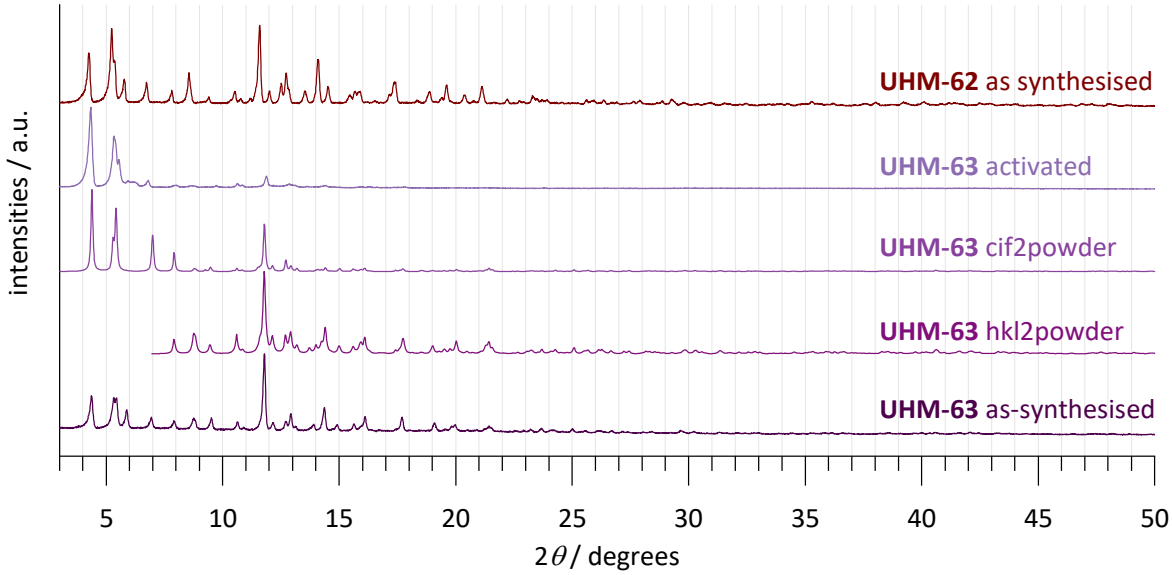

Figure S20: Powder X-ray diffractograms (from bottom to top) of **UHM-63** as-synthesised, a calculated powder diffractogram from the single crystal data (hkl2powder), a calculated diffractogram from the structural model established after refinement (cif2powder), an activated sample of **UHM-63**, and **UHM-62** as-synthesised for comparison. Please note that hkl2powder and cif2powder data is obtained from a single crystal diffraction experiment at 100 K, while as-synthesised and activated samples were measured at room temperature. The hkl2powder and cif2powder diffractograms are thus shifted to higher 2θ values.

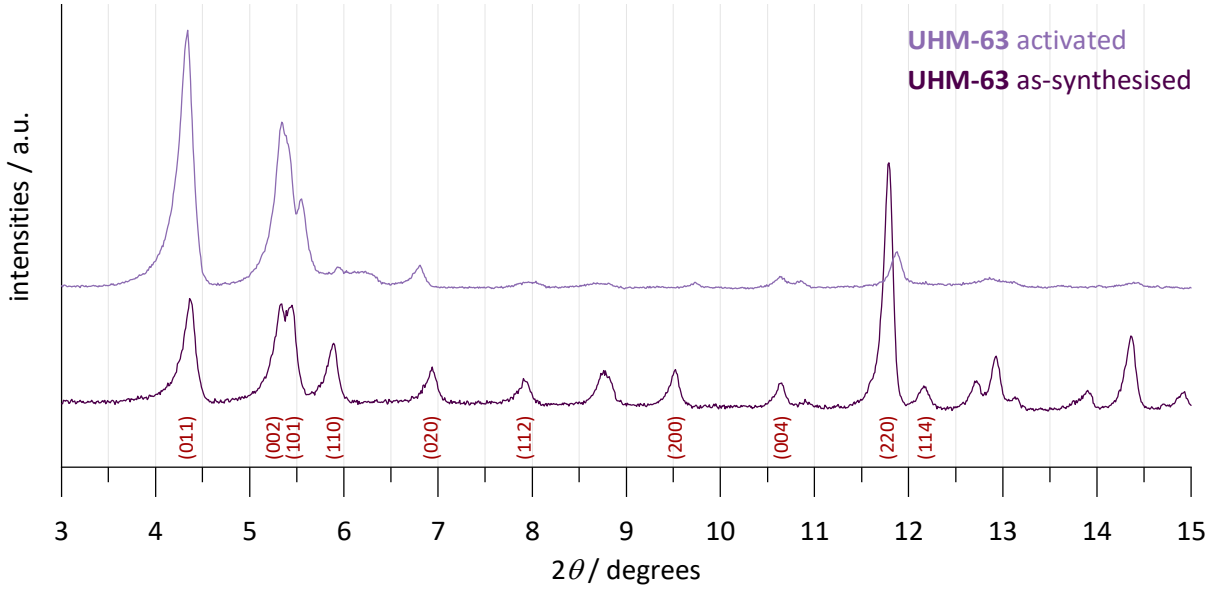

Figure S21: Powder X-ray diffractograms of **UHM-63** activated and **UHM-63** as-synthesised between 2θ angles of 3° and 15°. Reflections for **UHM-63** as-synthesised that can be assigned without doubt are labelled.

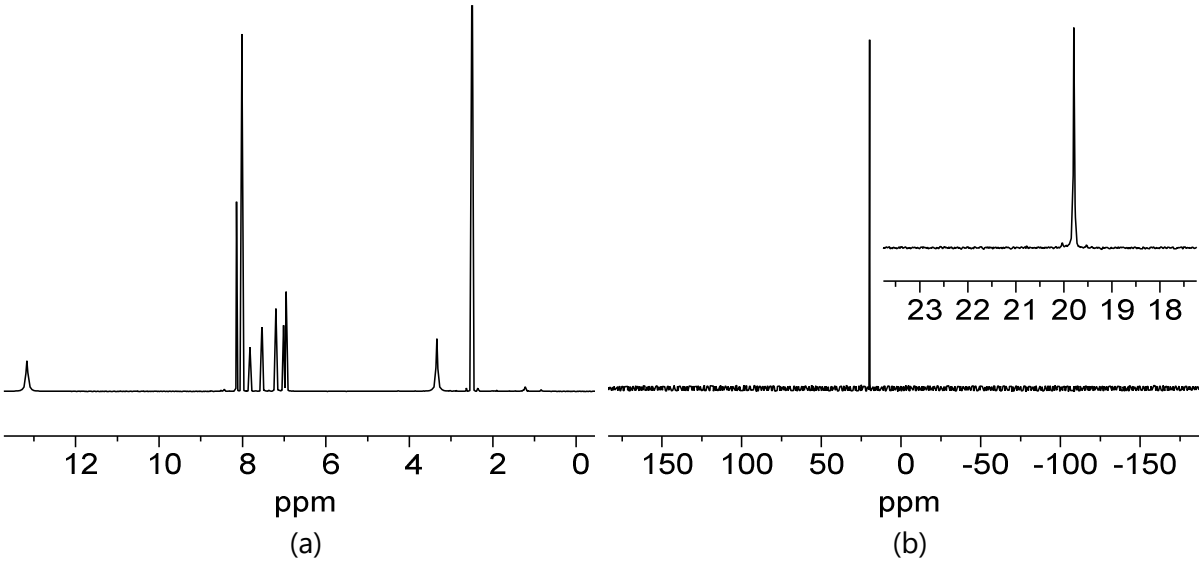

Figure S22: (a) ^{1}H NMR and (b) $^{31}P\{^{1}H\}$ NMR spectra of reisolated linker molecule from **UHM-63** in DMSO-d_6. No decomposition products of the linker molecule were identified.

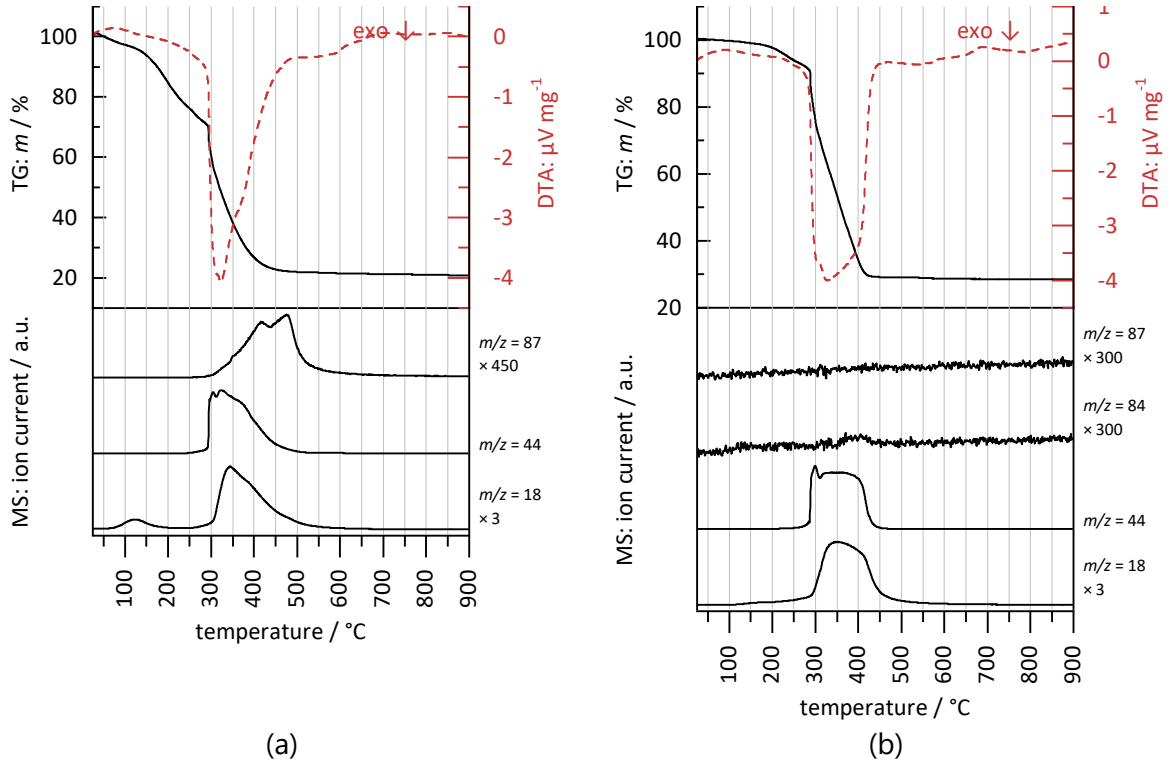

Figure S23: TG-DTA/MS data for (a) **UHM-63** as-synthesised and (b) **UHM-63** activated according to the procedure described. The *m/z* traces possibly correspond to H_2O (18), CO_2 (44), CH_2Cl_2 (84), and DMA (87).

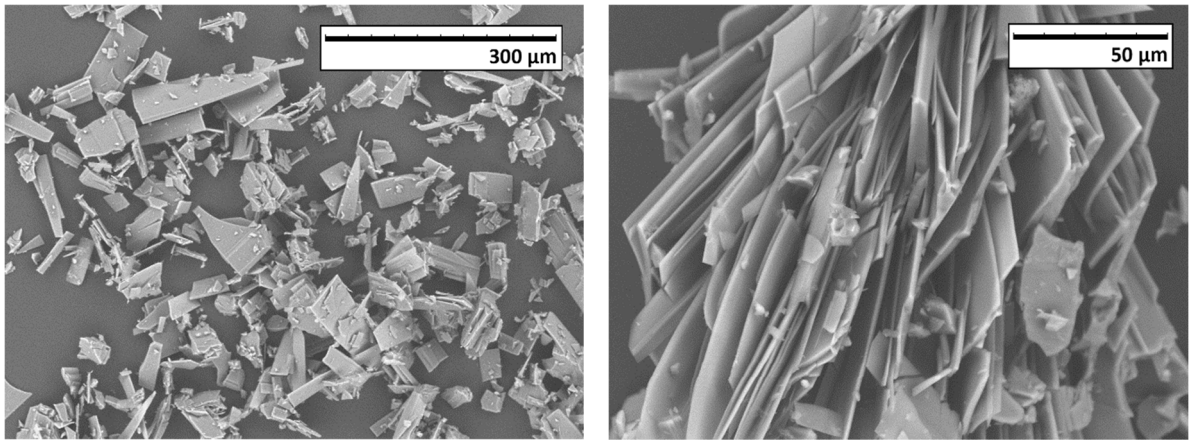

Figure S24: SEM images of as-synthesised **UHM-63**.

Physisorption data

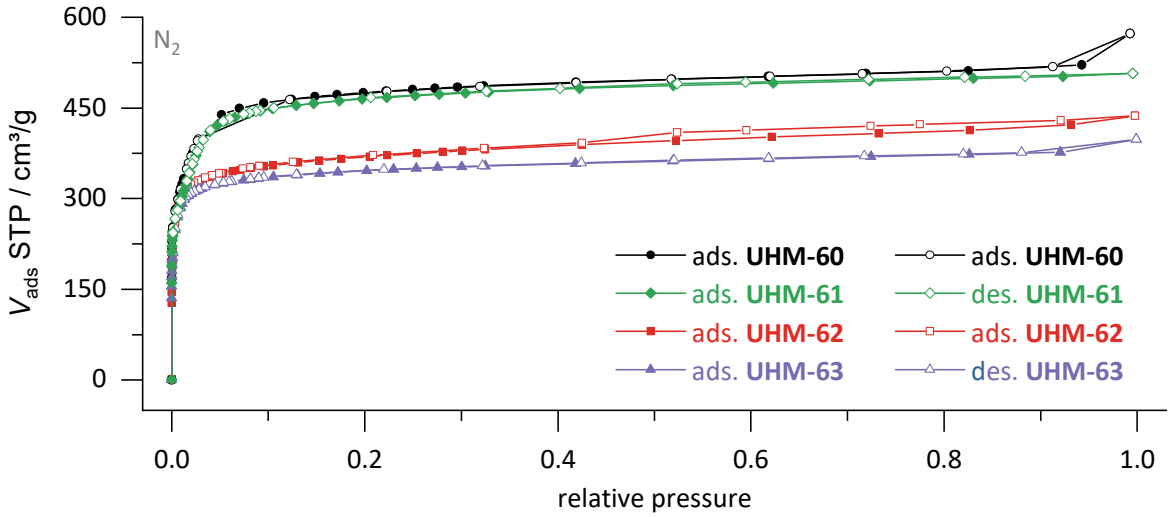

Figure S25: Nitrogen physisorption data for **UHM-60** (black), **UHM-61** (red), **UHM-62** (green), and **UHM-63** (blue).

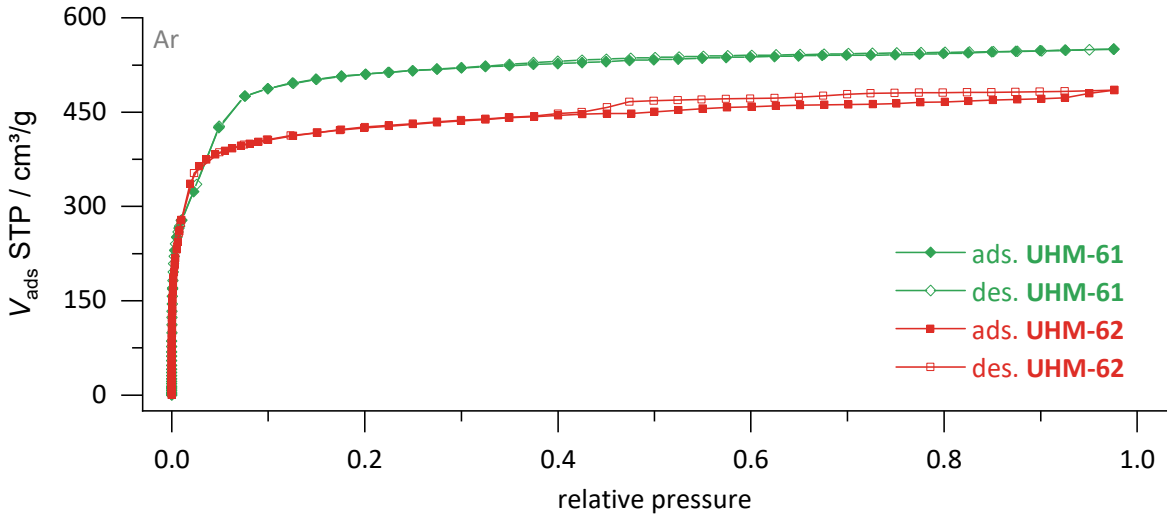

Figure S26: Argon physisorption data of **UHM-61** and **UHM-62**.

Table S3: Specific BET surface areas derived from N_2 and Ar physisorption experiments and total pore volumes determined from N_2 physisorption measurements.

MOF	spec. N_2 BET surface area / $m^2\ g^{-1}$	spec. Ar BET surface area / $m^2\ g^{-1}$	total pore volume (N_2) / $cm^3\ g^{-1}$
UHM-60	1939		0.89
UHM-61	1930	1772	0.78
UHM-62	1429	1457	0.68
UHM-63	1358		0.62

LITERATURE SURVEY

Topologies of MOFs employing the *m*-terphenyl tetracarboxylate linker molecule

Table S4 summarises the topologies reported for coordination polymers based on the [1,1′:3′,1′′-terphenyl]-3,3′′-5,5′′-tetracarboxylate linker molecule and the MOFs reported within the scope of this work. It becomes evident that the majority of Cu(II) MOFs exhibit underlying nets of type **sty** (**ssa**-derived) and **mfj** (derived from a quadrinodal (4,4,4,4)-c net with point symbol $\{4.6^4.8\}_2\{4^2.6^4\}\{6^4.8^2\}_2\{6^6\}$) with only few notable exceptions. **sty** has *pqrs* = 2243 and shows minimal transitivity, while **mfj** with *pqrs* = 4552 does not, as the structure exhibits only one type of secondary building unit (SBU) and one type of 3-c linker branch point, while the deconstruction gives two distinguishable 4-c nodes and 4-c nodes, respectively. Therefore, the requirements for a net of minimal transitivity are not met.[37] Metal ions used for the synthesis of MOFs apart from Cu(II) are Cd(II), Co(II), Eu(III), Fe(II), Gd(III), Mn(II), Ni(II), Pr(III), Sm(III), Tb(III), and Zn(II).

Table S4: Overview of literature-reported coordination polymers with *m*-terphenyl 3,3′′,5,5′′-tetracarboxylate linker molecules including corresponding CSD Refcodes, dimensionality of the structure, the metal ion used, the underlying net, its connectivity, and information regarding substitution of the linker backbone and the usage of a secondary ligand (bipy: bipyridine, bib: 1,4-bis(*N*-imidazolyl)benzene, phen: phenanthroline, bpen: *trans*-1,2-bis(4-pyridyl)ethylene). Secondary interactions like H- or π-bonding within the structures have been ignored. Structures bearing COOH functional groups on the central aryl were only considered if they were found to be uncoordinated after MOF synthesis. Those structures which were found to exhibit additional ligating groups (formiate ions, chloride ions, oxygen species) that interconnect neighbouring Cu(II) or Zn(II) paddle-wheels can be treated (a) in a fashion where two paddle-wheels form a single 8-c node, (b) in a way where the ligating group is treated as a link between two 4-c nodes, and (c) with the ligating group being excluded from the topological representation.

MOF	CSD Refcode and reference	dimen.	metal ion	underlying net	connectivity	linker substitution	secondary ligand
	BUBDEJ[38]	1D	Cd(II)	2,4C4	(2,4)-c		phen
	DEJYAV[39]	1D	Cd(II)	2,4C4	(2,4)-c		2,2′-bipy
	DORGAU[40]	3D	Cd(II)	3,3,3,3,5,10T1	(3,3,3,3,5,10)-c		4,4′-bipy
CHD-1	SEVWEY[41]	3D	Cd(II)	3,5T1	(3,5)-c		
	HORZEV[42]	1D	Co(II)	$4^4(0,2)$	3-c		phen
	KUWPAV[43]	3D	Co(II)	2,2,2,3M12-3	(3,10)-c		4,4′-bipy
	MUNQET[44]	3D	Co(II)	3,3,4,8T97	(3,3,4,8)-c	2′-aza	bib
	MUNQAP[44]	3D	Co(II)	3,4,5T332	(3,4,5)-c	2′-aza	bib
	MUDHOK[45]	3D	Co(II)	3,4T165	(3,4)-c		bib
	HORYIY[42] HORYIY01[40] HORYIY02[46] HORYIY03[47]	3D	Co(II)	**nof**	(3,3)-c		4,4′-bipy
	DORGOI[40]	3D	Co(II)	sqc27	(3,6)-c		bpen
	MUNPUI[44]	2D	Cu(II)	**sql**	4-c	2′-aza	bib

JLU-Liu22	ZUSNOS[48]	3D	Cu(II)	(a) $\{3.6^2\}_4\{3^2.6^7.7^2.8^5.9^4.10^4.11^4\}\{6^3.8^3\}\{6^3\}_2$ (b) 3,3,3,4,5T50 (c) 3,3,3,4,4T31	(3,3,3,4,8)-c (3,3,3,4,5)-c (3,3,3,4,4)-c	
UHM-62	**this work**	3D	Cu(II)	(a) **tst** (b) **tim** (c) 3,3,4,4T199	(3,3,4,8)-c (3,3,4,5)-c (3,3,4,4)-c	2′-$POEt_2$
UHM-63	**this work**	3D	Cu(II)	(a) **tst** (b) **tim** (c) 3,3,4,4T199	(3,3,4,8)-c (3,3,4,5)-c (3,3,4,4)-c	2′-$POPh_2$
BUT-301	XOHQET[49]	3D	Cu(II)	(a) **tst** (b) **tim** (c) 3,3,4,4T199	(3,3,4,8)-c (3,3,4,5)-c (3,3,4,4)-c	5′-NO_2
BUT-302	XOHQIX[49]	3D	Cu(II)	$\{6.8.9\}_4\{6.8^4.11\}\{6.8^4.12\}$	(3,3,4,4)-c	5′-NO_2
ZJNU-55	AWENAT02[50]	3D	Cu(II)	$\{6.8.9\}_2\{6.8^3.9^2\}$	(3,3,4)-c	4′,6′-diaza-5′-methyl
	WEJPOT[51]	3D	Cu(II)	$\{6^2.8^2.12^2\}\{6^2.8\}_4\{6^4.8^2\}$	(3,4,4)-c	2′-aza
	UWALEL[52]	3D	Cu(II)	3,3,4,4T234	(3,3,4,4)-c	2′-aza
	QIVZUT[53]	3D	Cu(II)	3,3,4T213	(3,3,4)-c	5′-NO_2
HHU-3 **ZJU-195**	[54,55] NEMCOA[56] CEKHUY[57] WAQKUX[58]	3D	Cu(II)	**mfj**	(3,3,4,4)-c	5′-NH_2
	[59]	3D	Cu(II)	**mfj**	(3,3,4,4)-c	5′-NO_2
PCN-306	[60]	3D	Cu(II)	**mfj**	(3,3,4,4)-c	
PCN-307	[60]	3D	Cu(II)	**mfj**	(3,3,4,4)-c	5′-CF_3
PCN-308	[60]	3D	Cu(II)	**mfj**	(3,3,4,4)-c	5′-CH_3
HHU-4	CEKJAG[57]	3D	Cu(II)	**mfj**	(3,3,4,4)-c	5′-OH
PCN-305 **NJU-Bai10**	FIBKEI[60] KIRFOI[61]	3D	Cu(II)	**mfj**	(3,3,4,4)-c	5′-aza
ZJNU-81	HIDTUM[62]	3D	Cu(II)	**mfj**	(3,3,4,4)-c	5′-Me
HHU-5	MIKVAG[63]	3D	Cu(II)	**mfj**	(3,3,4,4)-c	5′-(5-tetrazolyl)
HHU-5C	MIKVEK[63] VOGPEO[64]	3D	Cu(II)	**mfj**	(3,3,4,4)-c	5′-COOH
NJFU-3	WARXUL[65]	3D	Cu(II)	**mfj**	(3,3,4,4)-c	5′-OMe
	ATAYEB[66]	3D	Cu(II)	**sty**	(3,4)-c	5′-F-2′-NH_2
ZJNU-56	BAZSED[67]	3D	Cu(II)	**sty**	(3,4)-c	4′-NH_2-benzo[*e*′]
ZJNU-54	ERIWAF[68]	3D	Cu(II)	**sty**	(3,4)-c	2′-NH_2-4′,6′-diaza
	GACBIY[69]	3D	Cu(II)	**sty**	(3,4)-c	4′-COOH
	GAFRUD[70]	3D	Cu(II)	**sty**	(3,4)-c	2′-NH_2
ZJNU-69	HEMVIH[71]	3D	Cu(II)	**sty**	(3,4)-c	4′-OEt-benzo[*e*′]
ZJNU-70	HEMVON[71]	3D	Cu(II)	**sty**	(3,4)-c	4′-OMe-benzo[*e*′]
ZJNU-82	HIDVAU[62]	3D	Cu(II)	**sty**	(3,4)-c	2′-Me

ZJNU-83	HIDVEY[62]	3D	Cu(II)	**sty**	(3,4)-c	4′-Me	
	IDEWOG[72]	3D	Cu(II)	**sty**	(3,4)-c	2′-NH_2-5′-OMe	
ZJNU-71	LAYQEK[71,73]	3D	Cu(II)	**sty**	(3,4)-c	benzo[*d*′]	
	QEMFEW[74]	3D	Cu(II)	**sty**	(3,4)-c	2′-NH_2-5′-CF_3	
ZJNU-85	TEXXOM[75]	3D	Cu(II)	**sty**	(3,4)-c	pyrido[2,3-*e*′]	
ZJNU-86	TEXXUS[75]	3D	Cu(II)	**sty**	(3,4)-c	pyrido[3,2-*e*′]	
ZJNU-84	TEXYAZ[75]	3D	Cu(II)	**sty**	(3,4)-c	4′-aza-benzo[*e*′]	
ZJNU-57	YEVRID[76]	3D	Cu(II)	**sty**	(3,4)-c	2′,4′,6′-Me_3	
ZJNU-87	ZINQAR[77]	3D	Cu(II)	**sty**	(3,4)-c	4′,6′-diamino-5′-aza	
ZJNU-88	ZINQEV[77]	3D	Cu(II)	**sty**	(3,4)-c	4′,6′-dimethyl-5′-aza	
ZJNU-89	ZINQIZ[77]	3D	Cu(II)	**sty**	(3,4)-c	4′,6′-dimethoxy-5′-aza	
UHM-60	**this work**	3D	Cu(II)	**ucp**	(3,4)-c	2′-$POMe_2$	
UHM-61	**this work**	3D	Cu(II)	**ucp**	(3,4)-c	2′-$PSMe_2$ / 2′-$POMe_2$	
	OFOWUE[78]	2D	Eu(III)	3,3,4L34	(3,3,4)-c	5′-aza	
	XOFGAC[79]	3D	Eu(III)	3,3,8T34	(3,3,8)-c	2′-aza	
	ZIFZOG[80]	3D	Eu(III)	sqc495	(3,8)-c	5′-aza	
	MUNQOD[44]	3D	Fe(II)	3,3,6T199	(3,3,6)-c	2′-aza	bib
	OFOXEP[78]	2D	Gd(III)	3,3,4L34	(3,3,4)-c	5′-aza	
	XOFGEG[79]	3D	Gd(III)	3,3,8T34	(3,3,8)-c	2′-aza	
	[80]	3D	Gd(III)	sqc495	(3,8)-c	5′-aza	
	HORZAR[42]	1D	Mn(II)	4^4(0,2)	3-c		phen
	HORYUK[42]	2D	Mn(II)	3,4L87	(3,4)-c		2,2′-bipy
	QUSQUS[81]	3D	Mn(II)	(b) 3,3,5,5,6,8T1 (c) **lwh**	(3,3,5,5,6,8)-c (3,4,6)-c	2′-aza	
	MUNQIX[44]	3D	Mn(II)	3,6T194	(3,6)-c	2′-aza	bib
	OGUSIU[43]	3D	Mn(II)	sqc495	(3,8)-c		
	OGUSEQ[43]	2D	Ni(II)	3,4L87	(3,4)-c		
	[46]	3D	Ni(II)	$\{4.6.7.8.9.10\}_2\{4^2.7.9^2.11\}\{6^2.7\}_2$	(3,4,4)-c		4,4′-bipy
	HORYOE[42] HORYOE01[40] HORYOE02[82]	3D	Ni(II)	**nof**	(3,3)-c		4,4′-bipy
	DORGUO[40]	3D	Ni(II)	sqc27	(3,6)-c		bpen
	[78]	2D	Pr(III)	3,3,4L34	(3,3,4)-c	5′-aza	
	[78]	2D	Sm(III)	3,3,4L34	(3,3,4)-c	5′-aza	
	MUWRIH[83]	3D	Sm(III)	3,3,8T34	(3,3,8)-c	2′-aza	
	OFOXAL[78]	2D	Tb(III)	3,3,4L34	(3,3,4)-c	5′-aza	
	ZIFZUM[80]	3D	Tb(III)	sqc495	(3,8)-c	5′-aza	
	BUBDIN	2D	Zn(II)	3,3,4L111	(3,3,4)-c		phen
	GOGCUD[84]	2D	Zn(II)	**bex**	(3,4)-c	2′-NH_2-5′-Me	Rhodamine B
	QUSQOM[81]	3D	Zn(II)	(a) $\{3.7^2\}_{24}\{3^4.7^8.8^8.10^4.11^4\}_3\{7^6.8^6.11^3\}_4$	(3,6,8)-c	2′-aza	

				(b) 3,5,6T52 (c) **lwh**	(3,5,6)-c (3,4,6)-c		
	CIJLIT[85]	3D	Zn(II)	(b) $\{4.5.6\}_4\{4^4.5^4.6^2.7^5\}\{5^2.6^2.9^2\}$ (c) $\{6^2.7^2.11^2\}\{6^2.7^4\}\{6^2.7\}_4$	(3,4,6)-c (3,4,4)-c	5′-NO_2	
	DISWAG[82]	3D	Zn(II)	$\{5.10^5\}\{5.6.7\}_2\{5^2.8^2.10.11\}$	(3,4,4)-c		1,3-di(4-pyridyl)propane
CHD-2	SEVWIC[41]	3D	Zn(II)	3,4T35	(3,4)-c		
	MUWRUT[83]	3D	Zn(II)	3,5,8T20	(3,3,8)-c	2′-aza	
	DORFUN[40] MONDUQ[86]	3D	Zn(II)	**nof**	(3,3)-c		4,4′-bipy
	ATAYAX[66]	3D	Zn(II)	**sty**	(3,4)-c	5′-F-2′-NH_2	
	GAFROX[70]	3D	Zn(II)	**sty**	(3,4)-c	2′-NH_2	
	IDEWIA[72]	3D	Zn(II)	**sty**	(3,4)-c	2′-NH_2-5′-OMe	

Angular components of twist and fold between isophthalates within Cu(II) *m*-terphenyl tetracarboxylates

Table S5 summarises the internormal angles and angular components of twist and fold between the isophthalate moieties within the 1,1′:3′,1′′-terphenyl]-3,3′′-5,5′′-tetracarboxylate linker molecule and its substituted derivatives in Cu(II)-based MOFs. Structure numbers correspond to those used in Fig. 8 of the main paper. Underlying nets and, if applicable, linker substitutional patterns are also given.

Table S5: Literature-reported Cu(II) MOFs employing the *m*-terphenyl linker molecule as well as MOFs described herein with underlying nets, substitutional patterns of the linker backbone and respective internormal angles and angular components of twist and fold. All angles were obtained using the OLEX2 software.

MOF	structure number	CSD Refcode and reference	underlying net	linker substitution	internormal angle / degrees	twist angle / degrees	fold angle /degrees
UHM-60	1	**this work**	**ucp**	2′-$POMe_2$	51	0	51
UHM-61	1	**this work**	**ucp**	2′-$PSMe_2$ / 2′-$POMe_2$	51	0	51
UHM-62	2	**this work**	(a) **tst** (b) **tim** (c) 3,3,4,4T199	2′-$POEt_2$	50.8(3) 7.8(16) 24.1(15)	0 0 0	50.8(3) 7.8(16) 24.1(15)
UHM-63	3	**this work**	(a) **tst** (b) **tim** (c) 3,3,4,4T199	2′-$POPh_2$	48.0(4) 22.7(5)	0 0	48.0(4) 22.7(5)
BUT-301	4	XOHQET[49]	(a) **tst** (b) **tim** (c) 3,3,4,4T199	5′-NO_2	53.7(2) 17.44(19)	0 4.14(19)	53.7(2) 16.96(19)
PCN-305	5	FIBKEI[60]	**mfj**	5′-aza	64.79(10) 69.17(9)	0 73.47(9)	64.79(10) 31.05(16)
ZJNU-81	6	HIDTUM[62]	**mfj**	5′-Me	65.0(5) 68.6(4)	0 72.1(4)	65.0(5) 27.8(6)
HHU-5	7	MIKVAG[63]	**mfj**	5′-(5-tetrazolyl)	60.03(14)	0	60.03(14)

					70.74(10)	74.35(10)	31.32(18)
HHU-5C	8	MIKVEK[63]	**mfj**	5′-COOH	59.7(2) 71.33(14)	0 74.66(15)	59.7(2) 31.2(3)
	9	NEMCOA[56]	**mfj**	5′-NH_2	60.9(3) 68.9(2)	0 72.8(2)	60.9(3) 29.4(4)
	10	VOGPEO[64]	**mfj**	5′-COOH	58.5(4) 72.2(3)	0 76.0(3)	58.5(4) 34.4(6)
ZJU-195	11	WAQKUX[58]	**mfj**	5′-NH_2	60.9(4) 71.4(3)	0 75.2(3)	60.9(4) 32.9(6)
HHU-3	12	CEKHUY[57]	**mfj**	5′-NH_2	63.5(2) 68.1(2)	0 71.8(2)	63.5(2) 27.6(3)
HHU-4	13	CEKJAG[57]	**mfj**	5′-OH	65.6(2) 69.54(17)	0 73.89(17)	65.6(2) 31.8(3)
NJU-Bai10	14	KIRFOI[61]	**mfj**	5′-aza	54.4(2) 71.79(13)	0 75.00(14)	54.4(2) 31.6(3)
NJFU-3	15	WARXUL[65]	**mfj**	5′-OMe	65.6(2) 71.00(19)	0 74.95(19)	65.6(2) 32.9(4)
	16	ATAYEB[66]	**sty**	5′-F-2′-NH_2	60.5(4)	0	60.5(4)
ZJNU-56	17	BAZSED[67]	**sty**	4′-NH_2-benzo[*e*′]	71.0(3)	0	71.0(3)
	18	GACBIY[69]	**sty**	6′-COOH	70.8(4)	0	70.8(4)
	19	GAFRUD[70]	**sty**	2′-NH_2	60.73(16)	0	60.73(16)
ZJNU-69	20	HEMVIH[71]	**sty**	4′-OEt-benzo[*e*′]	67.1(2)	0	67.1(2)
ZJNU-70	21	HEMVON[71]	**sty**	4′-OMe-benzo[*e*′]	69.6(3)	0	69.6(3)
ZJNU-82	22	HIDVAU[62]	**sty**	2′-Me	60.01(17)	0	60.01(17)
ZJNU-83	23	HIDVEY[62]	**sty**	4′-Me	66.8(3)	0	66.8(3)
	24	IDEWOG[72]	**sty**	2′-NH_2-5′-OMe	60.0(5)	0	60.0(5)
ZJNU-71	25	LAYQEK[71,73]	**sty**	benzo[*d*′]	60.6(2)	0	60.6(2)
	26	QEMFEW[74]	**sty**	2′-NH_2-5′-CF_3	64.0(5)	0	64.0(5)
ZJNU-57	27	YEVRID[76]	**sty**	2′,4′,6′-Me_3	64.7(2)	0	64.7(2)
ZJNU-54	28	ERIWAF[68]	**sty**	2′-NH_2-4′,6′-diaza	57.3(3)	0	57.3(3)
ZJNU-85	29	TEXXOM[75]	**sty**	pyrido[2,3-*e*′]	62.68(16)	0	62.68(16)
ZJNU-86	30	TEXXUS[75]	**sty**	pyrido[3,2-*e*′]	63.90(15)	0	63.90(15)
ZJNU-84	31	TEXYAZ[75]	**sty**	4′-aza-benzo[*e*′]	63.60(16)	0	63.60(16)
ZJNU-87	32	ZINQAR[77]	**sty**	4′,6′-diamino-5′-aza	62.2(4)	0	62.2(4)
ZJNU-88	33	ZINQEV[77]	**sty**	4′,6′-dimethyl-5′-aza	65.42(15)	0	65.42(15)
ZJNU-89	34	ZINQIZ[77]	**sty**	4′,6′-dimethoxy-5′-aza	60.42(18)	0	60.42(18)
JLU-Liu22	35	ZUSNOS[48]	(a) $\{3.6^2\}_4\{3^2.6^7.7^2.8^5.9^4.10^4.11^4\}\{6^3.8^3\}\{6^3\}_2$ (b) 3,3,3,4,5T50 (c) 3,3,3,4,4T31		60.04(13) 28.75(10)	62.15(14) 10.02(10)	14.28(12) 27.19(10)
BUT-302	36	XOHQIX[49]	$\{6.8.9\}_4\{6.8^4.11\}\{6.8^4.12\}$	5′-NO_2	39.6(8)	8.5(9)	38.8(8)
	37	QIVZUT[53]	3,3,4T213	5′-NO_2	34.0(5)	7.5(5)	33.3(5)

	38	UWALEL[52]	3,3,4,4T234	2′-aza	36.6(3)	7.8(3)	35.9(3)
	39	WEJPOT[51]	$\{6^2.8^2.12^2\}\{6^2.8\}_4\{6^4.8^2\}$	2′-aza	64.2(3)	69.6(3)	27.0(4)

CO_2/CH_4 uptakes, isosteric heats of adsorption Q_{st}, and selectivities for literature-reported Cu(II) *m*-terphenyl MOFs

Table S6 lists specific BET surface areas, CO_2 uptakes, and isosteric heats of adsorption Q_{st} for CO_2 of Cu(II)-based MOFs employing the 1,1′:3′,1′′-terphenyl]-3,3′′-5,5′′-tetracarboxylate linker molecule and its substituted derivatives. CH_4 uptakes, Q_{st} for CH_4, and CO_2/CH_4 (50/50) selectivities are given in Table S7.

Table S6: Cu(II) MOFs with *m*-terphenyl linker backbones are given together with linker substitution, specific BET surface areas, CO_2 uptakes in units of cm^3 (STP) g^{-1}, mmol g^{-1}, mg g^{-1}, and wt.-%, as well as isosteric heats of adsorption Q_{st} for CO_2. Values shown in green font colour were calculated by us. Significant figures provided by the original authors were maintained throughout the calculation. We did not calculate the remaining values when uptakes were given in wt.-% only, as some authors report those based on the mass of adsorbate per mass of adsorbent instead of relating the mass of adsorbate to the sum of the mass of adsorbate plus the mass of the adsorbent. [a]297 K, [b]295 K, [c]278 K.

MOF	CSD Refcode and reference	linker substitution	S_{BET} / cm^3 (STP) g^{-1}	CO_2 uptake / cm^3 (STP) g^{-1}		CO_2 uptake / mmol g^{-1}		CO_2 uptake / mg g^{-1}		CO_2 uptake / wt.-%		Q_{st} (CO_2) / kJ mol^{-1}
				298 K	273 K	298 K	273 K	298 K	273 K	298 K	273 K	
	NEMCOA[56]	5′-NH_2	1480	89.98		3.989		175.5		14.93		26.72
	VOGPEO[64]	5′-COOH	1184	103.9	138.8	4.606	6.153	202.7	270.8	16.85	21.31	15.1
	ATAYEB[66]	5′-F-2′-NH_2	1580	106	185	4.70	8.20	207	361	20.9	36.4	39.5
	GAFRUD[70]	2′-NH_2	1410	104.39	164.65	4.6273	7.2985	203.64	321.20	20.500	32.1	37.51
	QEMFEW[74]	2′-NH_2-5′-CF_3	1584	106	181	4.70	8.02	207	353	20.8	35.5	
	QIVZUT[53]	5′-NO_2	235									
	UWALEL[52]	2′-aza	499	43.9	62.1	1.95	2.75	85.6	121	8.6	12.2	36.9
	WEJPOT[51]	2′-aza	1860		102		4.52		199		16.6	
BUT-301	XOHQET	5′-NO_2	1953									
BUT-302	XOHQIX	5′-NO_2	561									
HHU-3	CEKHUY[57]	5′-NH_2	2354	93	175	4.1	7.76	181	341	15.4	25.6	24.6
HHU-4	CEKJAG[57]	5′-OH	2353	88	164.7	3.9	7.301	172	321.3	14.7	24.4	23.9
HHU-5	MIKVAG[63]	5′-(5-tetrazolyl)	2070	107.1	188.8	4.747	8.369	208.9	368.3	17.28	26.92	25.6
HHU-5C	MIKVEK[63]	5′-COOH	2082	74.1	128.3	3.28	5.687	145	250.3	12.6	20.02	25.1
JLU-Liu22	ZUSNOS[48]		1487	95	170	4.2	7.54	185	332	19	33.4	30
NJFU-3	WARXUL[65]	5′-OMe	2531	95.6		4.24		186		15.8		24
NJU-Bai10	KIRFOI[61]	5′-aza	2883									
PCN-305	[60]	5′-aza	1720							[a]14.5	23.2	23.8
PCN-306	FIBKEI[60]		1927							[a]13.8	22.9	24.0
PCN-307	[60]	5′-CH_3	1376							[a]14.4	23.2	22.8
PCN-308	[60]	5′-CF_3	1418							[a]15.4	24.8	22.2
UHM-62	**this work**	2′-$POEt_2$	1429	84.0	114.2	3.74	5.071	164	223.2	14.1	18.25	28.9

ZJNU-54	ERIWAF[68]	2′-NH_2-4′,6′-diaza	2134	[b]120	[c]189	[b]5.32	[c]8.38	[b]234	[c]369	[b]19.0	[c]26.9	24.7
ZJNU-56	BAZSED[67]	4′-NH_2-benzo[*e*′]	1829	122	177	5.41	7.85	238	345	19.2	25.7	25.33
ZJNU-57	YEVRID[76]	2′,4′,6′-Me_3	1935	112.2		4.974		218.9		17.96		23.1
ZJNU-69	HEMVIH[71]	4′-OEt-benzo[*e*′]	1655	104.1		4.614		203.1		16.88		
ZJNU-70	HEMVON[71]	4′-OMe-benzo[*e*′]	1748	115.5		5.120		225.3		18.39		24.3
ZJNU-71	LAYQEK[71,73]	benzo[*d*′]	1860	115.6		5.124		225.5		18.40		
ZJNU-81	HIDTUM[62]	5′-Me	2720	99.0	159.1	4.39	7.052	193	310.4	16.2	23.69	24.8
ZJNU-82	HIDVAU[62]	2′-Me	2546	95.4	158.9	4.23	7.044	186	310.0	15.7	23.66	24.7
ZJNU-83	HIDVEY[62]	4′-Me	2279	102.7	171.4	4.552	7.598	200.3	334.4	16.69	25.06	22.5
ZJNU-84	TEXYAZ[75]	4′-aza-benzo[*e*′]	1926	122.6	[c]193.8	5.435	[c]8.591	239.2	[c]378.1	19.30	[c]27.43	24.5
ZJNU-85	TEXXOM[75]	pyrido[2,3-*e*′]	1206									
ZJNU-86	TEXXUS[75]	pyrido[3,2-*e*′]	595									
ZJNU-88	ZINQEV[77]	4′,6′-dimethyl-5′-aza	1696	99.2	[c]153.6	4.40	[c]6.809	194	[c]299.6	16.2	[c]23.06	
ZJNU-89	ZINQIZ[77]	4′,6′-dimethoxy-5′-aza	1618	103	[c]159.2	4.57	[c]7.057	201	[c]310.6	16.7	[c]23.70	
ZJU-195	WAQKUX[58]	5′-NH_2	1722	105	169.7	4.65	7.522	205	331.1	17.0	24.87	20.7

Table S7: Cu(II) MOFs based on the *m*-terphenyl linker backbone are listed together with specific surface areas, CH_4 uptakes in units of cm^3 (STP) g^{-1}, mmol g^{-1}, mg g^{-1}, and wt.-%, as well as isosteric heats of adsorption Q_{st} for CH_4. CO_2/CH_4 (50/50) selectivities are also given. Values shown in green font colour were calculated by us. Significant figures provided by the original authors were maintained throughout the calculation. [b]295 K, [c]278 K.

MOF	**CSD Refcode and reference**	**S_{BET} / cm^3 (STP) g^{-1}**	**CH_4 uptake / cm^3(STP) g^{-1}**		**CH_4 uptake / mmol g^{-1}**		**CH_4 uptake / mg g^{-1}**		**CH_4 uptake / wt.-%**		**Q_{st} (CH_4) / kJ mol^{-1}**	**CO_2/CH_4 selectivity (50/50)**	
			298 K	**273 K**	**298 K**	**273 K**	**298 K**	**273 K**	**298 K**	**273 K**		**298 K**	**273 K**
	NEMCOA[56]	1480									9.3		
	VOGPEO[64]	1184	25.1	32.3	1.11	1.43	17.8	22.9	1.75	2.24		6.8	8.2
	ATAYEB[66]	1580		41.8		1.84		29.6		2.87			
	GAFRUD[70]	1410											6.95
	UWALEL[52]	499	9.4	17.2	0.41	0.759	6.7	12.2	0.7	1.2		30.8	
	WEJPOT[51]	1860		28		1.2		20		1.9			
HHU-5	MIKVAG[63]	2070	22.4		0.989		15.9		1.56			6.2	
JLU-Liu22	ZUSNOS[48]	1487									11	9.4	
NJFU-3	WARXUL[65]	2531											7.9
PCN-305	[60]	1720											7.2
PCN-306	FIBKEI[60]	1927											7.5
PCN-307	[60]	1376											8.8
PCN-308	[60]	1418											7.8
UHM-62	**this work**	1429	16.4	24.1	0.728	1.06	11.7	17.1	1.15	1.68	16.0	6.1	9.7
ZJNU-54	ERIWAF[68]	2134	[b]25.9	[c]35.6	[b]1.14	[c]1.57	[b]18.3	[c]25.2	[b]1.80	[c]2.46		[b]6.1	
ZJNU-56	BAZSED[67]	1829	25.1		1.11		17.8		1.75		13.68		
ZJNU-57	YEVRID[76]	1935	24.3		1.07		17.2		1.69		20.3	5.5	
ZJNU-69	HEMVIH[71]	1655	19.8		0.87		14.0		1.38			7.14	

ZJNU-70	HEMVON[71]	1748	22.9		1.01		16.2		1.60		15.9	6.71	
ZJNU-71	LAYQEK[71,73]	1860	24.2		1.07		17.1		1.68			5.73	
ZJNU-81	HIDTUM[62]	2720	21.9		0.35		16		1.6			5.46	
ZJNU-82	HIDVAU[62]	2546	20.8		0.33		15		1.5			5.37	
ZJNU-83	HIDVEY[62]	2279	23		0.37		16		1.6			4.95	
ZJNU-84	TEXYAZ[75]	1926	24.8	[c]39.1	1.09	[c]1.73	17.6	[c]27.7	1.73	[c]2.69	18.9		
ZJNU-88	ZINQEV[77]	1696	23.3	[c]37.3	1.03	[c]1.65	16.5	[c]26.4	1.62	[c]2.57		5.4	[c]6.5
ZJNU-89	ZINQIZ[77]	1618	22.8	[c]34.9	1.01	[c]1.54	16.1	[c]24.7	1.59	[c]2.41		5.8	[c]7.5
ZJU-195	WAQKUX[58]	1722	24.5	45.8	1.08	2.02	17.3	32.4	1.71	3.14	19.9		

LITERATURE

[1] C. Eickmeier, S. Peters, K. Fuchs, N. Heine, S. Handschuh, C. Dorner-Ciossek, K. Klinder, M. Kostka, *Substituted 1,2-Ethylendiamines, Medicaments Comprising Said Compound; Their Use And Their Manufacture*, **2006**, WO2006103038.

[2] J. Jover, F. M. Miloserdov, J. Benet-Buchholz, V. V Grushin, F. Maseras, *Organometallics* **2014**, *33*, 6531–6543.

[3] G. R. Fulmer, A. J. M. Miller, N. H. Sherden, H. E. Gottlieb, A. Nudelman, B. M. Stoltz, J. E. Bercaw, K. I. Goldberg, *Organometallics* **2010**, *29*, 2176–2179.

[4] R. K. Harris, E. D. Becker, S. M. Cabral de Menezes, R. Goodfellow, P. Granger, *Pure Appl. Chem.* **2001**, *73*, 1795–1818.

[5] R. K. Harris, E. D. Becker, S. M. Cabral de Menezes, P. Granger, R. E. Hoffman, K. W. Zilm, *Pure Appl. Chem.* **2008**, *80*, 59–84.

[6] Agilent Technologies Ltd, Yarnton, Oxfordshire, England, **2014**.

[7] Bruker AXS Inc., Madison, Wisconsin, USA, **2014**.

[8] L. Palatinus, G. Chapuis, *J. Appl. Crystallogr.* **2007**, *40*, 786–790.

[9] L. Palatinus, S. J. Prathapa, S. van Smaalen, *J. Appl. Crystallogr.* **2012**, *45*, 575–580.

[10] G. M. Sheldrick, *Acta Crystallogr. A* **2008**, *64*, 112–122.

[11] G. M. Sheldrick, *Acta Crystallogr. A* **2015**, *71*, 3–8.

[12] G. M. Sheldrick, *Acta Crystallogr. C* **2015**, *71*, 3–8.

[13] L. J. Farrugia, *J. Appl. Crystallogr.* **2012**, *45*, 849–854.

[14] O. V. Dolomanov, L. J. Bourhis, R. J. Gildea, J. A. K. Howard, H. Puschmann, *J. Appl. Crystallogr.* **2009**, *42*, 339–341.

[15] A. L. Spek, *Acta Crystallogr. D* **2009**, *65*, 148–55.

[16] M. Nardelli, *J. Appl. Crystallogr.* **1999**, *32*, 563–571.

[17] A. L. Spek, *Acta Crystallogr. C* **2015**, *71*, 9–18.

[18] F. Rouquerol, J. Rouquerol, K. S. W. Sing, P. Llewellyn, G. Maurin, in *Adsorpt. by Powders Porous Solids*, Elsevier Ltd., Oxford, **2014**, pp. 239–253.

[19] E. W. Lemmon, M. O. McLinden, D. G. Friend, in *NIST Chem. WebBook, NIST Stand. Ref. Database Number 69* (Eds.: P.J. Linstrom, W.G. Mallard), National Institute Of Standards And Technology, Gaithersburg MD, 20899, **2018**.

[20] S. Lowell, J. E. Shields, M. A. Thomas, M. Thommes, in *Charact. Porous Solids Powders Surf. Area, Pore Size Density*, Springer Science+Business Media B.V., New York, **2004**.

[21] M. A. Neumann, *J. Appl. Crystallogr.* **2003**, *36*, 356–365.

[22] T. Loiseau, C. Mellot-Draznieks, H. Muguerra, G. Férey, M. Haouas, F. Taulelle, *C. R. Chim.* **2005**, *8*, 765–772.

[23] A. K. Rappé, C. J. Casewit, K. S. Colwell, W. A. Goddard III, W. M. Skiff, *J. Am. Chem. Soc.* **1992**, *114*, 10024–10035.

[24] L. Sarkisov, A. Harrison, *Mol. Simul.* **2011**, *37*, 1248–1257.

[25] V. A. Blatov, A. P. Shevchenko, D. M. Proserpio, *Cryst. Growth Des.* **2014**, *14*, 3576–3586.

[26] O. Delgado-Friedrichs, "The Gavrog Project," can be found under http://gavrog.org/, **2013**.

[27] M. Sartor, F. Hoffmann, M. Fröba, "Massive Open Online Course (iversity GmbH): The Fascination of Crystals and Symmetry, Chapter 07," can be found under https://iversity.org/en/courses/the-fascination-of-crystals-and-symmetry, **2014**.

[28] M. Sartor, F. Hoffmann, M. Fröba, "Fascination of Crystals and Symmetry - Chapter 7," can be found under https://www.youtube.com/watch?v=INRc_CfdaW0&list=PL6C90-24AMSOt8HrGv8DnlJa1lAeE3OoI, **2016**.

[29] M. O'Keeffe, O. M. Yaghi, *Chem. Rev.* **2012**, *112*, 675–702.

[30] C. M. Simon, B. Smit, M. Haranczyk, *Comput. Phys. Commun.* **2016**, *200*, 364–380.

[31] D. Hérault, D. H. Nguyen, D. Nuel, G. Buono, *Chem. Soc. Rev.* **2015**, *44*, 2508–2528.

[32] T. H. Kress, R. M. Leanna, *Synthesis (Stuttg).* **1988**, 803–805.

[33] M. Sartor, T. Stein, F. Hoffmann, M. Fröba, *Chem. Mater.* **2016**, *28*, 519–528.

[34] J. B. Anderson, G. L. Shoemaker, E. Kostiner, *J. Solid State Chem.* **1978**, *25*, 49–57.

[35] R. A. Chittenden, L. C. Thomas, *Spectrochim. Acta* **1964**, *20*, 1679–1696.

[36] L. C. Thomas, R. A. Chittenden, *Spectrochim. Acta* **1964**, *20*, 467–487.

[37] M. Li, D. Li, M. O'Keeffe, O. M. Yaghi, *Chem. Rev.* **2014**, *114*, 1343–1370.

[38] M.-L. Zhang, J.-J. Wang, Y.-X. Ren, *Wuji Huaxue Xuebao* **2014**, *30*, 2477.

[39] M.-L. Zhang, L. Qiao, Z.-Z. Ma, X.-L. Zhao, *Jiegou Huaxue* **2017**, *36*, 1532.

[40] Y.-P. Wu, *CSD Commun.* **2014**.

[41] J. Li, C. P. Men, Y. Q. Luo, S. J. Mo, W. H. Huang, L. Cui, *Z. Anorg. Allg. Chem.* **2018**, *644*, 228–234.

[42] X. Lv, L. Liu, C. Huang, L. Guo, J. Wu, H. Hou, Y. Fan, *Dalton Trans.* **2014**, *43*, 15475–15481.

[43] L. Zhang, L. Liu, C. Huang, X. Han, L. Guo, H. Xu, H. Hou, Y. Fan, *Cryst. Growth Des.* **2015**, *15*, 3426–3434.

[44] L. Fan, W. Fan, B. Li, X. Liu, X. Zhao, X. Zhang, *CrystEngComm* **2015**, *17*, 4669–4679.

[45] P. Yao, *Synth. React. Inorg. M.* **2015**, *45*, 1470–1473.

[46] X. Wang, J.-Y. Luo, J.-W. Tian, D.-D. Huang, Y.-P. Wu, S. Li, D.-S. Li, *Inorg. Chem. Commun.* **2018**, *98*, 141–144.

[47] Z. An, T. Zhou, *Chinese J. Struct. Chem.* **2019**, *38*, 777–782.

[48] D. Wang, B. Liu, S. Yao, T. Wang, G. Li, Q. Huo, Y. Liu, *Chem. Commun.* **2015**, *51*, 15287–

15289.

[49] M.-M. Xu, X.-J. Kong, T. He, X.-Q. Wu, L.-H. Xie, J.-R. Li, *Dalton Trans.* **2019**, *48*, 9225–9233.

[50] J. Jiao, H. Liu, F. Chen, D. Bai, S. Xiong, Y. He, *Inorg. Chem. Front.* **2016**, 1411–1418.

[51] J. Liu, W. Wang, Z. Luo, B. Li, D. Yuan, *Inorg. Chem.* **2017**, *56*, 10215–10219.

[52] B. Liu, H.-F. Zhou, L. Hou, Z. Zhu, Y.-Y. Wang, *Inorg. Chem. Front.* **2016**, *3*, 1326–1331.

[53] Y. Pan, W. Liu, D. Liu, Q. Ding, J. Liu, H. Xu, M. Trivedi, A. Kumar, *Inorg. Chem. Commun.* **2019**, *100*, 92–96.

[54] V. Sharma, D. De, P. K. Bharadwaj, *Inorg. Chem.* **2018**, *57*, 8195–8199.

[55] R. Saha, V. Sharma, D. De, P. K. Bharadwaj, P. K. Chattaraj, *Polyhedron* **2018**, *153*, 254–260.

[56] V. Sharma, D. De, R. Saha, R. Das, P. K. Chattaraj, P. K. Bharadwaj, *Chem. Commun.* **2017**, *53*, 13371–13374.

[57] Z. Lu, Y. Xing, L. Du, H. He, J. Zhang, C. Hang, *RSC Adv.* **2017**, *7*, 47219–47224.

[58] L. Zhang, K. Jiang, Y. Li, D. Zhao, Y. Yang, Y. Cui, B. Chen, G. Qian, *Cryst. Growth Des.* **2017**, *17*, 2319–2322.

[59] F. Wang, W. Liu, S. Li, R. W. Gable, H. Zhong, Q. Xu, G. Huang, A. Singh, J. Liu, A. Kumar, *Inorg. Chem. Commun.* **2018**, *97*, 109–112.

[60] Y. Liu, J.-R. Li, W. M. Verdegaal, T.-F. Liu, H.-C. Zhou, *Chem. Eur. J.* **2013**, *19*, 5637–5643.

[61] Z. Lu, L. Du, K. Tang, J. Bai, *Cryst. Growth Des.* **2013**, *13*, 2252–2255.

[62] Y. He, X. Gao, Y. Wang, M. He, S. Li, *Dalton Trans.* **2018**, *47*, 8983–8991.

[63] Z. Lu, F. Meng, L. Du, W. Jiang, H. Cao, J. Duan, H. Huang, H. He, *Inorg. Chem.* **2018**, *57*, 14018–14022.

[64] X. Duan, R. Song, J. Yu, H. Wang, Y. Cui, Y. Yang, B. Chen, G. Qian, *RSC Adv.* **2014**, *4*, 36419–36424.

[65] L. Du, Z. Lu, L. Xu, J. Zhang, *RSC Adv.* **2017**, *7*, 21268–21272.

[66] T. K. Pal, D. De, S. Senthilkumar, S. Neogi, P. K. Bharadwaj, *Inorg. Chem.* **2016**, *55*, 7835–7842.

[67] J. Jiao, D. Jiang, F. Chen, D. Bai, Y. He, *Dalton Trans.* **2017**, *46*, 7813–7820.

[68] J. Jiao, L. Dou, H. Liu, F. Chen, D. Bai, Y. Feng, S. Xiong, D.-L. Chen, Y. He, *Dalton Trans.* **2016**, *45*, 13373–13382.

[69] Y. T. Yan, W.-Y. Zhang, Y.-L. Wu, J. Li, Z.-P. Xi, Y.-Y. Wang, L. Hou, *Dalton Trans.* **2016**, *45*, 15473–15480.

[70] T. K. Pal, D. De, S. Neogi, P. Pachfule, S. Senthilkumar, Q. Xu, P. K. Bharadwaj, *Chem. Eur. J.* **2015**, *21*, 19064–19070.

[71] F. Chen, Y. Wang, D. Bai, M. He, X. Gao, Y. He, *J. Mater. Chem. A* **2018**, *6*, 3471–3478.

[72] M. Gupta, D. De, K. Tomar, P. K. Bharadwaj, *Inorg. Chim. Acta* **2018**, *482*, 925–934.

[73] D. Jiang, Y. He, D. Bai, F. Chen, Y. Wang, *Dalton Trans.* **2017**, *46*, 11469–11478.

[74] A. K. Gupta, D. De, K. Tomar, P. K. Bharadwaj, *Dalton Trans.* **2018**, *47*, 1624–1634.

[75] D. Bai, X. Gao, M. He, Y. Wang, Y. He, *Inorg. Chem. Front.* **2018**, *5*, 1423–1431.

[76] D.-L. Chen, Z. Tian, Y. He, M. He, L. Zhu, H. Zhong, X. Zhang, Y. Wang, Y. Zhang, *Dalton Trans.* **2018**, *47*, 2444–2452.

[77] Y. Wang, M. He, X. Gao, P. Long, Y. Zhang, H. Zhong, X. Wang, Y. He, *Dalton Trans.* **2018**, *47*, 12702–12710.

[78] X. Shi, Y. Fan, J. Xu, H. Qi, J. Chai, J. Sun, H. Jin, X. Chen, P. Zhang, L. Wang, *Inorg. Chim. Acta* **2018**, *483*, 473–479.

[79] B. Liu, W.-P. Wu, L. Hou, Y.-Y. Wang, *Chem. Commun.* **2014**, *50*, 8731–8734.

[80] J.-J. Huang, J.-H. Yu, F.-Q. Bai, J.-Q. Xu, *Cryst. Growth Des.* **2018**, *18*, 5353–5364.

[81] B. Liu, W.-P. Wu, L. Hou, Z.-S. Li, Y.-Y. Wang, *Inorg. Chem.* **2015**, *54*, 8937–8942.

[82] L.-G. Yu, Y.-G. Sun, Z.-L. Wang, *J. Mol. Struct.* **2019**, *1180*, 209–214.

[83] J.-Q. Liu, X.-F. Li, C.-Y. Gu, J. C. S. Da Silva, A. L. Barros, S. Alves-Jr, B.-H. Li, F. Ren, S. R. Batten, T. A. Soares, *Dalton Trans.* **2015**, *44*, 19370–19382.

[84] K. Tomar, W. Ji, P. K. Bharadwaj, C. Vijayan, M. Gupta, S. Lu, D. Kottilil, *ACS Appl. Nano Mater.* **2018**, *1*, 5408–5413.

[85] A. Ma, J. Wu, Y. Han, F. Chen, B. Li, S. Cai, H. Huang, A. Singh, A. Kumar, J. Liu, *Dalton Trans.* **2018**, *47*, 9627–9633.

[86] J.-J. Wang, X.-Y. Hou, L.-J. Gao, M.-L. Zhang, Y.-X. Ren, F. Fu, *Wuji Huaxue Xuebao* **2014**, *30*, 1616.

[87] J. Barthel, K. Bachhuber, R. Buchner, *Z. Naturforsch.* **2013**, *50a*, 65–74.

[88] Y. L. Zhao, Y. Li, S. M. Li, Y. G. Zhou, F. Y. Sun, L. X. Gao, F. S. Han, *Adv. Synth. Catal.* **2011**, *353*, 1543–1550.

APPENDIX

NMR Spectra

(2,6-Dichlorophenyl)dichlorophosphane (**1**)

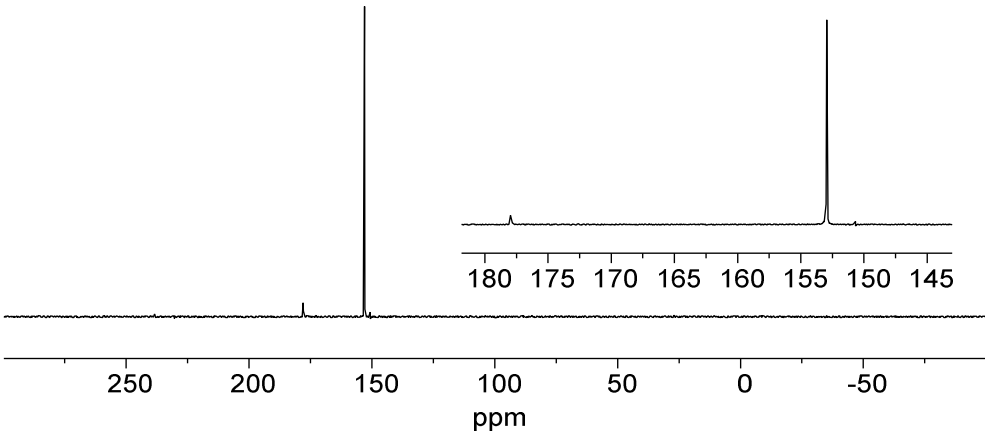

Figure S27: $^{31}P\{^{1}H\}$ NMR of **1** in C_6D_6.

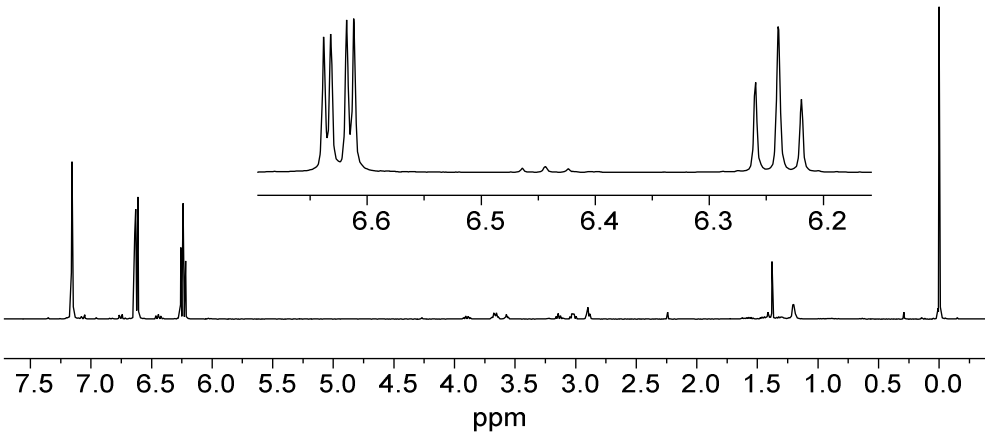

Figure S28: ^{1}H NMR of **1** in C_6D_6.

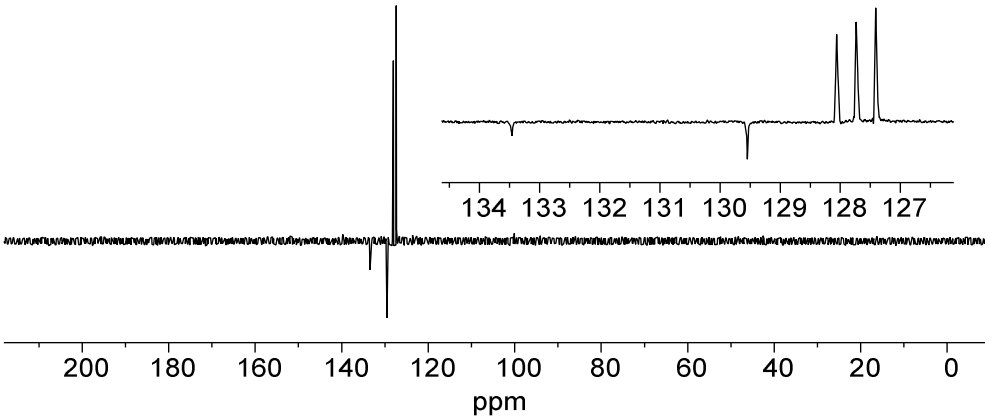

Figure S29: $^{31}C\{^{1}H\}$ NMR of **1** in C_6D_6.

(2,6-Dichlorophenyl)dimethylphosphane (**2a**)

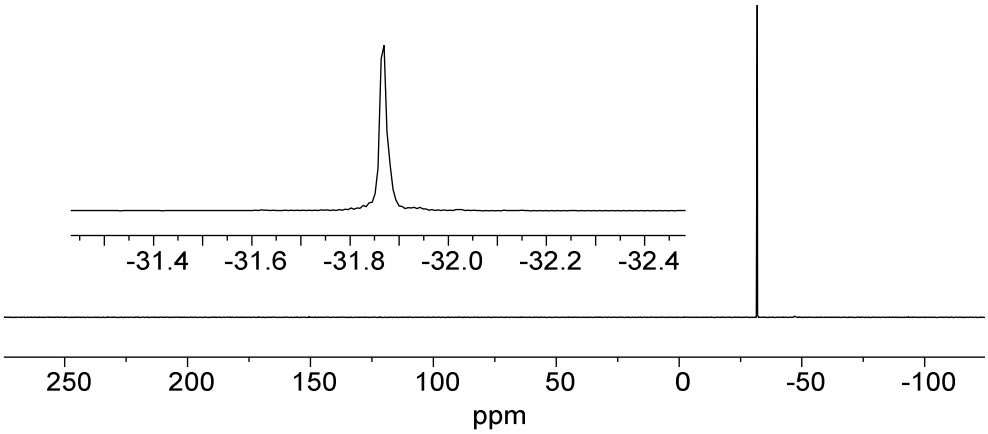

Figure S30: $^{31}P\{^{1}H\}$ NMR of **2a** in C_6D_6.

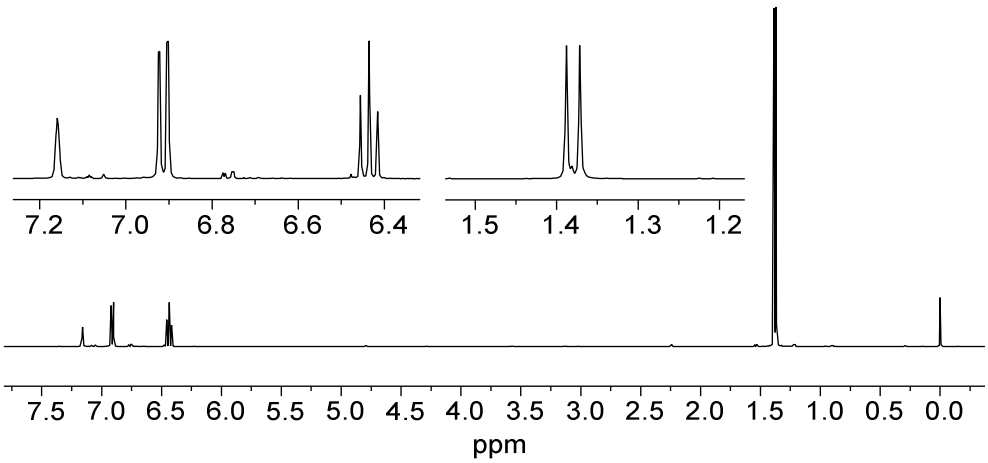

Figure S31: ^{1}H NMR of **2a** in C_6D_6.

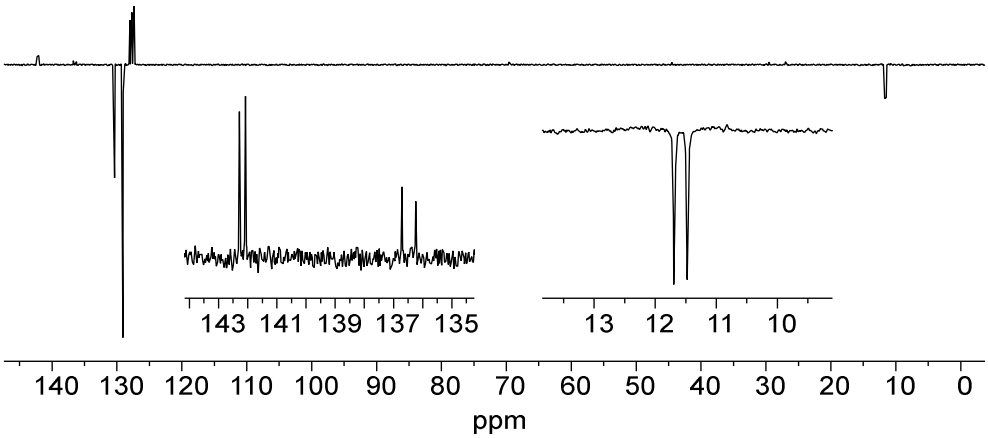

Figure S32: $^{13}C\{^{1}H\}$ NMR of **2a** in C_6D_6.

(2,6-Dichlorophenyl)diethylphosphane (**2b**)

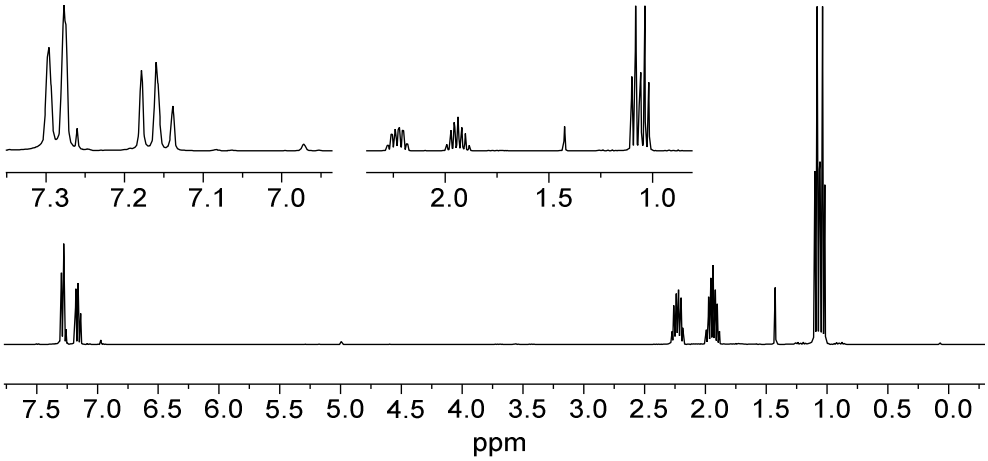

Figure S33: ^{1}H NMR of **2c** in $CDCl_3$.

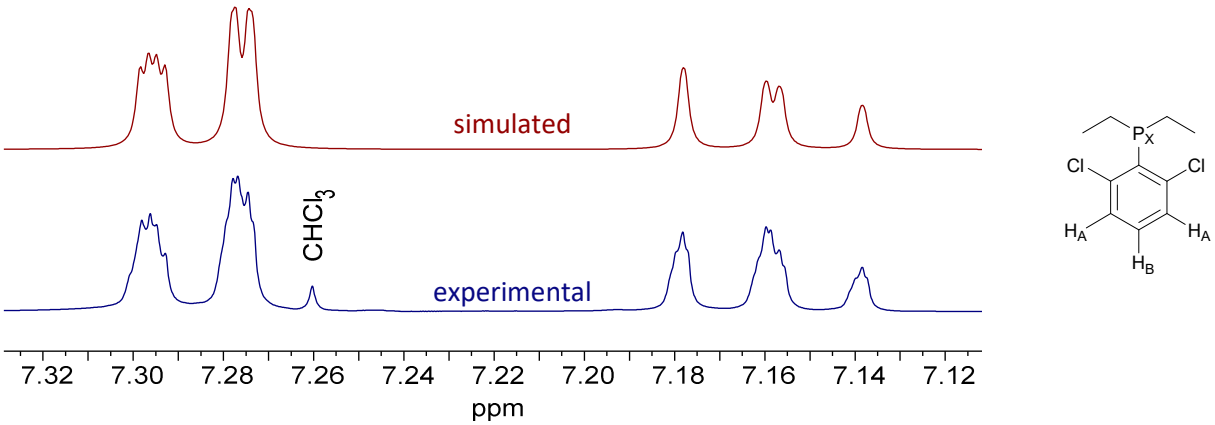

Figure S34: ^{1}H NMR iterative spin simulation of the A_2B part of the aromatic A_2BX spin system of **2c** in $CDCl_3$. The descriptors for nuclei according to Pople nomenclature are shown on the right-hand side.

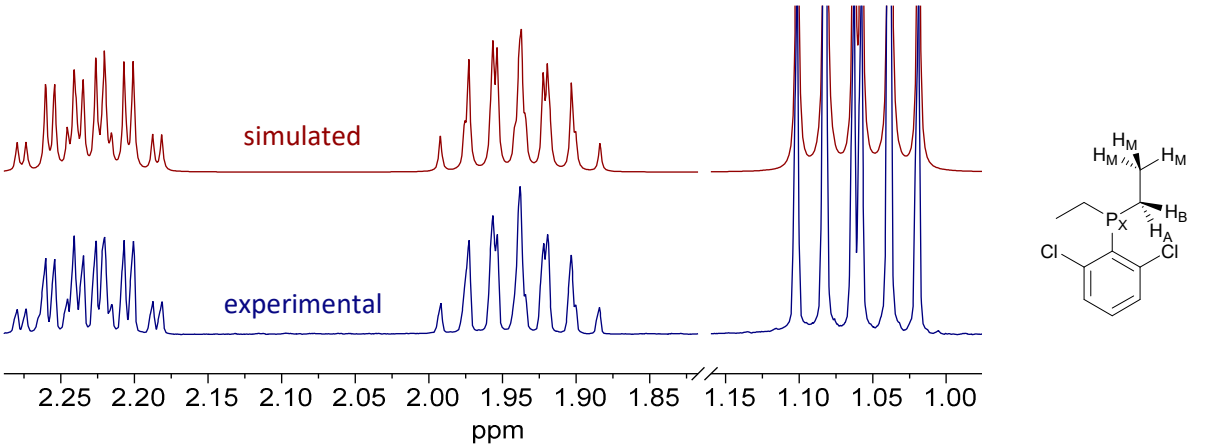

Figure S35: ^{1}H NMR iterative spin simulation of the ABM part of the aliphatic ABMX spin system of **2c** in $CDCl_3$. The descriptors for nuclei according to Pople nomenclature are shown on the right-hand side.

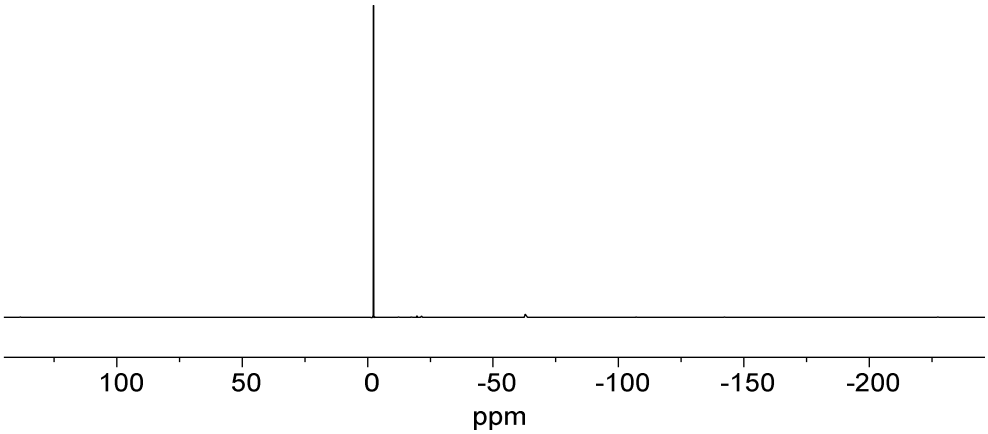

Figure S36: $^{31}P\{^{1}H\}$ NMR of **2c** in $CDCl_3$.

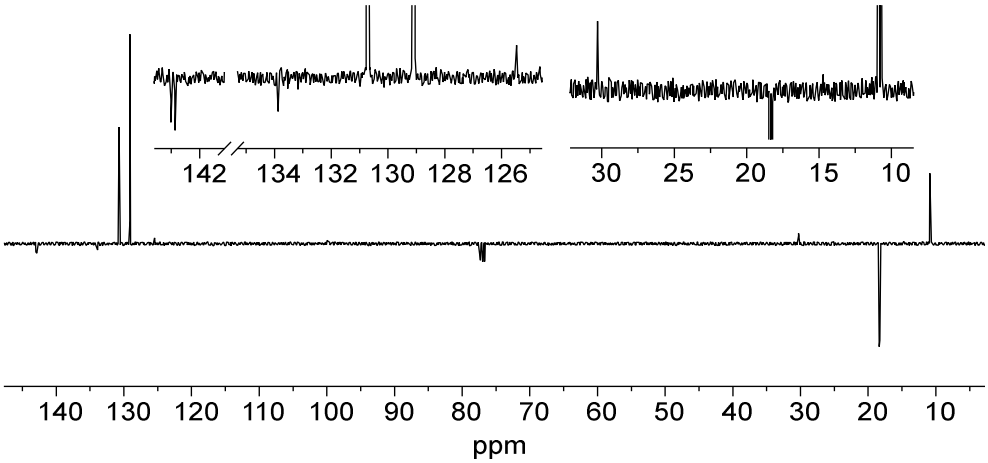

Figure S37: $^{13}C\{^{1}H\}$ NMR of **2c** in $CDCl_3$.

(2,6-Dichlorophenyl)diphenylphosphane (**2c**)

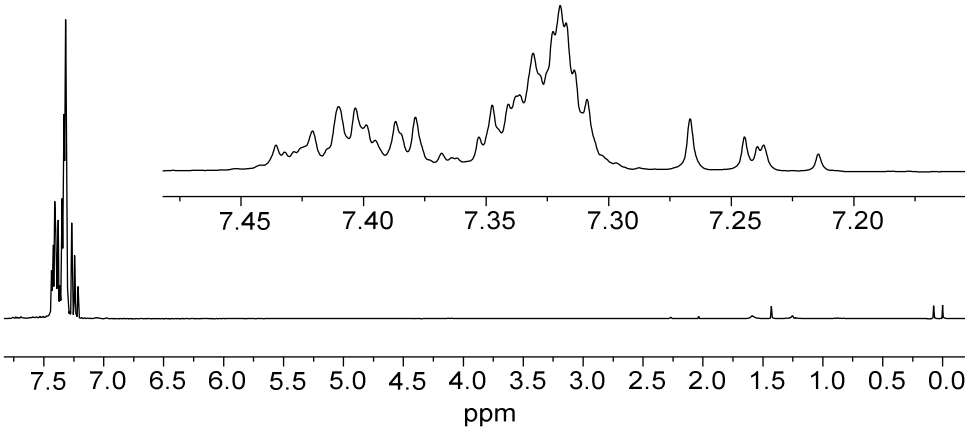

Figure S38: ^{1}H NMR of **2d** in $CDCl_3$.

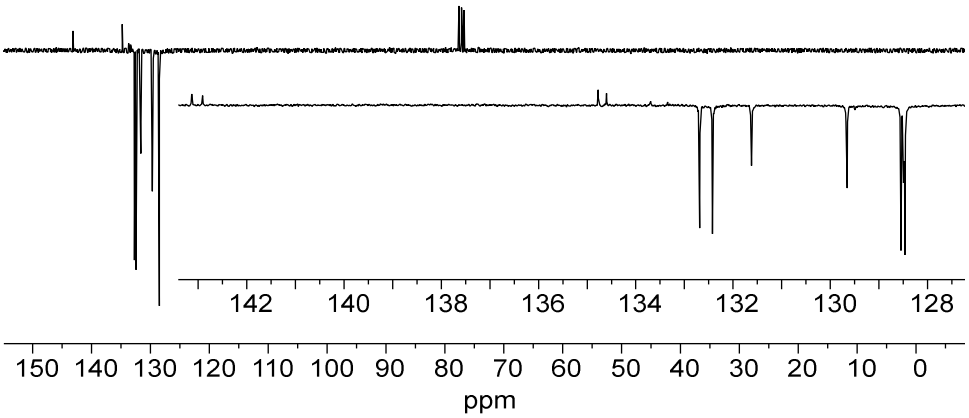

Figure S39: $^{13}C\{^{1}H\}$ NMR of **2d** in $CDCl_3$.

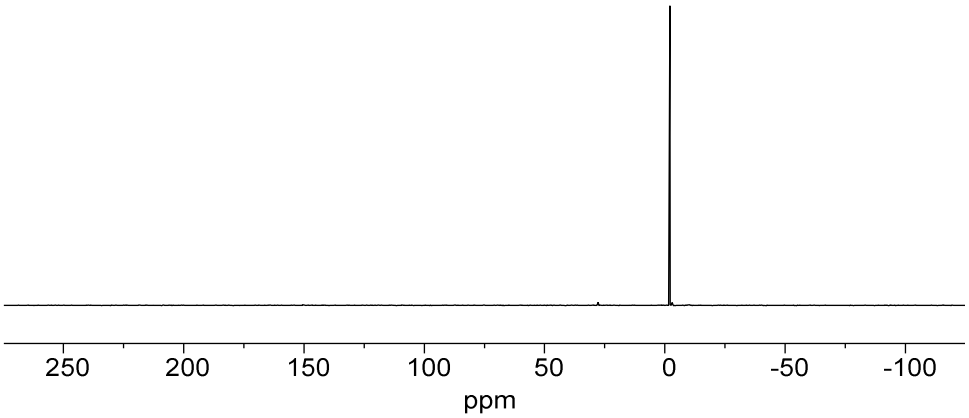

Figure S40: $^{31}P\{^{1}H\}$ NMR of **2d** in $CDCl_3$.

(3,3‘‘,5,5‘‘-Tetramethoxycarbonyl-1,1‘:3‘,1‘‘-terphen-2‘-yl)dimethylphosphane oxide (**3a**)

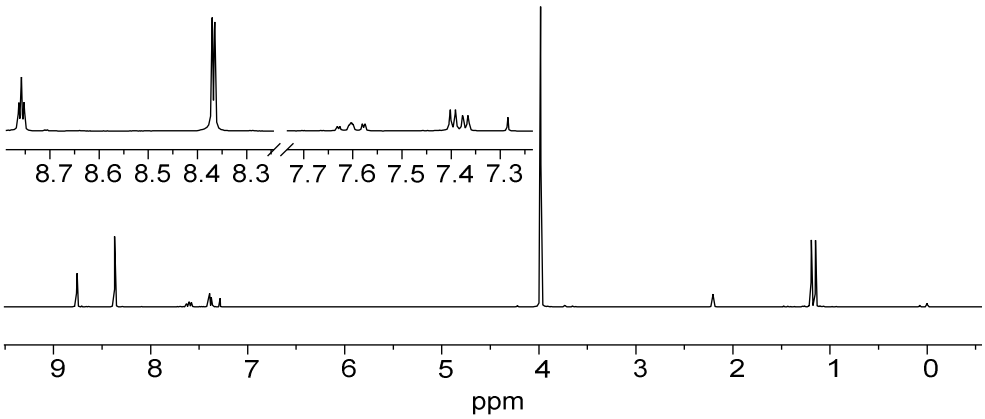

Figure S41: ^{1}H NMR of **3a** in $CDCl_3$.

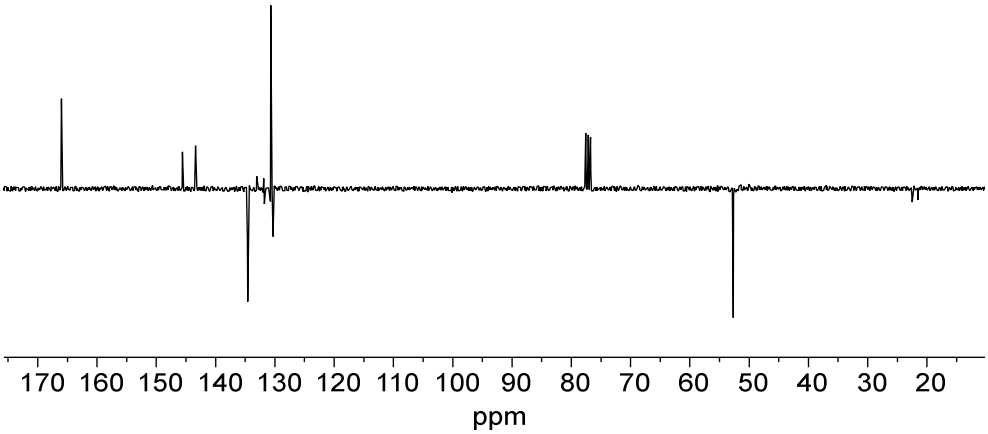

Figure S42: $^{13}C\{^{1}H\}$ NMR of **3a** in $CDCl_3$.

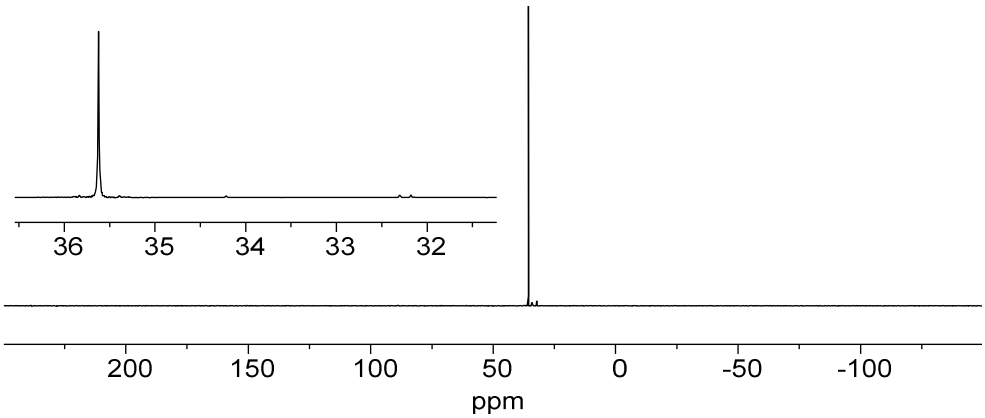

Figure S43: $^{31}P\{^{1}H\}$ NMR of **3a** in $CDCl_3$.

(3,3‘‘,5,5‘‘-Tetramethoxycarbonyl-1,1‘:3‘,1‘‘-terphen-2‘-yl)dimethylphosphane sulfide (**3b**)

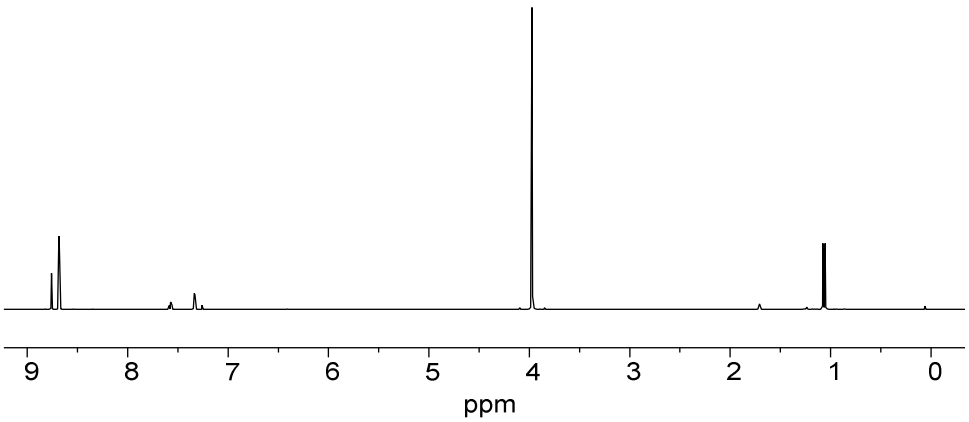

Figure S44: ^{1}H NMR of **3b** in $CDCl_3$.

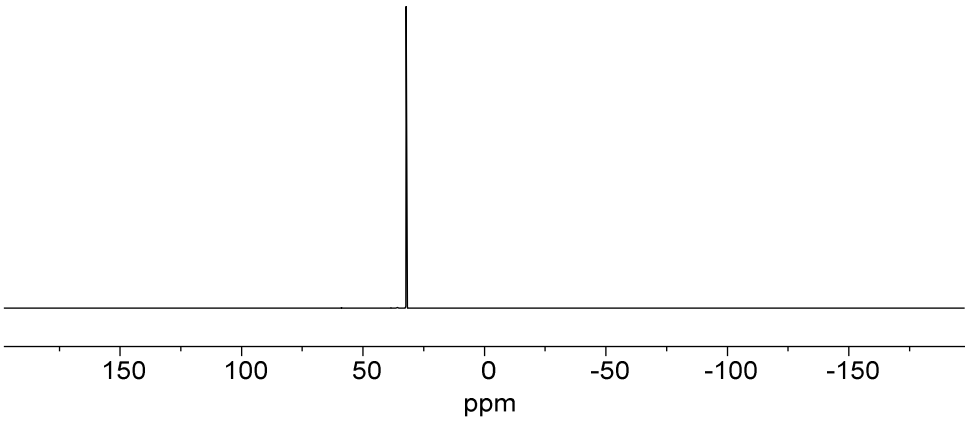

Figure S45: $^{31}P\{^{1}H\}$ NMR of **3b** in $CDCl_3$.

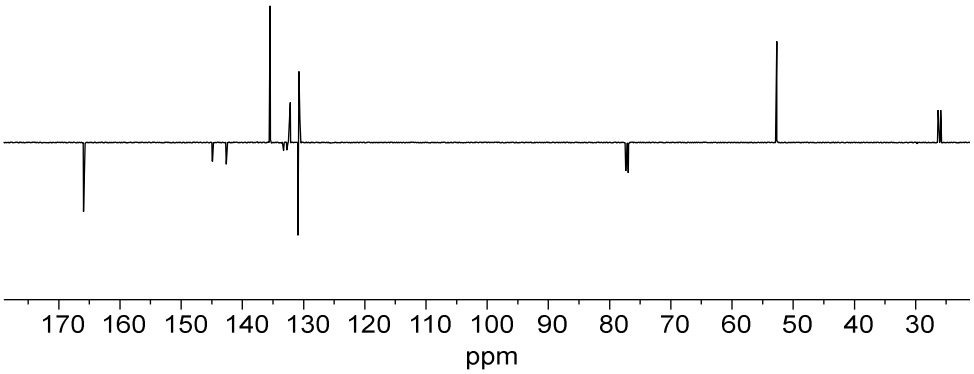

Figure S46: $^{13}C\{^{1}H\}$ NMR of **3b** in $CDCl_3$.

(3,3‘‘,5,5‘‘-Tetramethoxycarbonyl-1,1‘:3‘,1‘‘-terphen-2‘-yl)diethylphosphane oxide (**3c**)

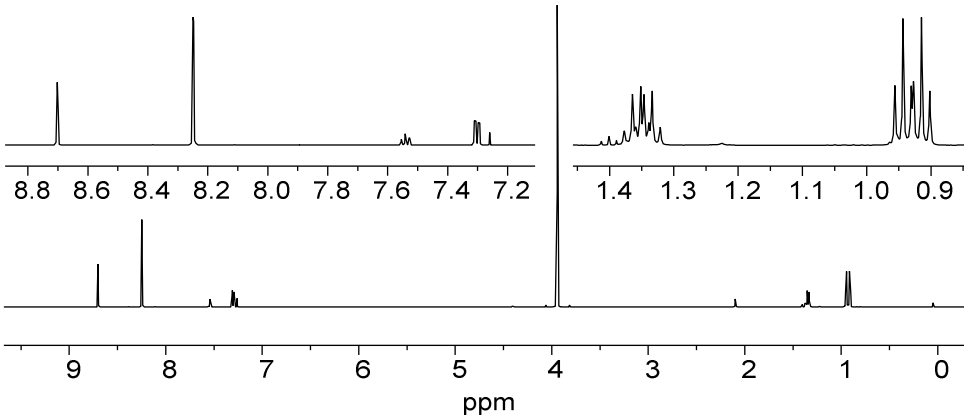

Figure S47: ^{1}H NMR of **3c** in $CDCl_3$.

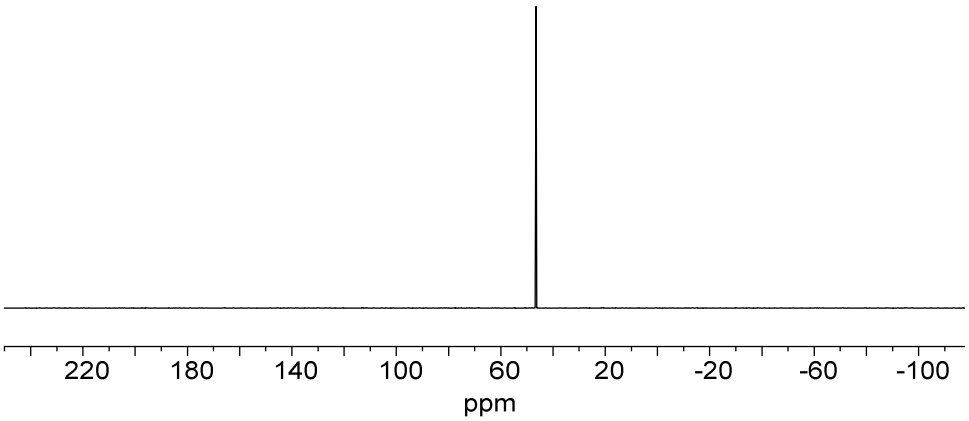

Figure S48: $^{31}P\{^{1}H\}$ NMR of **3c** in $CDCl_3$.

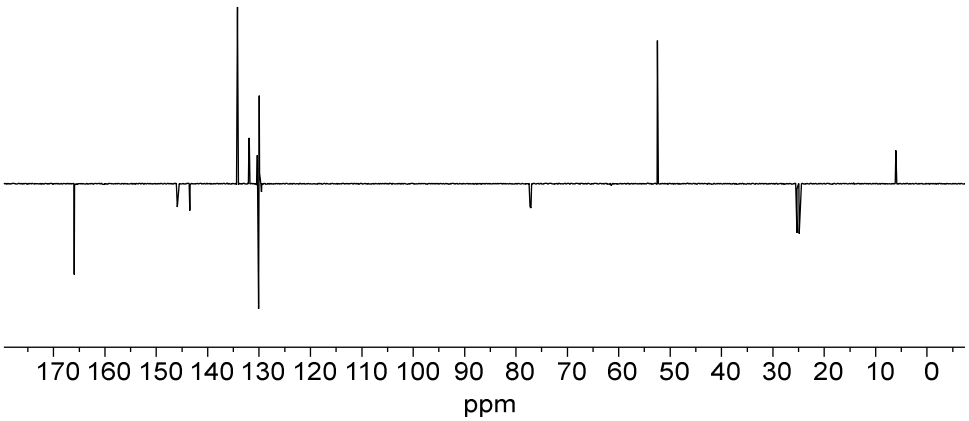

Figure S49: $^{13}C\{^{1}H\}$ NMR of **3c** in $CDCl_3$.

(3,3′′,5,5′′-Tetramethoxycarbonyl-1,1′:3′,1′′-terphen-2′-yl)diphenylphosphane oxide (**3d**)

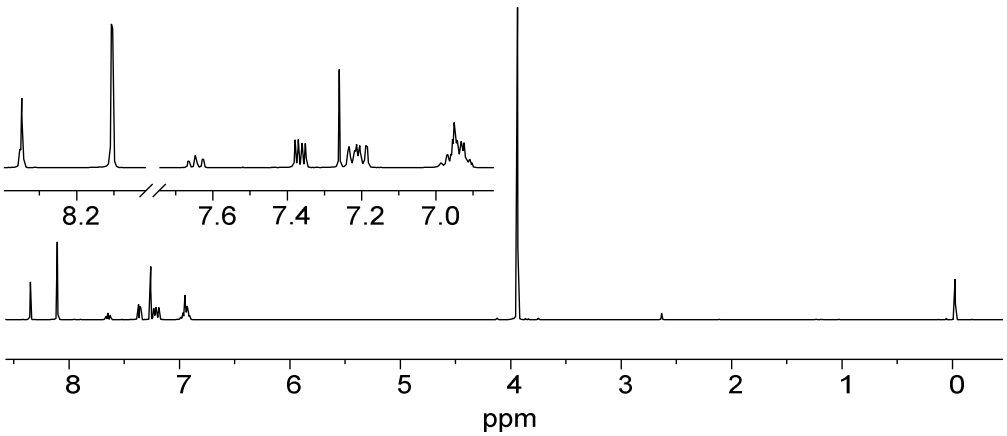

Figure S50: ^{1}H NMR of **3d** in $CDCl_3$.

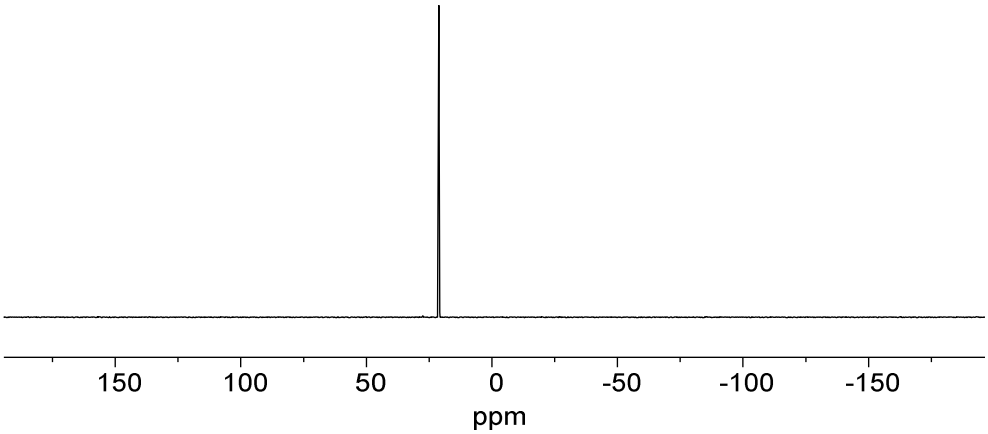

Figure S51: $^{31}P\{^{1}H\}$ NMR of **3d** in $CDCl_3$.

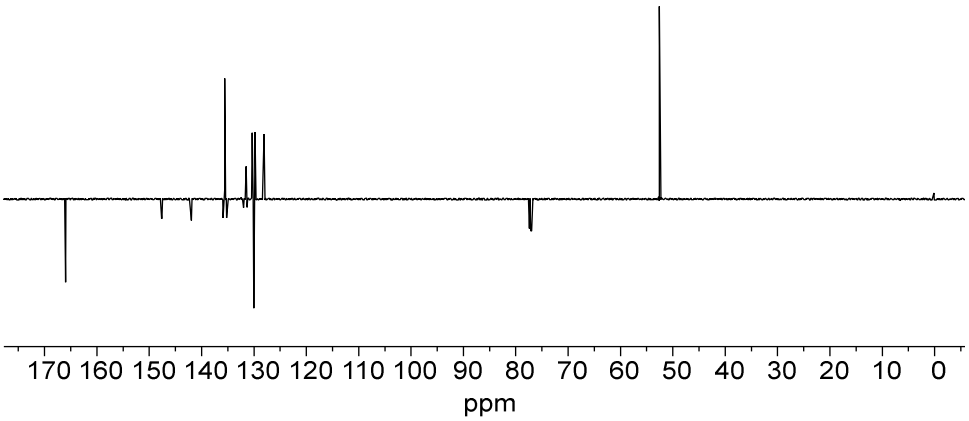

Figure S52: $^{13}C\{^{1}H\}$ NMR of **3d** in $CDCl_3$.

(3,3′′,5,5′′-Tetracarboxy-1,1′:3′,1′′-terphen-2′-yl)dimethylphosphane oxide (**4a**)

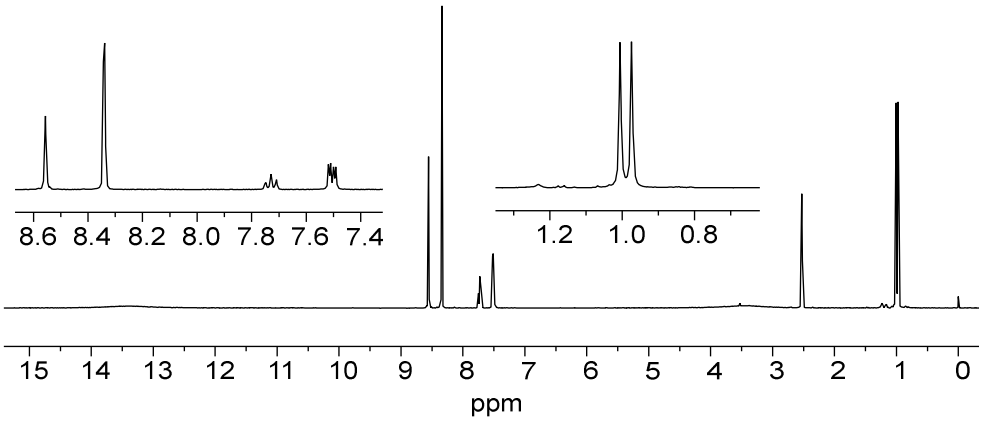

Figure S53: ^{1}H NMR of **4a** in DMSO-d_6.

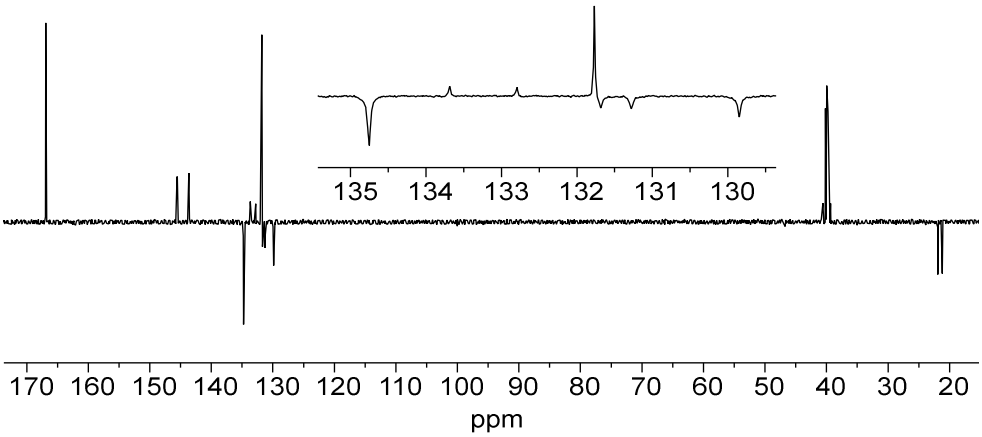

Figure S54: $^{13}C\{^{1}H\}$ NMR of **4a** in DMSO-d_6.

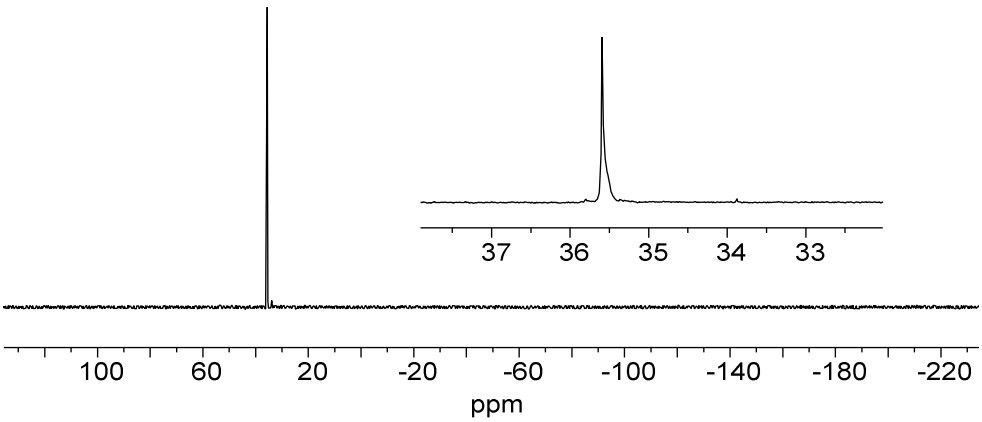

Figure S55: $^{31}P\{^{1}H\}$ NMR of **4a** in DMSO-d_6.

(3,3′′,5,5′′-Tetracarboxy-1,1′:3′,1′′-terphen-2′-yl)dimethylphosphane sulfide (**4b**)

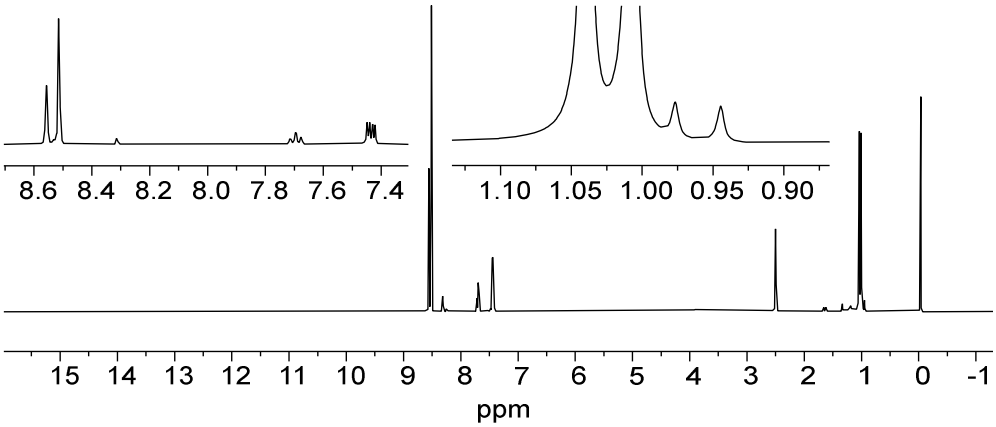

Figure S56: ^{1}H NMR of **4b** in DMSO-d_6. The right-hand expansion shows the region of resonances belonging to P-bound methyl groups. The doublet at 0.99 ppm (^{2}J(H,P) = 12.8 Hz) corresponds to the phosphine oxide **4a**, that at 1.02 ppm (^{2}J(H,P) = 12.8 Hz) to the phosphine sulfide **4b**. Deconvolution shows that approximately 5 % of phosphine oxide is present.

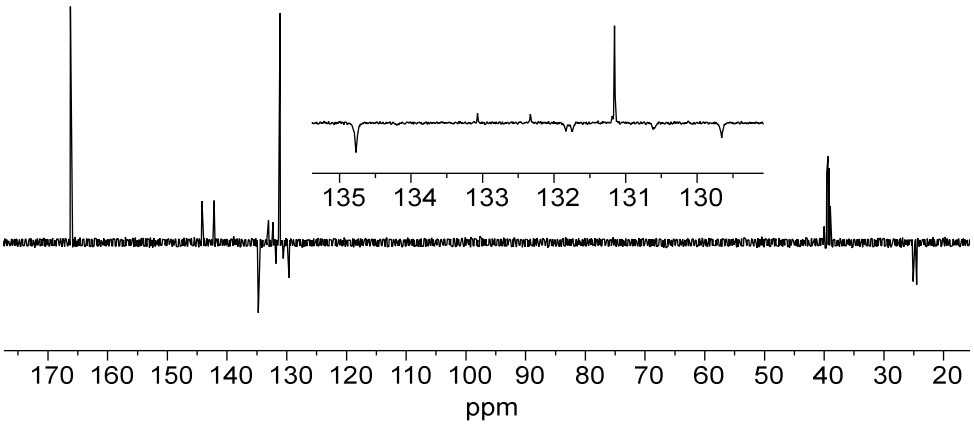

Figure S57: $^{13}C\{^{1}H\}$ NMR of **4b** in DMSO-d_6.

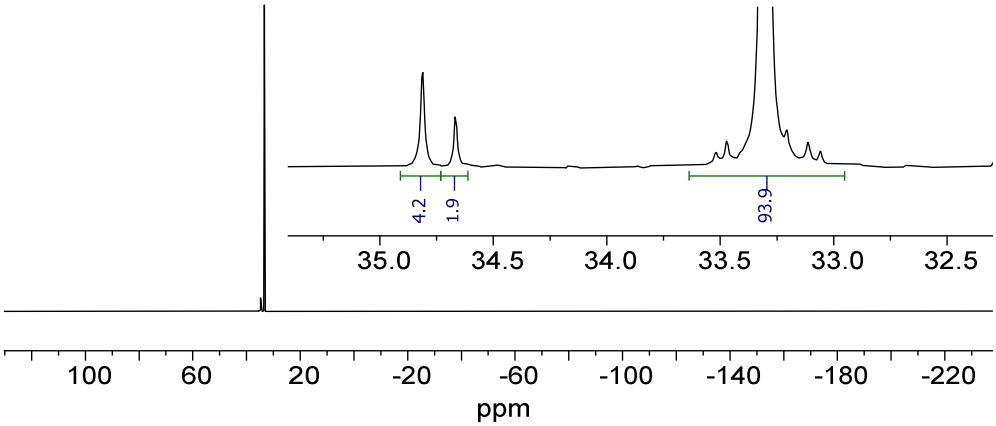

Figure S58: $^{31}P\{^{1}H\}$ NMR of **4b** in DMSO-d_6. Two contaminations corresponding to ^{31}P resonances at 34.8 ppm and 34.7 ppm are observed. The higher ppm resonance is expected to belong to the phosphine oxide **4a** as the relative proportion is also reflected by deconvolution of the corresponding resonances in the ^{1}H NMR spectrum, see Figure S56.

(3,3′′,5,5′′-Tetracarboxy-1,1′:3′,1′′-terphen-2′-yl)diethylphosphane oxide (**4c**)

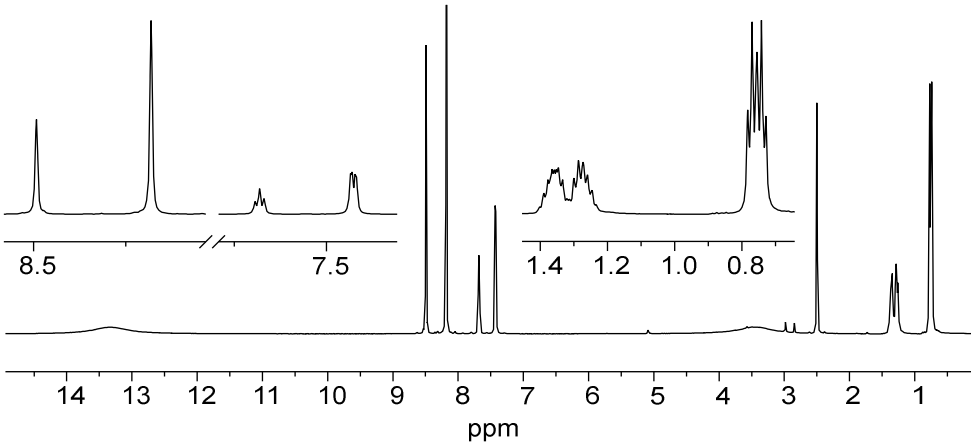

Figure S59: ^{1}H NMR of **4c** in DMSO-d_6.

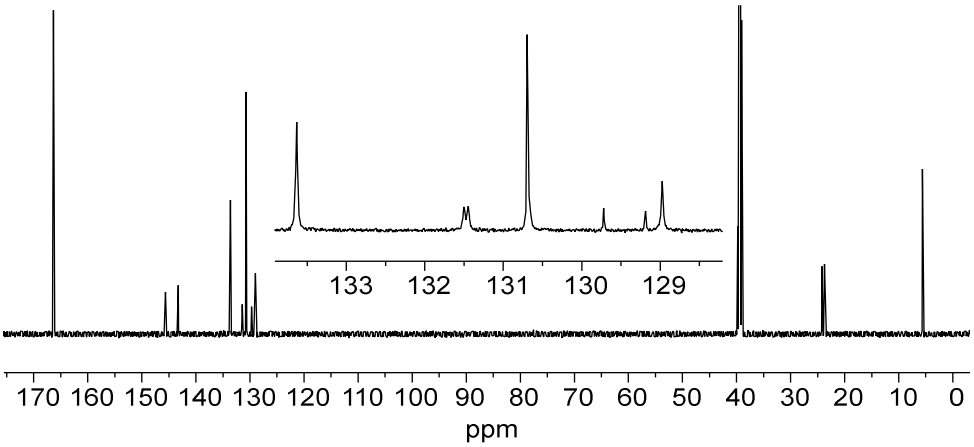

Figure S60: $^{13}C\{^{1}H\}$ NMR of **4c** in DMSO-d_6.

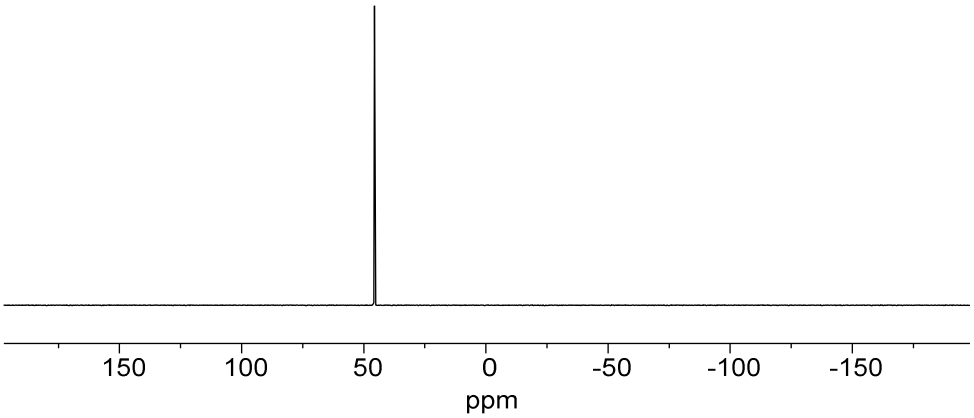

Figure S61: $^{31}P\{^{1}H\}$ NMR of **4c** in DMSO-d_6.

(3,3‘‘,5,5‘‘-Tetracarboxy-1,1‘:3‘,1‘‘-terphen-2‘-yl)diphenylphosphane oxide (**4d**)

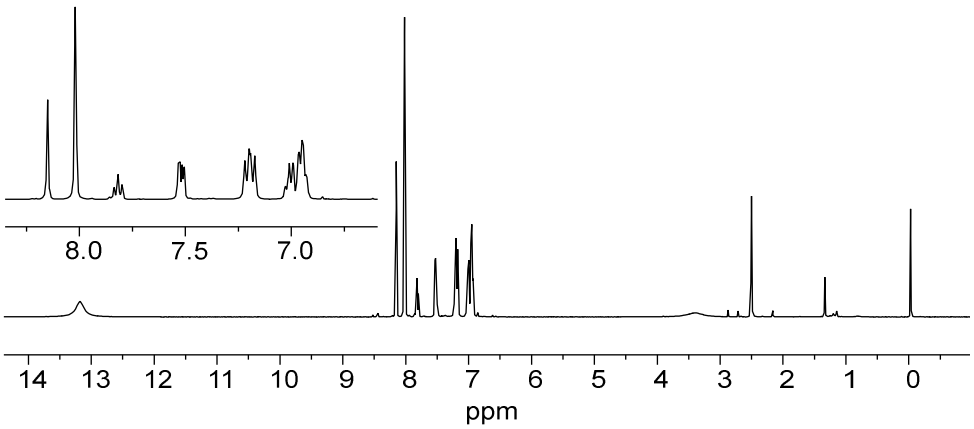

Figure S62: ^{1}H NMR of **4d** in DMSO-d_6.

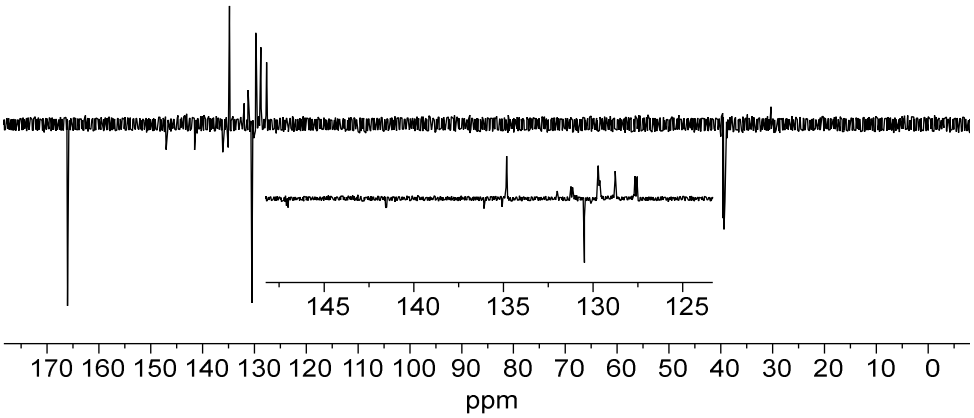

Figure S63: $^{13}C\{^{1}H\}$ NMR of **4d** in DMSO-d_6.

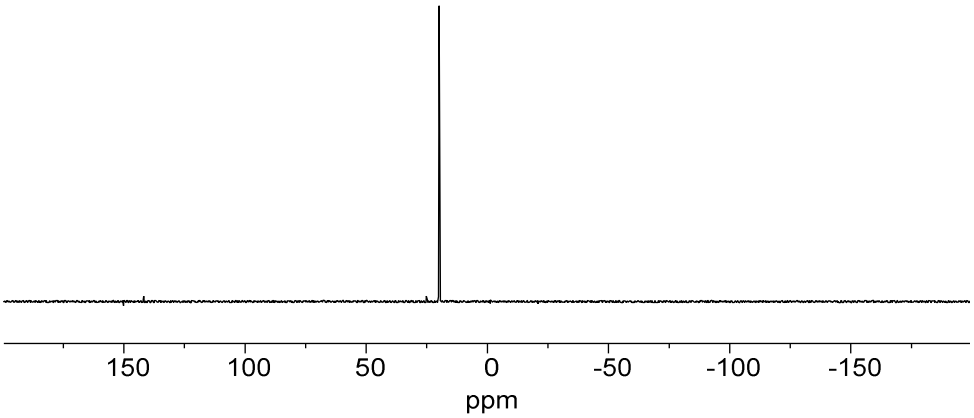

Figure S64: $^{31}P\{^{1}H\}$ NMR of **4d** in DMSO-d_6.

Single crystal structure analyses

(2,6-Dichlorophenyl)diphenylphosphane (**2d**)
CCDC Deposition Number 1942981

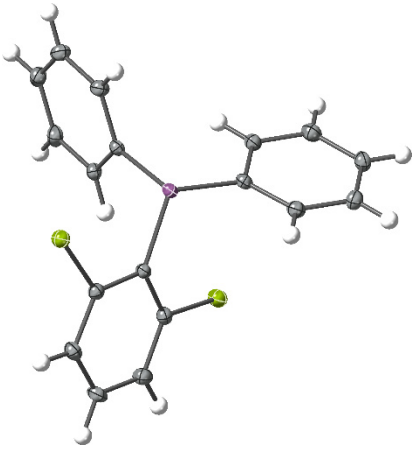

Figure S65: Molecular structure of **2d** with thermal ellipsoids at 50 % probability. H atoms displayed as spheres of an arbitrary radius.

Table S8: Crystal data, data collection, and refinement of **2d**.

Crystal data		
Cell	a = 8.2413(3) Å	α = 105.361(3)°
	b = 9.8910(3) Å	β = 104.778(3)°
	c = 11.4287(3) Å	γ = 110.456(3)°
	V = 776.87(5) Å³	
	from 12940 reflns. between θ_{min} = 4.3° and θ_{max} = 76.1°	
Chemical formula	$C_{18}H_{13}Cl_2P$	
Z / Z'	2 / 1	
M_r	331.15	
Crystal system, space group	Triclinic, $P\bar{1}$	
Crystal size	(0.39 × 0.30 × 0.21) mm^3	
Crystal colour, morphology	colourless, block	

Data collection	
F(000)	340.0
D_x	1.416 Mg m^{-3}
θ_{min}, θ_{max}	4.3°, 76.5°
Completeness at θ_{max}	0.986
Radiation type	Cu $K\alpha$ (λ = 1.54178 Å)
Temperature	100 K
μ	4.631 mm^{-1}
Diffractometer	Agilent SuperNova Dual Source
T_{min}, T_{max}	0.777, 1.000
hkl range	h: −9 → 10, k: −12 → 12, l: −14 → 14
No. of reflections	15427 measured, 3228 independent, 3145 (I > 2σ(I))
R_{int}	0.035
sin(θ_{max})/λ	0.631 Å^{-1}

Refinement

$R[F^2 > 2\sigma(F^2)]$	0.029
$wR(F^2)$	0.076
S	1.04
w	$1/(\sigma^2(F_o^2) + (0.0424P)^2 + 0.4588P)$ with $P = (F_o^2 + 2F_c^2)/3$
$(\Delta/\sigma)_{max}$	0.001
$\Delta\rho_{max}$, $\Delta\rho_{min}$	0.350 e Å^3, −0.334 e Å^3
No. of reflections	3228
No. of parameters / restraints	190 / 0

(3,3′′,5,5′′-Tetramethoxycarbonyl-1,1′:3′,1′′-terphen-2′-yl)dimethylphosphane oxide 1.5-ethanol solvate (**3a** · 1.5 EtOH)

CCDC Deposition Number 1942982

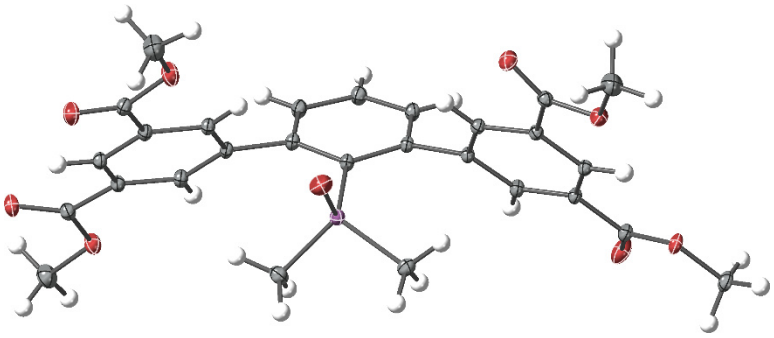

Figure S66: Molecular structure of **3a** · 1.5 EtOH with thermal ellipsoids at 50 % probability. H atoms displayed as spheres of an arbitrary radius. Co-crystallised solvent molecules not shown.

Table S9: Crystal data, data collection, and refinement of **3a** · 1.5 EtOH.

Crystal data		
Cell	a = 10.5051(2) Å	α = 66.318(1)°
	b = 12.1756(2) Å	β = 88.311(1)°
	c = 12.9793(3) Å	γ = 82.681(1)°
	V = 1507.51(5) Å^3	
	from 9902 reflns. between θ_{min} = 2.5° and θ_{max} = 34.3°	
Chemical formula	$C_{28}H_{27}O_9P \cdot 1.5(C_2H_6O)$	
Z / Z'	2 / 1	
M_r	607.57	
Crystal system, space group	Triclinic, $P\bar{1}$	
Crystal size	(0.14 × 0.14 × 0.12) mm^3	
Crystal colour, morphology	colourless, block	

Data collection	
F(000)	642.0
D_x	1.338 Mg m^{-3}
θ_{min}, θ_{max}	1.7°, 33.0°
Completeness at θ_{max}	0.972
Radiation type	Mo $K\alpha$ (λ = 0.71073 Å)
Temperature	100 K
μ	0.150 mm^{-1}
Diffractometer	Bruker AXS SMART APEX
T_{min}, T_{max}	0.710, 0.747
hkl range	h: −16 → 16, k: −18 → 18, l: −19 → 19
No. of reflections	41778 measured, 11051 independent, 9904 ($I > 2\sigma(I)$)
R_{int}	0.019
sin(θ_{max})/λ	0.766 Å^{-1}

Refinement	
$R[F^2 > 2\sigma(F^2)]$	0.038
$wR(F^2)$	0.108
S	1.04
w	$1/(\sigma^2(F_o^2) + (0.0544P)^2 + 0.6551P)$ with $P = (F_o^2 + 2F_c^2)/3$

$(\Delta/\sigma)_{max}$	0.000
$\Delta\rho_{max}$, $\Delta\rho_{min}$	0.554 e Å^3, −0.349 e Å^3
No. of reflections	11051
No. of parameters / restraints	400 / 5

Special details on the refinement

The ethanol molecule H61—O61—C60—C60^{i} is located around an inversion centre situated between C60 and C60^{i}. The molecule is equally involved in hydrogen bonding either with the ethanol molecule H51—O51—C50—C51 or H51^{i}—O51^{i}—C50^{i}—C51^{i}. Consequently, the occupancy of O61 was held fixed at 50 %. The methylene carbon atom C60 must become a methyl carbon atom C60^{i} after inversion. Consequently, hydrogen atom H61C has been added along the O61—C60 bond with fixed occupancy of 50 % to allow reproduction of the methyl group hydrogen atoms H60A^{i}, H60B^{i}, and H61C^{i}. Positioning of H61C was achieved using DFIX and SADI restraints, see .cif for details.[Symmetry code: (i) −*x*, −*y*, 1−*z*.]

(3,3‘‘,5,5‘‘-Tetramethoxycarbonyl-1,1‘:3‘,1‘‘-terphen-2‘-yl)dimethylphosphane sulfide (**3b**)

CCDC Deposition Number 1942983

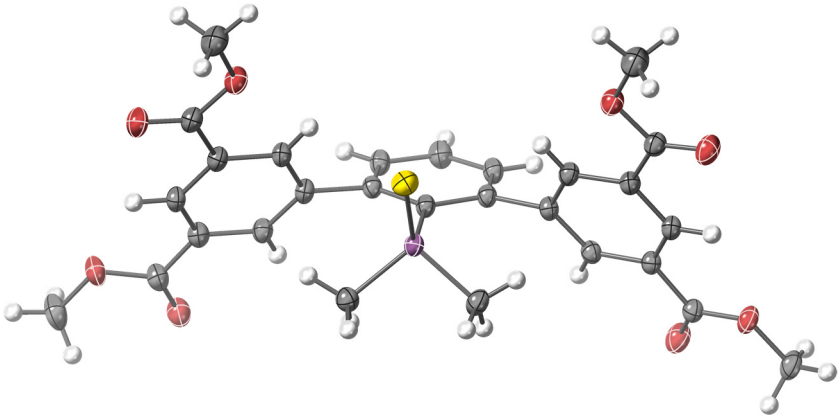

Figure S67: Molecular structure of **3b** with thermal ellipsoids at 50 % probability. H atoms displayed as spheres of an arbitrary radius.

Table S10: Crystal data, data collection, and refinement of **3b**.

Crystal data		
Cell	a = 10.9208(4) Å	α = 100.927(3)°
	b = 11.5897(3) Å	β = 109.264(3)°
	c = 11.7392(4) Å	γ = 103.651(3)°
	V = 1303.80(8) Å^3	
	from 22171 reflns. between θ_{min} = 4.1° and θ_{max} = 75.6°	
Chemical formula	$C_{28}H_{27}O_8PS$	
Z / Z'	2 / 1	
M_r	554.52	
Crystal system, space group	Triclinic, $P\bar{1}$	
Crystal size	(0.308 × 0.177 × 0.104) mm^3	
Crystal colour, morphology	colourless, plate	

Data collection	
F(000)	580
D_x	1.413 Mg m^{-3}
θ_{min}, θ_{max}	4.1°, 76.1°
Completeness at θ_{max}	0.993
Radiation type	Cu $K\alpha$ (λ = 1.54184 Å)
Temperature	100 K
μ	2.119 mm^{-1}
Diffractometer	Agilent SuperNova Dual Source
T_{min}, T_{max}	0.679, 1.000
hkl range	h: −13 → 13, k: −14 → 14, l: −14 → 14
No. of reflections	37479 measured, 5433 independent, 5029 (I > 2σ(I))
R_{int}	0.039
sin(θ_{max})/λ	0.630 Å^{-1}

Refinement	
$R[F^2 > 2\sigma(F^2)]$	0.042
$wR(F^2)$	0.106

S	1.03
w	$1/(\sigma^2(F_o^2) + (0.0547P)^2 + 0.8653P)$ with $P = (F_o^2 + 2F_c^2)/3$
$(\Delta/\sigma)_{max}$	0.000
$\Delta\rho_{max}$, $\Delta\rho_{min}$	0.520 e Å^3, −0.347 e Å^3
No. of reflections	5433
No. of parameters / restraints	349 / 0

Special details on the refinement

Six reflections with |error/esd| > 10 were omitted.

(3,3′′,5,5′′-Tetramethoxycarbonyl-1,1′:3′,1′′-terphen-2′-yl)diethylphosphane oxide deuterotrichloromethane solvate (**3c** · $CDCl_3$)

CCDC Deposition Number 1942984

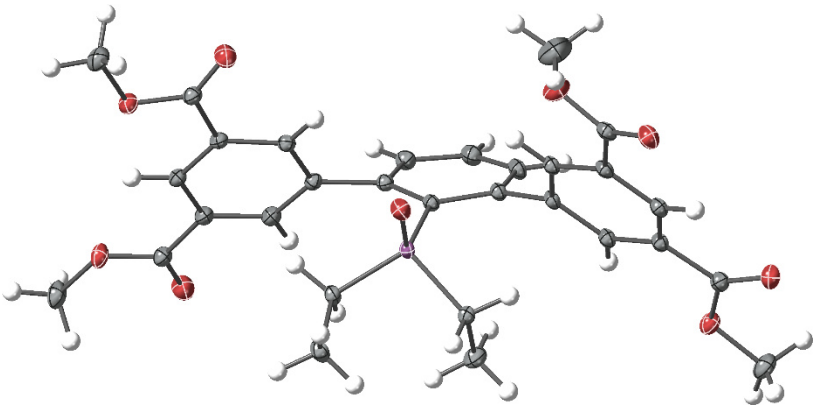

Figure S68: Molecular structure of **3c** · $CDCl_3$ with thermal ellipsoids at 50 % probability. H atoms displayed as spheres of an arbitrary radius. Co-crystallised solvent molecules not shown.

Table S11: Crystal data, data collection, and refinement of **3c** · $CDCl_3$.

Crystal data		
Cell	a = 10.6082(4) Å	α = 67.364(3)°
	b = 12.4315(4) Å	β = 88.560(3)°
	c = 12.9377(5) Å	γ = 81.914(3)°
	V = 1558.30(10) Å^3	
	from 44438 reflns. between θ_{min} = 2.9° and θ_{max} = 32.4°	
Chemical formula	$C_{31}H_{31}Cl_3DO_9P$	
Z / Z'	2 / 1	
M_r	686.89	
Crystal system, space group	Triclinic, $P\bar{1}$	
Crystal size	(0.40 × 0.20 × 0.16) mm^3	
Crystal colour, morphology	colourless, block	

Data collection	
F(000)	712
D_x	1.464 Mg m^{-3}
θ_{min}, θ_{max}	2.9°, 32.6°
Completeness at θ_{max}	0.948
Radiation type	Mo $K\alpha$ (λ = 0.71073 Å)
Temperature	100 K
μ	0.400 mm^{-1}
Diffractometer	Agilent SuperNova Dual Source
T_{min}, T_{max}	0.957, 1.000
hkl range	h: −16 → 15, k: −18 → 18, l: −19 → 19
No. of reflections	59878 measured, 10798 independent, 9368 (I > 2σ(I))
R_{int}	0.032
sin(θ_{max})/λ	0.759 Å^{-1}

Refinement	
$R[F^2 > 2\sigma(F^2)]$	0.040

$wR(F^2)$	0.111
S	1.04
w	$1/(\sigma^2(F_o^2) + (0.0518P)^2 + 0.9005P)$ with $P = (F_o^2 + 2F_c^2)/3$
$(\Delta/\sigma)_{max}$	0.001
$\Delta\rho_{max}$, $\Delta\rho_{min}$	0.752 e Å^3, −0.595 e Å^3
No. of reflections	10798
No. of parameters / restraints	463 / 61

Special details on the refinement

The initial cell a = 12.9377(5) Å, b = 15.1649(5) Å, c = 17.4406(5) Å, α = 80.861(3)°, β = 73.165(3)°, and γ = 72.667(3)° with Z = 4 and two formula units of **3c** within the asymmetric unit. Using the ADDSYM routine implemented in PLATON, a reduced cell of half the initial volume was found. The transformation matrix for cell and hkl data was 0 0.5 −0.5 0 −0.5 −0.5 −1 0 0. The co-crystallised deuterochloform solvent is disordered over three sites. The deuterium atoms were positioned by holding the D—C bond lengths fixed at a distance of 1.073 Å (DFIX restraint) and aligning the respective D…Cl distances to be the same (SADI restraint). Occupancy refinement gave s.o.f.s of 0.4263(9), 0.2630(14), and 0.3106(15) for the deuterochloroform molecules around carbon atoms C50A, C50B, and C50C, respectively. The sum of occupancy factors was restrained to 1.0 (SUMP instruction). $CDCl_3$ molecules belonging to carbon atoms C50B and C50C are very close to each other, so that (a) the anisotropic displacement parameters of near-congruent atoms were adjusted using the EADP constraint and (b) the 1,2 and 1,3 distances were fixed using the SAME restraint.

(3,3′′,5,5′′-Tetramethoxycarbonyl-1,1′:3′,1′′-terphen-2′-yl)diphenylphosphane oxide (**3d**) – monoclinic polymorph

CCDC Deposition Number 1942986

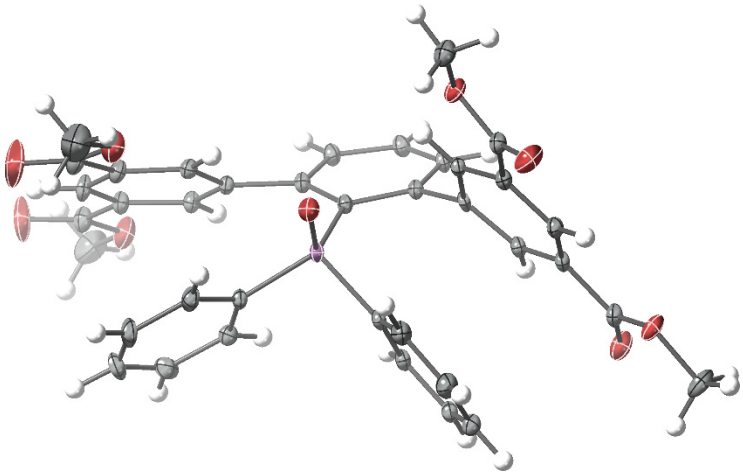

Figure S69: Molecular structure of **3d** (monoclinic polymorph) with thermal ellipsoids at 50 % probability. H atoms displayed as spheres of an arbitrary radius.

Table S12: Crystal data, data collection, and refinement of **3d** (monoclinic polymorph).

Crystal data		
Cell	a = 36.1084(4) Å	α = 90°
	b = 12.08210(10) Å	β = 99.4400(10)°
	c = 15.1558(2) Å	γ = 90°
	V = 6522.41(13) Å^3	
	from 28734 reflns. between θ_{min} = 3.8° and θ_{max} = 76.4°	
Chemical formula	$C_{38}H_{31}O_9P$	
Z / Z'	8 / 1	
M_r	662.60	
Crystal system, space group	Monoclinic, *C*2/*c*	
Crystal size	(0.28 × 0.07 × 0.03) mm^3	
Crystal colour, morphology	colourless, plate	

Data collection	
F(000)	2768
D_x	1.350 Mg m^{-3}
θ_{min}, θ_{max}	3.9°, 72.5°
Completeness at θ_{max}	1.000
Radiation type	Cu $K\alpha$ (λ = 1.54178 Å)
Temperature	100 K
μ	1.233 mm^{-1}
Diffractometer	Agilent SuperNova Dual Source
T_{min}, T_{max}	0.755, 1.000
hkl range	h: −44 → 44, k: −14 → 14, l: −18 → 18
No. of reflections	66459 measured, 6465 independent, 5841 (I > 2σ(I))
R_{int}	0.023
sin(θ_{max})/λ	0.619 Å^{-1}

Refinement

$R[F^2 > 2\sigma(F^2)]$	0.038
$wR(F^2)$	0.098
S	1.03
w	$1/(\sigma^2(F_o^2) + (0.0529P)^2 + 6.5889P)$ with $P = (F_o^2 + 2F_c^2)/3$
$(\Delta/\sigma)_{max}$	0.001
$\Delta\rho_{max}$, $\Delta\rho_{min}$	0.382 e Å^3, −0.496 e Å^3
No. of reflections	6465
No. of parameters / restraints	437 / 0

(3,3′′,5,5′′-Tetramethoxycarbonyl-1,1′:3′,1′′-terphen-2′-yl)diphenylphosphane oxide (**3d**) – triclinic polymorph

CCDC Deposition Number 1942987

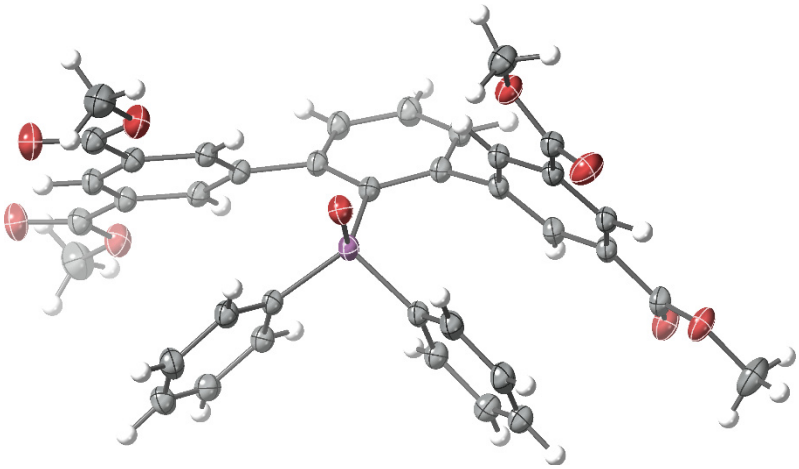

Figure S70: Molecular structure of **3d** (triclinic polymorph) with thermal ellipsoids at 50 % probability. H atoms displayed as spheres of an arbitrary radius.

Table S13: Crystal data, data collection, and refinement of **3d** (triclinic polymorph).

Crystal data		
Cell	a = 8.2514(4) Å	α = 101.701(3)°
	b = 11.6965(5) Å	β = 97.017(3)°
	c = 17.6863(6) Å	γ = 102.970(4)°
	V = 1603.49(12) Å^3	
	from 15424 reflns. between θ_{min} = 4.0° and θ_{max} = 76.2°	
Chemical formula	$C_{38}H_{31}O_9P$	
Z / Z'	2 / 1	
M_r	662.60	
Crystal system, space group	Triclinic, $P\bar{1}$	
Crystal size	(0.40 × 0.30 × 0.25) mm^3	
Crystal colour, morphology	colourless, block	

Data collection	
F(000)	692
D_x	1.372 Mg m^{-3}
θ_{min}, θ_{max}	4.0°, 77.7°
Completeness at θ_{max}	0.976
Radiation type	Cu $K\alpha$ (λ = 1.54178 Å)
Temperature	100 K
μ	1.254 mm^{-1}
Diffractometer	Agilent SuperNova Dual Source
T_{min}, T_{max}	0.643, 1.000
hkl range	h: −10 → 10, k: −14 → 14, l: −22 → 22
No. of reflections	32088 measured, 6679 independent, 5812 (I > 2σ(I))
R_{int}	0.051
sin(θ_{max})/λ	0.634 Å^{-1}

Refinement

$R[F^2 > 2\sigma(F^2)]$	0.045
$wR(F^2)$	0.128
S	1.03
w	$1/(\sigma^2(F_o^2) + (0.0795P)^2 + 0.4780P)$ with $P = (F_o^2 + 2F_c^2)/3$
$(\Delta/\sigma)_{max}$	0.001
$\Delta\rho_{max}$, $\Delta\rho_{min}$	0.565 e Å^3, −0.372 e Å^3
No. of reflections	6679
No. of parameters / restraints	437 / 0

(3,3′′,5,5′′-Tetramethoxycarbonyl-1,1′:3′,1′′-terphen-2′-yl)diphenylphosphane oxide 2-chloroform solvate (**3d** · 2 $CHCl_3$)

CCDC Deposition Number 1942985

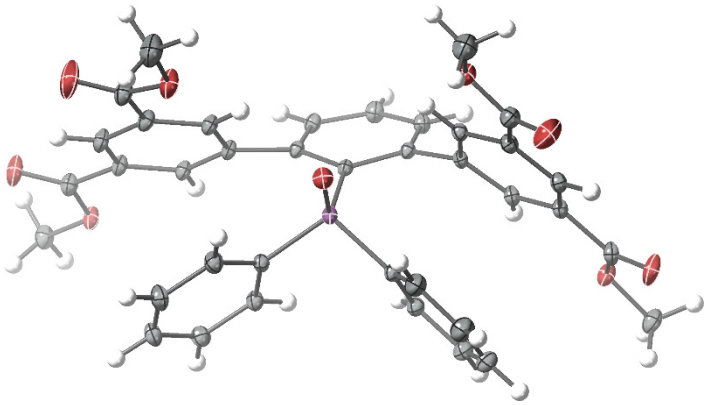

Figure S71: Molecular structure of **3d** · 2 $CHCl_3$ with thermal ellipsoids at 50 % probability. H atoms displayed as spheres of an arbitrary radius. Co-crystallised solvent molecules not shown.

Table S14: Crystal data, data collection, and refinement of **3d** · 2 $CHCl_3$.

Crystal data		
Cell	a = 10.24130(10) Å	α = 90°
	b = 22.4781(3) Å	β = 94.4590(10)°
	c = 17.7231(2) Å	γ = 90°
	V = 4067.60(8) Å^3	
	from 26357 reflns. between θ_{min} = 3.4° and θ_{max} = 31.9°	
Chemical formula	$C_{40}H_{33}Cl_6O_9P$	
Z / Z'	4 / 1	
M_r	901.33	
Crystal system, space group	Monoclinic, $P2_1/n$	
Crystal size	(0.20 × 0.16 × 0.07) mm^3	
Crystal colour, morphology	colourless, block	

Data collection	
F(000)	1848
D_x	1.472 Mg m^{-3}
θ_{min}, θ_{max}	2.9°, 32.6°
Completeness at θ_{max}	0.946
Radiation type	Mo $K\alpha$ (λ = 0.71073 Å)
Temperature	100 K
μ	0.516 mm^{-1}
Diffractometer	Agilent SuperNova Dual Source
T_{min}, T_{max}	0.954, 1.000
hkl range	h: −15 → 14, k: −33 → 32, l: −26 → 25
No. of reflections	78872 measured, 14097 independent, 11252 (I > 2σ(I))
R_{int}	0.028
sin(θ_{max})/λ	0.759 Å^{-1}

Refinement	
$R[F^2 > 2\sigma(F^2)]$	0.047

$wR(F^2)$	0.122
S	1.04
w	$1/(\sigma^2(F_o^2) + (0.0492P)^2 + 3.5090P)$ with $P = (F_o^2 + 2F_c^2)/3$
$(\Delta/\sigma)_{max}$	0.001
$\Delta\rho_{max}$, $\Delta\rho_{min}$	1.047 e Å^3, −0.880 e Å^3
No. of reflections	14097
No. of parameters / restraints	549 / 112

Special details on the refinement

The co-crystallised chloroform molecules occupy two sites where both show disorder over four sites, respectively. The first site is occupied by chloroform molecules with carbon atoms C60A (0.49661(244)), C60B (0.09018(73)), C60C (0.26231(265)), and C60D (0.15077(251)), respectively, where the individually refined s.o.f.s and respective e.s.d.s are given in parentheses. The second site is occupied by the molecules around the carbon atoms C70A (0.43109(222)), C70B (0.31316(224)), C70C (0.18556(205)), and C70D (0.07013(144)), respectively. The sums of s.o.f.s of molecules belonging to C60A > C60D and C70A > C70D, respectively, was restrained to 1.0 (SUMP instruction). Furthermore, (a) anisotropic displacement parameters of near-congruent atoms were adjusted using the EADP constraint and (b) the 1,2 and 1,3 distances were fixed using the SAME restraint. The displacement parameters of the disordered chloroform molecules were refined isotropic.

UHM-62

CCDC Deposition Number 1942989

Table S15: Crystal data, data collection, and refinement of **UHM-62**.

Crystal data		
Cell	a = 18.3318(4) Å	α = 90°
	b = 25.8343(5) Å	β = 90°
	c = 33.4448(6) Å	γ = 90°
	V = 15839.1(5) Å^3	
	from 20450 reflns. between θ_{min} = 3.9° and θ_{max} = 75.2°	
Chemical formula	$C_{230}H_{290}ClCu_{12}N_{25}O_{89}P_6$	
Z / Z'	2 / 0.125	
M_r	5812.60	
Crystal system, space group	Orthorhombic, *Immm*	
Crystal size	(0.12 × 0.10 × 0.06) mm^3	
Crystal colour, morphology	blue, block	

Data collection	
F(000)	6024
D_x	1.219 Mg m^{-3}
θ_{min}, θ_{max}	3.4°, 67.5°
Completeness at θ_{max}	0.996
Radiation type	Cu $K\alpha$ (λ = 1.54184 Å)
Temperature	100 K
μ	1.634 mm^{-1}
Diffractometer	Agilent SuperNova Dual Source
T_{min}, T_{max}	0.900, 1.000
hkl range	h: −21 → 21, k: −30 → 30, l: −40 → 39
No. of reflections	82481 measured, 7651 independent, 6192 (I > 2σ(I))
R_{int}	0.052
sin(θ_{max})/λ	0.599 Å^{-1}

Refinement	
$R[F^2 > 2\sigma(F^2)]$	0.061
$wR(F^2)$	0.195
S	1.05
w	$1/(\sigma^2(F_o^2) + (0.1298P)^2 + 9.0209P)$ with $P = (F_o^2 + 2F_c^2)/3$
$(\Delta/\sigma)_{max}$	0.000
$\Delta\rho_{max}$, $\Delta\rho_{min}$	0.841 e Å^3, −0.601 e Å^3
No. of reflections	6198
No. of parameters / restraints	434 / 494

Special details on the refinement

All data beyond 2θ = 135° and eight reflections with |error/e.s.d.| > 10 were omitted. Enhanced rigid bond restraints (RIGU) were applied to all non-hydrogen atoms. Atom sets A, B, and C were obtained, where B and C are disordered sites of one chemical site. Aryls C20B C21B C22B C23B C22B^{i} C21B^{i} and C20C C21C C22C C23C C22C^{i} C21C^{i} were restrained using the FLAT instruction. Aryls C20A C21A C22A C23A C22A^{ii} C21A^{ii}, C20B C21B C22B C23B C22B^{i} C21B^{i}, and C20C C21C C22C C23C C22C^{i} C21C^{i} were idealised by applying DFIX and SADI restraints to 1,2-

(1.39 Å) and 1,3-distances, respectively. All diphenylphosphoryl functional groups were idealised by restraining (DFIX) distances P40*n*—O40*n* (1.488 Å), P40*n*—C20*n* (1.842 Å), P40*n*—C40*n* (1.820 Å), and C40*n*—C41*n* (1.530 Å) (*n* = A, B, C).[9] Using DANG restraints, the 1,3-distances C40A…C40A^{iii} and C40*m*…C40*m*^{i} (*m* = B, C) were set to 2.822 Å (DANG), P40n…C41*n* to 2.80 Å. The pairs of C12*m*, C13*m*, and C20*m* were equalised using EADP. The anisotropic displacement parameters of the soft ethyl groups C40A, C41A as well as C41B, C41C were restrained to show a more isotropic behaviour (ISOR). ISOR was also applied to the dimethylammonium cation. Herein, N60—C60 was held fixed at 1.51 Å (DFIX) and the C60…C60^{iv} distance at 2.53 Å (DANG).[Symmetry codes: (i) *x*, *y*, −*z*; (ii) *x*, −*y*, *z*; (iii) 1 −*x*, *y*, *z*; (iv) *x*, −*y*, −*z*.]

PLATON/SQUEEZE was employed to mask electron density contributions that could not modelled by means of chemically sensible molecules. $R[F^2 > 2\sigma(F^2)]$ dropped from 0.1184 to 0.0605. With a multiplicity of 16 for the space group *Immm*, 1860/16 = 116 electrons were removed from a volume of 8542 Å^3/16 ≈ 534 Å^3 per asymmetric unit. This corresponds to approximately three DMF molecules (40 electrons and 144 Å^3 per molecule[87]) per asymmetric unit.

[9] Bond lengths and interatomic distances were taken from single crystal data of **3c** · $CDCl_3$.

UHM-63

CCDC Deposition Number 1942990

Table S16: Crystal data, data collection, and refinement of **UHM-63**.

Crystal data		
Cell	a = 18.6420(4) Å	α = 90°
	b = 25.2812(4) Å	β = 90°
	c = 33.3107(6) Å	γ = 90°
	V = 15699.1(5) Å^3	
	from 58750 reflns. between θ_{min} = 3.9° and θ_{max} = 69.0°	
Chemical formula	$C_{276.93}H_{285.74}Cl_{0.47}Cu_{12}N_{24.47}O_{90.54}P_6$	
Z / Z'	2 / 0.125	
M_r	6370.09	
Crystal system, space group	Orthorhombic, *Immm*	
Crystal size	(0.20 × 0.20 × 0.08) mm^3	
Crystal colour, morphology	blue, block	

Data collection	
F(000)	6578
D_x	1.348 Mg m^{-3}
θ_{min}, θ_{max}	3.5°, 67.5°
Completeness at θ_{max}	0.962
Radiation type	Cu $K\alpha$ (λ = 1.54184 Å)
Temperature	100 K
μ	1.894 mm^{-1}
Diffractometer	Agilent SuperNova Dual Source
T_{min}, T_{max}	0.811, 1.000
hkl range	h: −20 → 22, k: −27 → 29, l: −39 → 38
No. of reflections	58750 measured, 7346 independent, 3745 ($I > 2\sigma(I)$)
R_{int}	0.077
sin(θ_{max})/λ	0.599 Å^{-1}

Refinement	
$R[F^2 > 2\sigma(F^2)]$	0.117
$wR(F^2)$	0.372
S	1.21
w	$1/(\sigma^2(F_o^2) + (0.2000P)^2)$ with $P = (F_o^2 + 2F_c^2)/3$
$(\Delta/\sigma)_{max}$	0.000
$\Delta\rho_{max}$, $\Delta\rho_{min}$	1.026 e Å^3, −1.176 e Å^3
No. of reflections	7346
No. of parameters / restraints	368 / 426

Special Details on the Refinement

All data beyond 2θ = 135° and two reflections with $F_o^2 >> F_c^2$ were omitted. Enhanced rigid bond restraints (RIGU) were applied to all non-hydrogen atoms. ISOR was applied to the soft disordered phenyl group C40B > C45B. Aryl C20B C21B C22B C23B C22B^{i} C21B^{i} was restrained using the FLAT instruction. Additionally, 1,2-distances were idealised to be 1.39 Å (DFIX) and 1,3-distances were equalised using the SADI restraint. 1,2- and 1,3-distances were also idealised for aryls C20A C21A C22A C23A C22A^{ii} C21A^{ii} and C10A C11A C12A C13A C12A^{iii}

C11A[iii]. The diphenylphosphoryl functional groups were idealised using DFIX restraints (1.488 Å for P—O, 1.806 Å for P—C_{phenyl}, 1.830 Å for P—$C_{central\ aryl}$).[10] The P-bound phenyls C40A > C45A and C40B > C45B were idealised using AFIX 66. The dimethylammonium ion was idealised using the following restraints: the N60—C60 bond length was fixed at 1.51 Å using DFIX, the C60…C60[iv] distance was fixed at 2.53 Å using DANG. The interstitial site between Cu3 and Cu3[v] was found to be of mixed occupancy between O1 and Cl1. Both atoms were refined using the same (EADP) isotropic displacement parameters as well as the same coordinates (EXYZ) to give an occupancy of 0.53(3) in favor of Cl1. Consequently, the occupancy for the dimethylammonium cation was linked to the occupancy of Cl1.[Symmetry codes: (i) *x*, *y*, −*z*; (ii) 1−*x*, −*y*, *z*; (iii) 1−*x*, *y*, *z*; (iv) *x*, −*y*, −*z*; (v) −*x*, *y*, −*z*.]

PLATON/SQUEEZE was employed to mask electron density contributions that could not modeled by means of chemically sensible molecules. $R[F^2 > 2\sigma(F^2)]$ dropped from 0.1637 to 0.1169. With a multiplicity of 16 for the space group *Immm*, 1957/16 = 122 electrons were removed from a volume of 7352 Å^3/16 ≈ 460 Å^3 per asymmetric unit. This corresponds to approximately three DMF molecules (40 electrons and 144 Å^3 per molecule[87]) per asymmetric unit.

[10] Bond lengths and interatomic distances were taken from single crystal data of **3d** (monoclinic polymorph).